Exploiting coordination and energy transfer in multinuclear lanthanide complexes

Qidian Li

St Cross College

University of Oxford



A thesis submitted for the degree of

Doctor of Philosophy

Hilary Term 2026

Contents

Abstract v

Acknowledgements vii

Abbreviations viii

Chapter 1 Introduction 1

1.1 Lanthanide Luminescence Characteristics 2

1.2 Lanthanide Photophysics 4

1.3 Antenna effect 6

1.4 Mechanisms of Energy Transfer 9

1.5 Quenching 9

1.6 Stability and the macrocyclic effect 11

1.7 Isomerism 11

1.8 Self-Assembly 13

1.9 NMR 15

1.10 Glycolysis products sensing 16

1.11 Aim 19

1.12 References 20

Chapter 2 Binuclear complexes as imaging agents for anionic guests 32

2.1 Background 32

2.2 Binuclear nitro-m-xylyl complex—Ln.NMM 33

2.3 Synthesis of nitro-m-xylyl bridged binuclear complexes (Ln.NMM) 34

2.4 Binding Studies 36

2.4.1 Photophysical titration experiment 36

2.4.2 NMR binding study 41

2.5 CEST experiments 42

2.6 Conclusion 45

2.7 References 47

Chapter 3 Self-assembly heterometallic complexes: controlling processes by competitive binding --- The interaction of homometallic binuclear nitro-m-xylyl complexes and the 8-coordinate aminoisophthalate complexes vs glucose phosphate 49

3.1 Eu.NMM + Tb.iphth / G6P competitive binding 49

3.2 The idea of Competitive Binding 49

3.3 Possible future applications 52

3.4 How did we choose these three candidates? 53

3.5 Synthesis of Tb.iphth complex 54

3.6 Part 1: Experiment for Investigating the Energy Transfer between Eu.NMM and Tb.iphth. 56

3.7 Part 2: Experiment for Competitive Binding Assay of EuNMM and Tb.iphth with G6P 64

3.8 FBP for Competitive Binding 72

3.9 Gd.NMM for Competitive Binding with G6P 75

3.10 Comparative Binding Behaviour of FBP and G6P in the Gd.NMM–Tb.iphth System 80

3.11 Conclusion 84

3.12 References 87

Chapter 4 The exploration of a new Glucose Imaging Probe - Synthesis of a new kinetically stable 7- and 8-coordinate heterometallic complexes and their interactions with anionic guests 88

4.1 Background and Rationale 88

4.2 Synthesis of a new Tb-Eu bimetallic complex 92

4.2.1 Azidobenzyl-DO3A complex 93

4.2.2 Propargyl-DO3A complex 101

4.2.3 Click Chemistry to access Heterometallic Arrays 103

4.3 Photophysical Properties 106

4.4 Binding Studies with Anionic Guests 110
4.4.1 Interaction with Glucose-6-Phosphate 110
4.5 Coordination and Structural Characterisation 117
4.6 Conclusion 119
4.7 References 120
Chapter 5 Summary 121
Chapter 6 Experimental 123
6.1 Synthesis and chemical characterisation 123
6.2 Photophysics Experimental 149
6.3 References 152

Abstract

Lanthanide complexes possess unique photophysical properties, making them attractive candidates for responsive imaging probes. This thesis explores how coordination environment, self-assembly, and intermetallic energy transfer can be exploited in multinuclear lanthanide complexes to achieve luminescent responses, particularly on sensing anionic glycolytic intermediates.

Binuclear nitro-m-xylyl lanthanide complexes (Ln.NMM) were first investigated as kinetically stable platforms for binding dianionic guests via self-assembly. Their interactions with phosphorylated glycolysis products, including glucose-6-phosphate and fructose-1,6-bisphosphate, were characterised using luminescence spectroscopy and paramagnetic NMR techniques. These studies demonstrate that guest binding perturbs the local coordination environment, leading to measurable changes in lanthanide emission behaviour.

Building on this foundation, competitive binding and energy-transfer processes were examined in heterometallic systems formed through self-assembly between homometallic binuclear complexes (Eu.NMM) and mononuclear isophthalate lanthanide complex (Tb.iphth). The results reveal that guest binding can control intermetallic communication and modulate Eu–Tb energy-transfer pathways, enabling ratiometric luminescence responses to biologically relevant anions.

Finally, a new class of heterometallic europium–terbium complexes (TbEu complex & EuTb complex) incorporating both seven- and eight-coordinate metal centres was designed and synthesised using click chemistry. Photophysical and binding studies show that glucose-6-

phosphate binding induces changes in terbium emission intensity, consistent with reduced quenching and altered energy transfer.

Overall, this work demonstrates how coordination environment, ligand architecture, and multinuclear assembly can be used to design responsive lanthanide systems. The insights gained provide a framework for developing next-generation luminescent probes for metabolic sensing and bioimaging applications.

Acknowledgements

Firstly, I would like to thank my mum and dad, who supported me selflessly throughout this DPhil project and were always there for me, day and night, providing me with a safe and supportive home.

I would like to thank my professor Steve, who gave me this precious opportunity to study in Oxford. Without you, I cannot imagine where I would be today. When I had lots of self-doubt, it was you to give me hope and confidence again and again.

I would like to thank Margaret, who is my spiritual guide, who taught me Love. When I had lots of troubles and was in a dark hole, it was you who dragged me out of it. You brought me to this new life knowing Jesus and taught me to face life without fear.

I would like to thank Lei and Feige for the great support they gave me over the past two years. Without you, I would have felt deeply alone during my most difficult time in Oxford. You are like an elder brother and sister to me, offering warmth, kindness, and wise advice.

I would like to thank my uncle, Dr Wu Zhiheng, and my aunt, Xiao Fengjuan. When I felt lost in my project, it was your guidance and trust in me that taught me how to navigate and survive the DPhil journey.

I would like to thank my colleagues and friends in Oxford — Carlson, Agnes, Kezi, Grace, Cameron, Deborah, Xuejian, Tamar, Euan, Andrew, and Matt. We solved problems together and shared our successes.

For a long time, I believed I was walking this journey alone. In looking back, I now realise that so many people were standing behind me, supporting me every step of the way.

"Never Give Up. Love is the Key. Love is the Solution.

Abbreviations

a.u.	Arbitrary units
br	Broad
CO	Carbon monoxide
CEST	Chemical Exchange Saturation Transfer
d	Doublet
DCM	Dichloromethane
DMSO	Dimethyl sulfoxide
DO3A	1,4,7,10-Tetraazacyclododecane-1,4,7-triacetic acid
DO3A-tBu	Tri-tert-butyl 1,4,7,10-tetraazacyclododecane-1,4,7-triacetate hydrobromide salt
DOTA	1,4,7,10-Tetraazacyclododecane-1,4,7,10-tetraacetic acid
δ	Chemical shift
ESI-MS	Electrospray ionisation mass spectrometry
Eu	Europium
FBP	Fructose-1,6-bisphosphate
Gd	Gadolinium
G6P	Glucose-6-phosphate
HEPES	4-(2-Hydroxyethyl)-1-piperazineethanesulfonic acid
IR	Infrared
Ln	Lanthanide
λ	Wavelength
m	Multiplet
M	Molar concentration (mol L^{-1})
MALDI	Matrix-assisted laser desorption/ionisation
MRI	Magnetic resonance imaging
MS	Mass spectrometry
m/z	Mass-to-charge ratio
nm	Nanometre(s)
NMR	Nuclear magnetic resonance

ppm	Parts per million
s	Singlet
SAP	Square antiprismatic
τ	Luminescence lifetime
TFA	Trifluoroacetic acid
TSAP	Twisted square antiprismatic
UV	Ultraviolet
v/v	Volume per volume

Chapter 1 Introduction

This thesis will focus on the coordination behaviour and energy transfer of multinuclear lanthanide complexes. The inert lanthanide chelators are used to maintain the high purity of heterometallic samples. There are three separate projects in this work.

General Aspects of Lanthanides

The lanthanide elements are elements 57 to 71 on the periodic table. The chemical properties of lanthanides are highly similar, which mainly results from their unique electronic structure, especially the characteristics of the 4f orbitals.

Because of its electronic structure and bonding character, the 4f orbitals are shielded by the outer $5s^2 5p^6$ electrons (xenon core), resulting in minimal overlap with the ligand orbitals.[1] Therefore, the 4f orbitals hardly participate in bonding, and the chemical bonds of lanthanide complexes are mainly ionic, with a weak covalent character.[2,3,4] Crystal field effects can be ignored because 4f electrons are not directly affected by the ligand field, unlike the d orbitals of transition metals.[5,6]

For its oxidation state and Lewis acidity, the +3 oxidation state (Ln^{3+}) is the most stable and common valence state of lanthanides in aqueous solution.[2,7] Trivalent Ln ions are hard Lewis acids and preferentially bind to Lewis basic atoms (such as O, N) (e.g. water, carboxylates, amine ligands).[2,3]

For its coordination characteristics, the coordination number is high (8~10) because the Ln^{3+} ion radius is large and can accommodate more ligands.[2,8] The coordination geometry is mainly determined by steric hindrance rather than electronic effects (unlike transition metals, which are often affected by the ligand field stabilisation energy). Common geometric configurations include square antiprismatic, dodecahedral.[2,3]

Because the bonding is mainly electrostatic, ligand exchange is usually fast (labile complexes).[9] Strong chelating and macrocyclic ligands (such as DOTA, DO3A, shown in Figure 1.1) are required to improve the stability of the complex (especially in biomedical applications, such as MRI contrast agents).[8]



(a) (b)

Figure 1.1 Strong chelating ligands (a) DOTA and (b) DO3A.

1.1 Lanthanide Luminescence Characteristics

The lanthanides have distinctive characteristics arising from the 4f-4f transitions nature that are suitable for bioimaging probes or anion sensing.

They have wide emission wavelength coverage. Due to the electronic transition between 4f energy levels, lanthanide ions can emit light across a broad spectral range, spanning the ultraviolet, visible, and near-infrared regions.[3,10,11]

Lanthanides have long luminescence lifetimes (μs to ms).[12] Due to partially forbidden 4f-4f transitions, lanthanide complexes exhibit luminescence lifetimes 1000× longer than organic dyes (1–10 ns).[13] This character can be used for the time-gated detection: applying a microsecond delay between excitation and emission allows complete suppression of short-lived autofluorescence and scattering noise.[14] It also has a superior signal-to-noise ratio, which enables high-contrast imaging in complex biological media, such as blood and tissues.[15]

Lanthanides have sharp emission peaks. The 4f-4f transitions in lanthanides are partially forbidden, resulting in low transition probabilities and highly narrow, sharp emission lines. Since outer electrons shield 4f orbitals, their emissions serve as spectral fingerprints, largely unaffected by the surrounding matrix.[12]

Sharp emission peaks also mean a narrow bandwidth. They will have line-like emission spectra, unlike the broad peaks of organic dyes.[12] This characteristic allows multiplex detection, which resolves multiple lanthanide signals such as Eu^{3+}, Sm^{3+}, Dy^{3+} without crosstalk between species.[16] It is also valuable for precision quantification, reducing background interference for accurate data analysis.[17]

The 4f orbitals experience minimal influence from the ligand (crystal) field, ensuring that the emission wavelength and spectral shape remain nearly constant across different environments.[3] Unlike organic dyes that degrade under prolonged illumination, lanthanide complexes resist photobleaching.[18] This character allows the long-term live-cell tracking, which is ideal for dynamic processes.[19]

Lanthanides have small Stokes shifts. The shielding effect of outer orbitals ensures that the coordination geometry remains nearly unchanged between the ground and excited states. In other words, there is minimal structural relaxation upon excitation, leading to minimal energy loss between absorption and emission.[3] This character can eliminate self-absorption, preventing signal attenuation caused by the reabsorption of emitted light. It can also allow multiplexing compatibility, which enables simultaneous multi-target detection with minimal spectral overlap.[20]

1.2 Lanthanide Photophysics

The luminescence observed in lanthanides is due to the electronic transitions within the $^{2S+1}L_J$ states in the 4f orbitals. Each lanthanide element has its own absorption and emission spectra.[21-24]

Lanthanide ions have spectra containing a great number of sharp spectral lines compared with the d transition metals (Figure 1.2).[25] This is because each 4f electronic configuration corresponds to a large number of electronic microstates. Furthermore, the positions of lanthanide emission peaks are generally insensitive to ligand type, whereas their relative intensities vary significantly with the local environment.

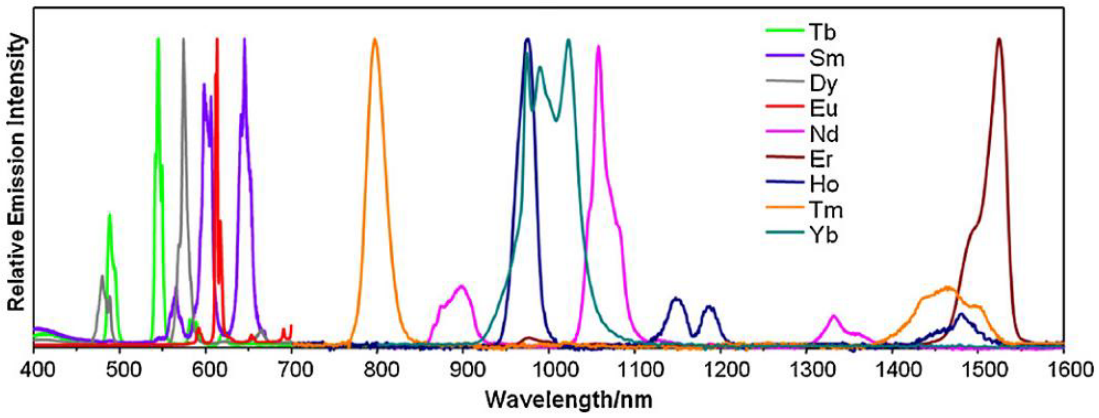


Figure 1.2 Emission spectra of luminescent lanthanide complexes in solution.[25]

Taking europium(III) as an example, its emission peaks originate from the transition from the excited state $^5D_0$ to the ^7F_J ($\Delta J = 0–6$).[26] At room temperature, emission from higher excited states ($^5D_1$, $^5D_2$, $^5D_3$) is occasionally observed in europium complex, although these excited states are efficiently quenched through nonradiative decay processes. In other words, no peaks are generated from these excited states. The ligand field influence on Ln^{3+} ions is relatively weak, but it can still break the degeneracy of the electronic state, leading to the splitting of the energy level into different sublevels.[27] This is called Stark splitting into mj sublevels. Stark splitting allows spectroscopic access to subtle changes in local coordination geometry without altering emission energies.[6]

Some transitions are called hypersensitive transitions, with the $\Delta J = 2$ transition in Eu^{3+} being the most typical. These transitions are extremely sensitive to the coordination environment and local symmetry of the metal centre; therefore, their spectral changes are often used as spectroscopic probes for structural changes, coordination or binding events, and pH changes.[31-33] For complexed lanthanides, intense hypersensitive transitions are obtained compared to lanthanide aquo ion.

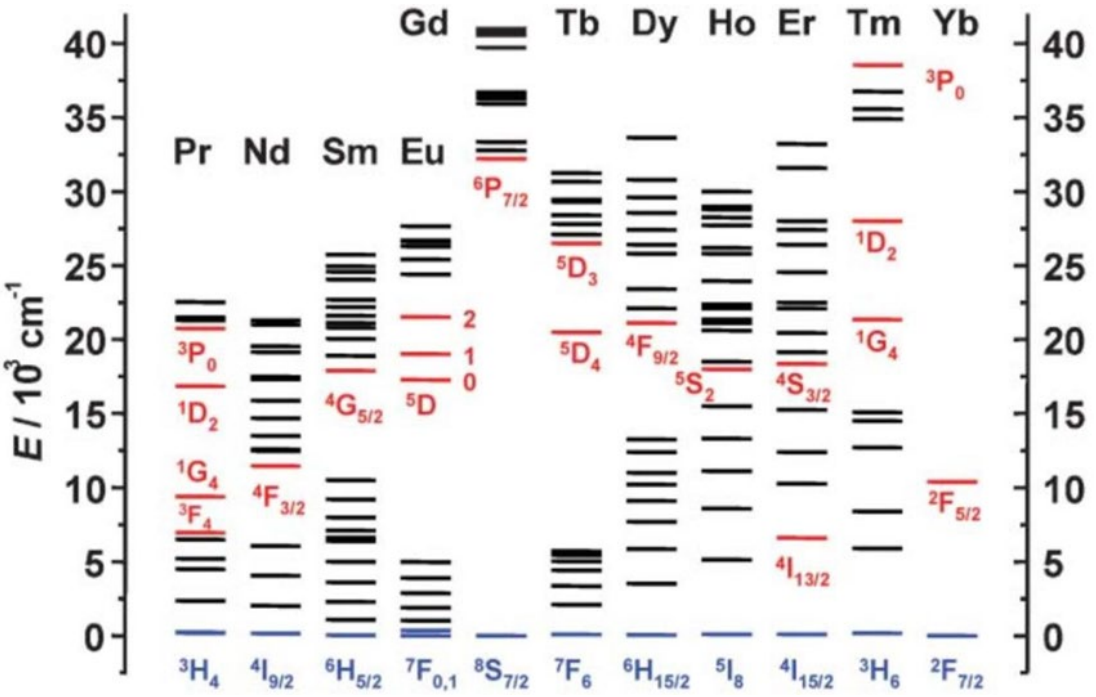


Figure 1.3 Energy levels for lanthanide ions in aqua. Key levels that are luminescent (red).[28-30]

1.3 Antenna effect

The antenna effect is the luminescence sensitization of lanthanide through chromophores, which was first reported by Weissmann in 1942.[34] The antenna is usually an organic chromophore, which absorbs incident light and transfers the energy to the lanthanide centre (Figure 1-4).[35] With this energy transfer process, stronger luminescence will be achieved than the lanthanide ion absorbing light energy directly via f–f transitions by itself. A significant Stokes shift usually exists between the absorption of the chromophore and the emission of the lanthanide ion. This results in a considerable reduction of background interference and self-absorption, providing the distinct advantages of such applications in detection and analysis.

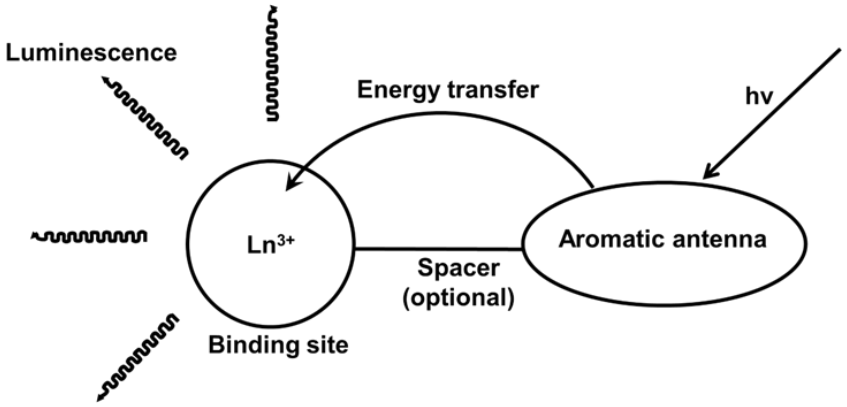


Figure 1.4 Illustration of the antenna effect.[35]

The process involves four steps (Figure 1.5)[36]: Step one, the aromatic chromophore acts as a light-absorbing antenna, strongly harvesting incident photons. Step two, the chromophore is excited to a singlet excited state (S_1). Step three, the chromophore is rapidly transferred to a triplet excited state (T_1) via the intersystem crossing (ISC). Spin-orbit coupling significantly improves the intersystem crossing (ISC) process, especially if heavy atoms are present in the molecule. Step four, The long-lived triplet state transfers the energy to the lanthanide ion, populating its emissive excited state—such as the $^5D_4$ level in terbium(III) or the $^5D_0$ level in europium(III).

To achieve efficient sensitization, several criteria apply: the chromophore should be structurally rigid to suppress the non-radiative vibrational relaxation and energy loss.[3] The triplet excited state of the chromophore should be approximately 1500 cm^{-1} higher than the emissive level of the lanthanide ion. This energy gap can form an effective spectral overlap in the system for energy transfer, and it can suppress the thermally activated back energy transfer.[37]

Moreover, luminescence is sensitive to quenching; therefore, interactions with high-energy vibrational oscillators—such as O–H in water molecules—should be avoided.[7] This mechanism is the foundation for designing antennas for Eu^{3+}/Tb^{3+} systems and is widely applied in ratiometric sensing and bioanalytical platforms.

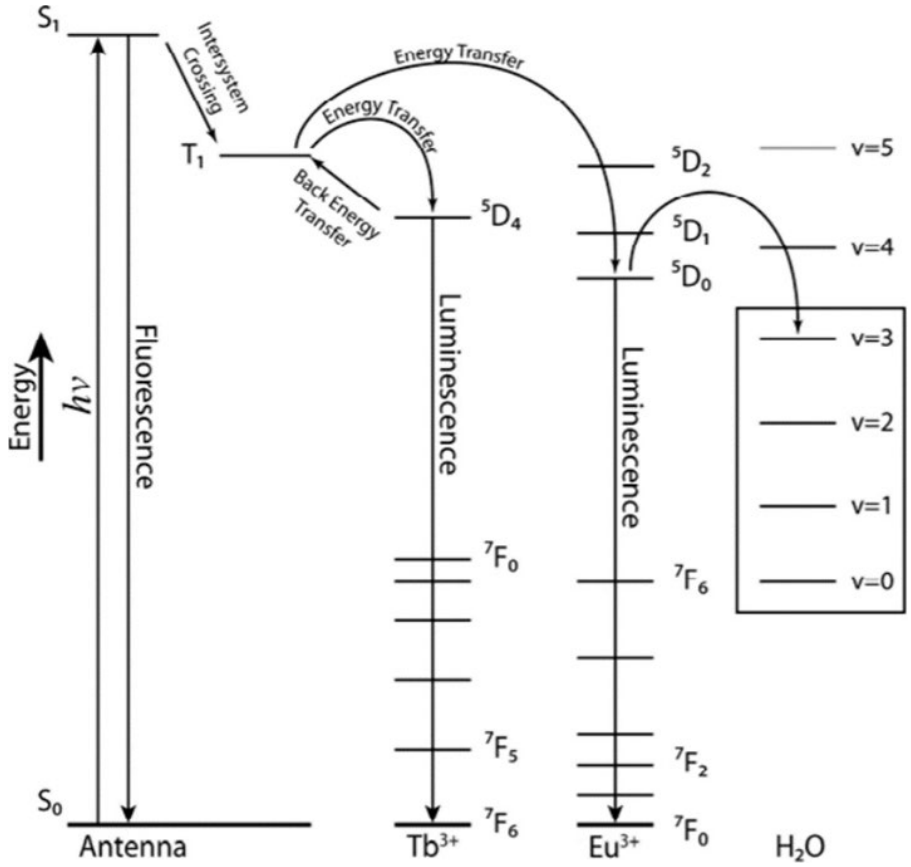


Figure 1.5 Diagram[36] showing the mechanisms of energy transfer involved in sensitisation of Tb(III) and Eu(III) emission. The vibrational energy levels of water are also shown, to illustrate quenching.

Luminescence in lanthanide complexes is critically dependent on efficient energy transfer from organic chromophores (antenna effect) to the metal centre.[6] Solvent quenching and non-

radiative decay pathways remain major challenges, necessitating careful ligand design to shield the metal ion.[7] Recent studies have demonstrated that binuclear lanthanide complexes can enhance luminescence through intermetallic communication, enabling applications in anion sensing and dual-modal imaging. [8,9]

1.4 Mechanisms of Energy Transfer

Dexter energy transfer is achieved through a two-electron exchange mechanism between the donor and acceptor, requiring direct overlap of the orbitals. Its efficiency decreases exponentially with distance (e^{-r}), and it is effective over very short distances (~0.5 Å) . For lanthanides, through ligand-coupling superexchange, a larger distance can be approached (~20 Å). Dexter transfer is short-range (< 1 nm) and overlap-dependent, so it is generally suppressed in lanthanide systems unless mediated by ligands.[38,39]

Förster resonance energy transfer (FRET) is a long-range (typically 1–10 nm) energy transfer mechanism achieved via through-space dipole-dipole coupling, which does not require orbital overlap. Its efficiency exhibits an inverse distance dependence (r^{-6}). This mechanism depends on good spectral overlap between donor emission and acceptor absorption, and is particularly important in lanthanide–lanthanide energy transfer.[40]

1.5 Quenching

Quenching refers to any process that reduces the intensity and/or lifetime of lanthanide luminescence by introducing non-radiative deactivation pathways that compete with radiative emission.[41] In lanthanide complexes, quenching is dominated by vibrational coupling to high-

energy oscillators (O–H, N–H) and by interactions with external quenchers (O_2, solvent, additives).[7]

The degree of O-H bond vibrations is typically assessed using the *q* value.[42-45] The *q* value is the number of solvent molecules (usually water) directly coordinated to a lanthanide ion in its first coordination sphere. In other words, *q* shows how many O–H oscillators are close enough to the metal centre to directly quench lanthanide luminescence. Each coordinated water molecule introduces O–H oscillators that provide efficient non-radiative decay pathways. Therefore, higher *q* means stronger vibrational quenching; lower *q* means longer lifetime and higher luminescence efficiency. This makes *q* a direct structural–photophysical parameter.

To calculate the *q* value (inner-sphere hydration number), the key is to measure the luminescence lifetimes in H_2O and D_2O (τ_{H_2O} and τ_{D_2O}). The lanthanide-specific modified Horrocks equation (Equation 1.2) can be used to calculate this number.[42-45]

$$q = A\left(\frac{1}{\tau_{H2O}} - \frac{1}{\tau_{D2O}} - B\right) \quad (1.1)$$

Equation 1.1 General form of lanthanide-specific modified Horrocks equation.[42] *(A and B depend on the specific lanthanide ion).*

$$q_{Eu} = 1.2\left(\frac{1}{\tau_{H2O}} - \frac{1}{\tau_{D2O}} - 0.25 - 0.075x\right) \quad (1.2)$$

Equation 1.2 Europium-specific modified Horrocks equation. (x=number of close diffusing N-H oscillators.)

$$q_{Tb} = 5\left(\frac{1}{\tau_{H2O}} - \frac{1}{\tau_{D2O}} - 0.06\right) \quad (1.3)$$

Equation 1.3 Terbium-specific modified Horrocks equation.

1.6 Stability and the macrocyclic effect

Lanthanide complexes have garnered significant attention due to their unique photophysical properties and coordination chemistry. The Ln^{3+} ions, with their partially filled 4f orbitals, exhibit characteristic luminescence arising from intra-4f transitions, which are shielded from environmental perturbations, enabling high quantum yields and long lifetimes.[3] However, their applications are often limited by poor water solubility and low kinetic stability.

Coordination chemistry plays a pivotal role in tuning the properties of lanthanide complexes. Lanthanides typically adopt coordination numbers of 8–9, with geometries dictated by steric factors rather than electronic effects.[2] Macrocyclic ligands like DOTA (1,4,7,10-tetraazacyclododecane-1,4,7,10-tetraacetic acid) and its derivative DO3A have been extensively explored due to their ability to enforce preorganized, kinetically inert complexes through the macrocyclic effect.[46] For instance, $[Gd(DOTA)]^-$ exhibits exceptional kinetic and thermodynamic stability against demetallation, making it a cornerstone in MRI contrast agents.[47]

1.7 Isomerism

The geometrical isomerism derived from DOTA and DO3A ligands has two interchangeable coordination geometries. These geometries are known as the square antiprism (SAP) and the twisted square antiprism (TSAP). The lanthanide ion is in a coordination geometry of nine that involves four carboxylate oxygen atoms and four nitrogen atoms, which act as ligands, and one molecule of water. The donor set forms two square faces, the N_4 plane and the O_4 plane, and the Ln^{3+} sits between them. The main difference between the SAP and TSAP arrangements is

in the angle by which the planes of the nitrogen and oxygen donors are twisted relative to one another. This twisting angle is about 40 degrees for SAP and 30 degrees for TSAP.[48,49]

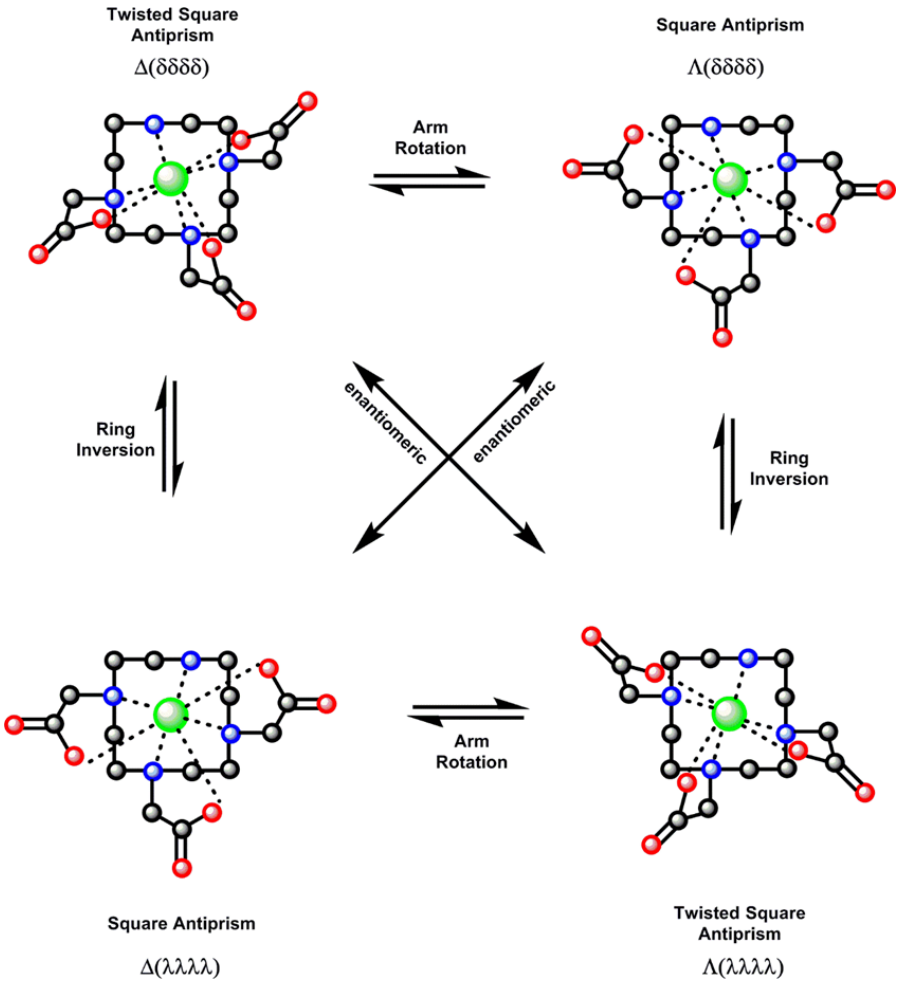


Figure 1.6. SAP and TSAP isomers of DO3A complex.[50]

Despite minor geometric differences, these two isomers exhibit distinct coordination kinetics. Compared to SAP, the TSAP configuration has a more open coordination environment, leading to a significantly faster exchange rate for its apical water molecule. Faster water exchange leads to more O–H vibrational quenching, directly influencing luminescence quenching and relaxation.

The SAP and TSAP can interconvert via pendant arm rotation and ring inversion. The rate of the interconversion is dependent on the ligand's structure. DO3A has a lower interconversion energy barrier compared with DOTA because it has fewer acetate arms. So DO3A undergoes rapid interconversion on the NMR timescale, leading to broad peaks. DOTA has a slower interconversion rate, leading to sharper peaks.[51,52]

The preference for TSAP or SAP seems to be largely determined by the lanthanide ion's ionic radius. The larger, earlier members of the lanthanide series tend to stabilise the more space-demanding TSAP configuration, while the smaller, later members prefer the more compact SAP configuration. This is in agreement with the lanthanide contraction.[53]

These configurations in paramagnetic Eu(III) complexes can be distinguished by ^{1}H NMR chemical shift. Signals in the range of 15 to 20 ppm are linked to the TSAP configuration; those in the range of 30 to 40 ppm are associated with the SAP configuration.[54] This shows that there is a difference in the proton spatial distribution relative to the metal's magnetic axis. Therefore, understanding the SAP–TSAP configuration equilibrium provides an important structural basis for explaining the solution structure, kinetic behaviour, and related photophysical properties of DOTA/DO3A lanthanides.

1.8 Self-Assembly

The spontaneous organization of lanthanide ions (Ln^{3+}) with ligands or guests into a non-covalent system is called self-assembly. The lanthanides have a flexible coordination number, which is useful in this process, and the main driving force to self-assembly is electrostatic.[55,56]

In our group, it has been reported that self-assembly can replace water molecules in coordination or introduce bridging ligands to link different metal ions. The key function of self-assembly is to change the coordination environment in a lanthanide complex. Once the structures change along with the coordination change, the luminescence behaviours of lanthanide ions will be different. These behaviours include "on/off" luminescence effects,[57] variations in lifetimes,[58] or changes in energy-transfer pathways.[59] It is reported that lanthanide complexes can self-assemble with different anionic groups, such as carboxylates,[60] phosphates.[61] In short, self-assembly is useful in designing responsive luminescent probes, chemical probes, and functional supramolecular structures.

Gunnlaugsson and colleagues explored the self-assembly behaviour of p-xylyl terbium DO3A-trisamide complex (Figure 1.20) in solution with various dicarboxylate guests.[58] It is reported that the terbium's luminescence intensity and lifetime were influenced by the presence of dicarboxylate guests.

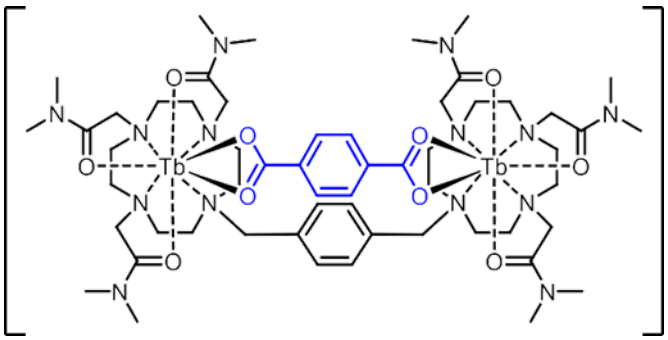


Figure 1.20 The bis-p-xylyl DO3AM Tb(III) complex self-assembles with dicarboxylate guest.[58]

The Faulkner group later investigated similar behaviour. The m-xylyl-based binuclear

lanthanide complexes (Ln. NMM) can self-assemble with the dianionic guests. In 2011, Tilney *et al.* reported that an amino-m-xylyl complex showed selective binding to isophthalate over other aryldicarboxylates (Figure 1.21).[60]

This work was extended by Sørensen *et al.* in 2015, who examined phosphate binding to m-xylyl complexes.[62] They found that phosphate binds strongly to the europium complex of the nitro-substituted derivative, but not to that of the amino-substituted analogue.

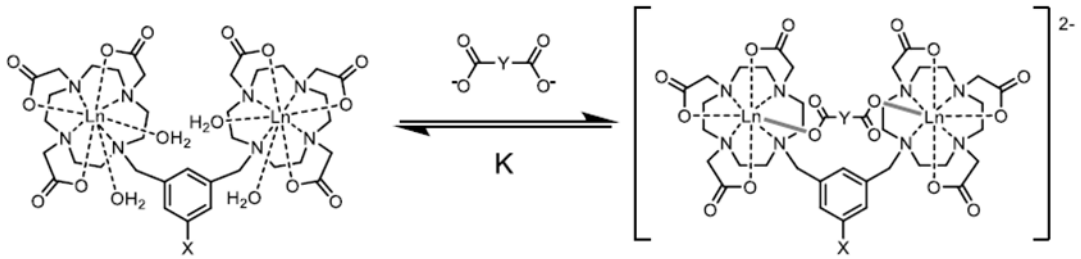


Figure 1.21 Xylyl-based binuclear lanthanide complexes (Ln. NMM) self-assemble with the dianionic guests where X = NO_2, NH_2; Y = aromatic ring.[60]

1.9 NMR

For a long time, NMR spectroscopy has exploited paramagnetic properties of lanthanides.[63,64] Shift and relaxation properties, specific to lanthanides, may affect NMR parameters of nearby nuclei. For biomedical applications, NMR probe development is widely applied, including shift reagents for *in vivo* magnetic resonance spectroscopy and chiral lanthanide shift reagents for enantiomer NMR separation. The utilisation of lanthanide-induced shifts and the acceleration of relaxation rates have been widely reviewed.[65]

A. Lanthanide-induced shifts (LIS)

For the ligand's nuclei, coordinated to an Ln^{3+} ion, three factors contribute to the LIS (Δ); contact (Δc), diamagnetic (Δd), and pseudo-contact shift (Δp) (eq.).[66]

$$\Delta = \Delta d + \Delta c + \Delta p$$

Δd shifts are usually small, and often they are not considered except for atoms that have direct coordination to Ln^{3+} ions. Unpaired electron density, through-bond transmission at the Ln^{3+} ion to the concerned nucleus, results in Δc (also known as fermi) shifts. The dipolar shift or the pseudo-contact contribution arises when the magnetic moment of the unpaired electrons of the Ln^{3+} interacts through space.

B. Applications in aqueous media

Spectral simplification and resolution enhancement through the utilisation of lanthanide complexes, as shift reagents in NMR, have attracted much interest among researchers.[67,68] Lanthanide-induced shifts are widely used in determining the solution structures of lanthanide chelates, through angular and distance information.[69] The majority of paramagnetic probes in biological research for deriving useful structural information on amino acids or proteins, are lanthanide complexes.[63]

1.10 Glycolysis products sensing

For many organisms, glucose is a main source of energy, with glucose uptake being an important mechanistic and biological process. Glucose transport occurs across the cell membrane via phosphorylation processes, helping it to easily get trapped. This is performed by

intracellular hexose kinases and a family of glucose transporters (GLUT).[70]

The measurement of glucose uptake is key to several biological processes. When compared to normal tissue, tumours are heavily dependent on glycolytic processes.[71] Changes in the rate of metabolism can be reflected in changes in glucose uptake, as specific processes generate changes in glucose uptake levels. Glucose uptake measurement in cancer cells helps monitor glucose transporter expression as well as identifying inhibitors that prevent glucose transportation. When fats and muscle cells are stimulated by insulin, alterations in glucose uptake reflect changes in GLUT4 translocation.[72] Additionally, glucose measurement also tracks the transformation of certain cell types from one stage to another, particularly immunologically relevant cells.

For many years, the radio-labelled analogue [^{3}H]2-Deoxy-D-glucose (^{3}H-2DG), in combination with the measurement of [^{3}H]2-Deoxy-D-glucose-6-phosphate (^{3}H-2DG6P), has been considered a gold standard in the measurement of glucose uptake.[73] This method works well; but it is very sensitive and requires multiple wash steps. This method is not utilised in many studies, as researchers are keen to escape from the difficulties of handling and disposing radioactive materials. Commercially available non-radioactive techniques utilize non-radiolabelled 2-Deoxy-D-glucose that monitors 2-Deoxy-D-glucose-6-phosphate accumulation through the glucose-6- phosphate dehydrogenase.[74] 2-Deoxy-D-glucose-6-phosphate is oxidised by this enzyme, leading to the formation of nicotinamide adenine dinucleotide phosphate which is utilised for probe generation or fluorescence assays.

These assays are amenable for multi-cell plate formats, but they need multiple steps for

processing. The absorbance assay has a higher sensitivity due to a cyclic reaction and can therefore, detect low levels of 2DG6P. Both assays are limited as they have a small signal window, that is, the signal above no 2DG6P background.

The imaging of glycolysis metabolites requires new methods. For this reason, studying and imaging tumour growth and redox stress can be performed using glycolysis methods, while CEST methods (chemical exchange saturation transfer), such as glucoCEST image glucose production. In living organisms, there are several important fructose bisphosphates (FBPs) substrates that include fructose-1,6-bisphosphate and fructose-2,6-bisphosphate. These molecules are found in glycolysis, produced by fructose-6-phosphate phosphorylation.[75,76]

Metabolic studies led to the discovery of FBPs in eukaryotes in the 20th century, possibly the last such discovery in that century. Intracellular FBPs are important in controlling cellular glucose homeostasis; pyruvate kinase is allosterically activated by fructose-1,6-bisphosphatase.[77] Fructose-2,6-bisphosphate is both a potent inhibitor and activator of fructose-1,6-bisphosphatase[78] and phosphofructokinase[79], respectively.

Therefore, glycolytic/gluconeogenic flux FBPs are significantly regulated by FBPs to provide a switching mechanism between the two opposing carbohydrate metabolism pathways. The binding and sequestration of ferrous iron is also related to FBPs.[80] The treatment and diagnosis of some diseases also involves FBP, including some cancers,[81] diabetes[82] and liver injury.[83] FBPs therefore play important roles in clinical diagnoses, pharmaceutical analysis and biochemical studies.

Currently, several methods can assay FBPs. Enzymatic methods are the most common and include: spectrophotometric phosphofructokinase-DNPH techniques,[84,85] colorimetric aldolase-DNPH methods,[86,87] and chromatography coupled enzymatic methods.[88] Enzymatic techniques are often difficult to perform, which may be attributed to alterations in factors such as pH and effecters. However, these methods are very sensitive. Radioactive labelled competitive binding assays are sensitive,[88] but may be problematic due to sensitive enzymes. Such new assay methods must be developed for FBPs.

1.11 Aim

The aim of this thesis was to design, synthesise, and study responsive lanthanide coordination complexes for the sensing of on glycolysis-related molecules, such as glucose-6-phosphate and fructose-1,6-bisphosphate. This work focused on homo- and hetero-metallic europium(III) and terbium(III) systems. These systems were designed to exhibit responsive luminescence behaviour through changes in supramolecular self-assembly and control of the energy-transfer pathways that lead to luminescence and non-radiative decay. This thesis combined synthetic chemistry, luminescence spectroscopy, and binding studies. These systems may have future applications in metabolic imaging.

1.12 References

(1) Gschneidner, K. A.; Eyring, L.; Lander, G. H.; Choppin, G. R. *Handbook on the Physics and Chemistry of Rare Earths*; Elsevier, 1994.

(2) Cotton, S. *Lanthanide and Actinide Chemistry*; John Wiley & Sons, 2006.

(3) Bünzli, J.-C. G.; Piguet, C. Taking Advantage of Luminescent Lanthanide Ions. *Chemical Society Reviews* **2005**, *34* (12), 1048-1077.

(4) Parker, D.; Dickins, R. S.; Puschmann, H.; Crossland, C.; Howard, J. A. Being Excited by Lanthanide Coordination Complexes: Aqua Species, Chirality, Excited-State Chemistry, and Exchange Dynamics. *Chem. Rev.* **2002**, *102* (6), 1977-2010.

(5) Jørgensen, C. K. *Modern Aspects of Ligand Field Theory*; North-Holland Publishing, 1971.

(6) Liu, G.; Jacquier, B. *Spectroscopic Properties of Rare Earths in Optical Materials*; Springer Science & Business Media, 2006.

(7) (a) Kaltsoyannis, N.; Scott, P. *The f Elements*; Oxford University Press, 1999. (b) Beeby, A.; Clarkson, I. M.; Dickins, R. S.; Faulkner, S.; Parker, D.; Royle, L.; De Sousa, A. S.; Williams, J. G.; Woods, M. Non-Radiative Deactivation of the Excited States of Europium, Terbium and Ytterbium Complexes by OH, NH and CH Oscillators: A Study in H_2O and D_2O. *J. Chem. Soc., Perkin Trans. 2* **1999**, (3), 493-504.

(8) Bünzli, J.-C. G. On the Design of Highly Luminescent Lanthanide Complexes. *Coord. Chem. Rev.* **2015**, *293*, 19-47.

(9) Caravan, P.; Ellison, J. J.; McMurry, T. J.; Lauffer, R. B. Gadolinium(III) Chelates as MRI Contrast Agents: Structure, Dynamics, and Applications. *Chem. Rev.* **1999**, *99* (9), 2293-2352.

(10) Hasegawa, Y.; Nakanishi, T. Luminescent Lanthanide Coordination Polymers for Photonic Applications. *Rsc Adv.* **2015**, *5* (1), 338-353.

(11) Auzel, F. Upconversion and Anti-Stokes Processes with f and d Ions in Solids. *Chem. Rev.* **2004**, *104* (1), 139-174.

(12) Bünzli, J.-C. G. Lanthanide Luminescence for Biomedical Analyses and Imaging. *Chem. Rev.* **2010**, *110* (5), 2729-2755.

(13) Lakowicz, J. R. *Principles of Fluorescence Spectroscopy*; Springer, 2006.

(14) Hemmilä, I.; Laitala, V. Progress in Lanthanides as Luminescent Probes. *J. Fluoresc.* **2005**, *15* (4), 529-542.

(15) Yuan, J.; Wang, G. Lanthanide-Based Luminescence Probes and Time-Resolved Luminescence Bioassays. *TRAC-Trends Anal. Chem.* **2006**, *25* (5), 490-500.

(16) Montgomery, C. P.; Murray, B. S.; New, E. J.; Pal, R.; Parker, D. Cell-Penetrating Metal Complex Optical Probes: Targeted and Responsive Systems Based on Lanthanide Luminescence. *Acc. Chem. Res.* **2009**, *42* (7), 925-937.

(17) Hagan, A. K.; Zuchner, T. Lanthanide-Based Time-Resolved Luminescence Immunoassays. *Anal. Bioanal. Chem.* **2011**, *400* (9), 2847-2864.

(18) Zheng, W.; Huang, P.; Tu, D.; Ma, E.; Zhu, H.; Chen, X. Lanthanide-Doped Upconversion Nano-Bioprobes: Electronic Structures, Optical Properties, and Biodetection. *Chem. Soc. Rev.* **2015**, *44* (6), 1379-1415.

(19) Chen, G.; Qiu, H.; Prasad, P. N.; Chen, X. Upconversion Nanoparticles: Design, Nanochemistry, and Applications in Theranostics. *Chem. Rev.* **2014**, *114* (10), 5161-5214.

(20) Bünzli, J.-C. G. Lanthanide Light for Biology and Medical Diagnosis. *J. Lumin.* **2016**, *170*, 866-878.

(21) Nič, M.; Jirát, J.; Košata, B.; Jenkins, A.; McNaught, A. *IUPAC Compendium of Chemical Terminology*; IUPAC, 2009.

(22) Van Grieken, R.; De Bruin, M. Nomenclature for Radioanalytical Chemistry (IUPAC Recommendations 1994). *Pure Appl. Chem.* **1994**, *66* (12), 2513-2526.

(23) Melhuish, W. VI: Molecular Luminescence Spectroscopy. *Pure Appl. Chem.* **1984**, *56* (2), 231-245.

(24) Verhoeven, J. Glossary of Terms used in Photochemistry (IUPAC Recommendations 1996). *Pure Appl. Chem.* **1996**, *68* (12), 2223-2286.

(25) (a) Shriver, D. F.; Atkins, P. W.; Overton, T. L.; Rourke, J. P.; Weller, M. T.; Armstrong, F. *Inorganic Chemistry; ed.; 2006.*; Oxford University Press, 2006. (b) Martinić, I.; Eliseeva, S. V.; Petoud, S. Near-Infrared Emitting Probes for Biological Imaging: Organic Fluorophores, Quantum Dots, Fluorescent Proteins, Lanthanide(III) Complexes and Nanomaterials. *J. Lumin.* **2017**, *189*, 19-43.

(26) Binnemans, K. Interpretation of Europium (III) Spectra. *Coord. Chem. Rev.* **2015**, *295*, 1-45.

(27) Hänninen, P.; Härmä, H. *Lanthanide Luminescence: Photophysical, Analytical and Biological Aspects*; Springer Science & Business Media, 2011.

(28) Carnall, W.; Fields, P.; Rajnak, K. Electronic Energy Levels of the Trivalent Lanthanide Aquo Ions. IV. Eu^{3+}. *J. Chem. Phys.* **1968**, *49* (10), 4450-4455.

(29) Carnall, W.; Fields, P.; Rajnak, K. Electronic Energy Levels in the Trivalent Lanthanide Aquo Ions. I. Pr^{3+}, Nd^{3+}, Pm^{3+}, Sm^{3+}, Dy^{3+}, Ho^{3+}, Er^{3+}, and Tm^{3+}. *J. Chem. Phys.* **1968**, *49* (10), 4424-4442.

(30) Carnall, W.; Fields, P.; Rajnak, K. Electronic Energy Levels of the Trivalent Lanthanide Aquo Ions. II. Gd^{3+}. *J. Chem. Phys.* **1968**, *49* (10), 4443-4446.

(31) Jørgensen, C. K.; Judd, B. Hypersensitive Pseudoquadrupole Transitions in Lanthanides. *Mol. Phys.* **1964**, *8* (3), 281-290.

(32) Judd, B. Hypersensitive Transitions in Rare-Earth Ions. *J. Chem. Phys.* **1965**, *44*, 839.

(33) Mason, S.; Peacock, R.; Stewart, B. Dynamic Coupling Contributions to the Intensity of Hypersensitive Lanthanide Transitions. *Chem. Phys. Lett.* **1974**, *29* (2), 149-153.

(34) Weissman, S. Intramolecular Energy Transfer the Fluorescence of Complexes of Europium. *J. Chem. Phys.* **1942**, *10* (4), 214-217.

(35) Alpha, B.; Ballardini, R.; Balzani, V.; Lehn, J. M.; Perathoner, S.; Sabbatini, N. Antenna Effect in Luminescent Lanthanide Cryptates: A Photophysical Study. *Photochem. Photobiol.* **1990**, *52* (2), 299-306.

(36) Orcutt, K. M.; Jones, W. S.; McDonald, A.; Schrock, D.; Wallace, K. J. A Lanthanide-Based Chemosensor for Bioavailable Fe^{3+} Using a Fluorescent Siderophore: An Assay Displacement Approach. *Sensors* **2010**, *10* (2), 1326-1337.

(37) Parker, D. Luminescent Lanthanide Sensors for pH, pO_2 and Selected Anions. *Coord. Chem. Rev.* **2000**, *205* (1), 109-130.

(38) Dexter, D. L. A Theory of Sensitized Luminescence in Solids. *J. Chem. Phys.* **1953**, *21* (5), 836-850.

(39) Lazarides, T.; Sykes, D.; Faulkner, S.; Barbieri, A.; Ward, M. D. On the Mechanism of d‐f Energy Transfer in RuII/LnIII and OsII/LnIII Dyads: Dexter‐Type Energy Transfer Over a Distance of 20 Å. *Chem. - Eur. J.* **2008**, *14* (30), 9389-9399.

(40) Főrster, T. 10th Spiers Memorial Lecture. Transfer mechanisms of electronic excitation. *Faraday Discuss.* **1959**, *27*, 7-17.

(41) Acuña, A.; Adam, W.; Amat, F.; Armesto, D.; Atvars, T.; Bard, A.; Bill, E.; Björn, L.; Bohne, C.; Bolton, J. Glossary of Terms used in Photochemistry. *Pure Appl. Chem.* **2007**, *79* (3), 293-465.

(42) Beeby, A.; Clarkson, I. M.; Dickins, R. S.; Faulkner, S.; Parker, D.; Royle, L.; De Sousa, A. S.; Williams, J. G.; Woods, M. Non-radiative deactivation of the excited states of europium, terbium and ytterbium complexes by proximate energy-matched OH, NH and CH oscillators:

an improved luminescence method for establishing solution hydration states. *J. Chem. Soc., Perkin Trans. 2* **1999**, (3), 493-504.

(43) Horrocks Jr, W. D.; Sudnick, D. R. Lanthanide Ion Probes of Structure in Biology. Laser-Induced Luminescence Decay Constants Provide a Direct Measure of the Number of Metal-Coordinated Water Molecules. *J. Am. Chem. Soc.* **1979**, *101* (2), 334-340.

(44) Horrocks Jr, W. D.; Sudnick, D. R. Lanthanide Ion Luminescence Probes of the Structure of Biological Macromolecules. *Acc. Chem. Res.* **1981**, *14* (12), 384-392.

(45) Supkowski, R. M.; Horrocks Jr, W. D. On the Determination of the Number of Water Molecules, q, Coordinated to Europium (III) Ions in Solution from Luminescence Decay Lifetimes. *Inorganica Chim. Acta* **2002**, *340*, 44-48.

(46) Woods, M.; Sherry, A. D. Lanthanide Macrocyclic Complexes: Stability, Dynamics, and Applications. *Chem. Soc. Rev.* **2003**, *32*, 190-198.

(47) Aime, S.; Caravan, P. Biodistribution of Gadolinium-Based Contrast Agents, Including Gadolinium Deposition. *J. Magn. Reson. Imaging* **2009**, *30* (6), 1259-1267.

(48) Parker, D. Excitement in f Block: Structure, Dynamics and Function of Nine-Coordinate Chiral Lanthanide Complexes in Aqueous Media. *Chem. Soc. Rev.* **2004**, *33* (3), 156-165.

(49) Aime, S.; Barge, A.; Botta, M.; De Sousa, A. S.; Parker, D. Direct NMR Spectroscopic Observation of a Lanthanide ‐ Coordinated Water Molecule Whose Exchange Rate is Dependent on the Conformation of the Complexes. *Angew. Chem. Int. Ed.* **1998**, *37* (19), 2673-2675.

(50) Aime, S.; Botta, M.; Ermondi, G. NMR Study of Solution Structures and Dynamics of Lanthanide (III) Complexes of DOTA. *Inorg. Chem.* **1992**, *31* (21), 4291-4299.

(51) Cakić, N.; Verbić, T. Ž.; Jelić, R. M.; Platas-Iglesias, C.; Angelovski, G. Synthesis and Characterisation of Bismacrocyclic DO3A-amide Derivatives–an Approach Towards Metal-Responsive PARACEST Agents. *Dalton Trans.* **2016**, *45* (15), 6555-6565.

(52) Placidi, M. P.; Natrajan, L. S.; Sykes, D.; Kenwright, A. M.; Faulkner, S. Bimetallic Lanthanide Complexes Derived from Macrocycle‐Appended m‐Xylyl Derivatives: Synthesis and Spectroscopic Properties. *Helv. Chim. Acta* **2009**, *92* (11), 2427-2438.

(53) Aime, S.; Botta, M.; Fasano, M.; Marques, M. P. M.; Geraldes, C. F.; Pubanz, D.; Merbach, A. E. Conformational and Coordination Equilibria on DOTA Complexes of Lanthanide Metal Ions in Aqueous Solution Studied by ^{1}H-NMR Spectroscopy. *Inorg. Chem.* **1997**, *36* (10), 2059-2068.

(54) Bleaney, B. Nuclear Magnetic Resonance Shifts in Solution Due to Lanthanide Ions. *J. Magn. Reson.* **1972**, *8* (1), 91-100.

(55) Elhabiri, M.; Hamacek, J.; Humbert, N.; Bünzli, J.-C. G.; Albrecht-Gary, A.-M. Proton-Assisted Dissociation of a Triple-Stranded Dinuclear Europium Helicate. *New J. Chem.* **2004**, *28* (9), 1096-1099.

(56) Floquet, S.; Borkovec, M.; Bernardinelli, G.; Pinto, A.; Leuthold, L. A.; Hopfgartner, G.; Imbert, D.; Bünzli, J. C. G.; Piguet, C. Programming Heteropolymetallic Lanthanide Helicates: Thermodynamic Recognition of Different Metal Ions Along the Strands. *Chem. - Eur. J.* **2004**, *10* (5), 1091-1105.

(57) Faulkner, S.; Burton-Pye, B. P.; Khan, T.; Martin, L. R.; Wray, S. D.; Skabara, P. J. Interaction Between Tetrathiafulvalene Carboxylic Acid and Ytterbium DO3A: Solution State Self-Assembly of a Ternary Complex Which is Luminescent in the near IR. *Chem. Commun.* **2002**, (16), 1668-1669.

(58) Harte, A. J.; Jensen, P.; Plush, S. E.; Kruger, P. E.; Gunnlaugsson, T. A Dinuclear Lanthanide Complex for the Recognition of Bis (Carboxylates): Formation of Terbium (III) Luminescent Self-Assembly Ternary Complexes in Aqueous Solution. *Inorg. Chem.* **2006**, *45* (23), 9465-9474.

(59) Faulkner, S.; Burton-Pye, B. P. pH Dependent Self-Assembly of Dimetallic Lanthanide Complexes. *Chem. Commun.* **2005**, (2), 259-261.

(60) Tilney, J. A.; Sørensen, T. J.; Burton-Pye, B. P.; Faulkner, S. Self-Assembly Between Dicarboxylate Ions and a Binuclear Europium Complex: Formation of Stable Adducts and Heterometallic Lanthanide Complexes. *Dalton Trans.* **2011**, *40* (45), 12063-12066.

(61) Caffrey, D. F.; Gunnlaugsson, T. Displacement Assay Detection by a Dimeric Lanthanide Luminescent Ternary Tb (III)–Cyclen Complex: High Selectivity for Phosphate and Nitrate Anions. *Dalton Trans.* **2014**, *43* (48), 17964-17970.

(62) Sørensen, T. J.; Hill, L. R.; Faulkner, S. Thermodynamics of Self‐Assembly of Dicarboxylate Ions with Binuclear Lanthanide Complexes. *ChemistryOpen* **2015**, *4* (4), 509-515.

(63) Evans, C. H. *Biochemistry of the Lanthanides*; Springer Science & Business Media, 2013.

(64) Bertini, I.; Luchinat, C. *NMR of Paramagnetic Substances*; Elsevier: Amsterdam, 1996.

(65) (a) Peters, J.; Huskens, J.; Raber, D. Lanthanide Induced Shifts and Relaxation Rate Enhancements. *Prog. Nucl. Magn. Reson. Spectrosc.* **1996**, *28* (3-4), 283-350. (b) Reuben, J. Aqueous Lanthanide Shift Reagents. 8. Chiral Interactions and Stereochemical Assignments of Chemically and Isotopically Chiral Ligands. *J. Am. Chem. Soc.* **1980**, *102* (7), 2232-2237.

(66) Parker, D.; Dickins, R. S.; Puschmann, H.; Crossland, C.; Howard, J. A. Being Excited by Lanthanide Coordination Complexes: Aqua Species, Chirality, Excited-State Chemistry, and Exchange Dynamics. *Chem. Rev.* **2002**, *102* (6), 1977-2010.

(67) Sherry, A. D.; Geraldes, C. F. G. C. Lanthanide Probes in NMR. *In Lanthanide Probes in Life*, Chemical and Earth Sciences; Bünzli, J.-C. G., Choppin, G. R., Eds.; Elsevier: Amsterdam, 1989; 93–126.

(68) Wenzel, T. G. *NMR Shift Reagents*; Boca Raton, 1987.

(69) Geraldes, C. F. G. C. NMR in Supramolecular Chemistry. In *NMR in Supramolecular Chemistry*, Pans, M. Ed.; Kluwer, 1999.

(70) Heinrich, P. C.; Müller, M.; Graeve, L. *Löffler/Petrides Biochemie und Pathobiochemie*; Springer-Verlag, 2014.

(71) Annibaldi, A.; Widmann, C. Glucose Metabolism in Cancer Cells. *Curr. Opin. Clin. Nutr. Metab. Care* **2010**, *13* (4), 466-470.

(72) Govers, R. Cellular Regulation of Glucose Uptake by Glucose Transporter GLUT4. *Adv. Clin. Chem.* **2014**, *66*, 173-240.

(73) Yamamoto, N.; Ueda‐Wakagi, M.; Sato, T.; Kawasaki, K.; Sawada, K.; Kawabata, K.; Akagawa, M.; Ashida, H. Measurement of Glucose Uptake in Cultured Cells. *Curr. Protoc. Pharmacol.* **2015**, *71* (1), 12.14. 11-12.14. 26.

(74) Saito, K.; Lee, S.; Shiuchi, T.; Toda, C.; Kamijo, M.; Inagaki-Ohara, K.; Okamoto, S.; Minokoshi, Y. An Enzymatic Photometric Assay for 2-Deoxyglucose Uptake in Insulin-Responsive Tissues and 3T3-L1 Adipocytes. *Anal. Biochem.* **2011**, *412* (1), 9-17.

(75) Frenzel, J.; Schellenberger, W.; Eschrich, K.; Hofmann, E. Regulation of the fructose 6-Phosphate/Fructose 2, 6-Bisphosphate Cycle by enzyme phosphorylation and Sn-Glycerol 3-Phosphate. *Biol. Chem. Hoppe-Seyler* **1990**, *371*, 841-850.

(76) Lorentzen, E.; Siebers, B.; Hensel, R.; Pohl, E. Structure, Function and Evolution of the Archaeal Class I Fructose-1, 6-Bisphosphate Aldolase. *Biochem. Soc. Trans.* **2004**, *32* (2), 259-263.

(77) Collins, R.; McNally, T.; Fothergill-Gilmore, L.; Muirhead, H. A Subunit Interface Mutant of Yeast Pyruvate Kinase Requires the Allosteric Activator Fructose 1, 6-Bisphosphate for Activity. *Biochem. J.* **1995**, *310* (1), 117-123.

(78) Myers, R. W.; Baginsky, W. F.; Gattermeir, D. J.; Geissler, W. M.; Harris, G. Enzymatic Preparation of High-Specific-Activity β -d-[6, 6′ -3H] Fructose-2, 6-Bisphosphate: Application to a Sensitive Assay for Fructose-2, 6-Bisphosphatase. *Anal. Biochem.* **2010**, *406* (2), 97-104.

(79) Pilkis, S.; El-Maghrabi, M. R.; Pilkis, J.; Claus, T. H.; Cumming, D. Fructose 2, 6-Bisphosphate. A new Activator of Phosphofructokinase. *J. Biol. Chem.* **1981**, *256* (7), 3171-3174.

(80) Bajić, A.; Zakrzewska, J.; Godjevac, D.; Andjus, P.; Jones, D. R.; Spasić, M.; Spasojević, I. Relevance of the Ability of Fructose 1, 6-Bis (Phosphate) to Sequester Ferrous but not Ferric Ions. *Carbohydr. Res.* **2011**, *346* (3), 416-420.

(81) Azambuja, A. A.; Lunardelli, A.; Nunes, F. B.; Gaspareto, P. B.; Donadio, M. V. F.; de Figueiredo, C. E. P.; de Oliveira, J. R. Effect of Fructose-1, 6-Bisphosphate on the Nephrotoxicity Induced by Cisplatin in Rats. *Inflammation* **2011**, *34* (1), 67-71.

(82) Atsumi, T.; Chiba, H.; Yoshioka, N.; Bucala, R.; Koike, T. Increased Fructose 2, 6-Bisphosphate in Peripheral Blood Mononuclear Cells of Patients with Diabetes. *Endocr. J.* **2007**, *54* (4), 517-520.

(83) Cuesta, E.; Boada, J.; Calafell, R.; Perales, J. C.; Roig, T.; Bermudez, J. Fructose 1, 6-Bisphosphate Prevented Endotoxemia, Macrophage Activation, and Liver Injury Induced by D-Galactosamine in Rats. *Crit. Care Med.* **2006**, *34* (3), 807-814.

(84) Bruni, P.; Vasta, V.; Farnararo, M. An Endpoint Enzymatic Assay for Fructose 2, 6-Bisphosphate Performed in 96-Well Plates. *Anal. Biochem.* **1989**, *178* (2), 324-326.

(85) Uyeda, K.; Furuya, E.; Luby, L. J. The Effect of Natural and Synthetic D-Fructose 2, 6-Bisphosphate on the Regulatory Kinetic Properties of Liver and Muscle Phosphofructokinases. *J. Biol. Chem.* **1981**, *256* (16), 8394-8399.

(86) Wang, C.; Xu, C.; Yu, H.; Pan, L. Determination of Fructose-1, 6-Diphosphate with Aldolase-DNPH by the Colorimetric Method. *J. Biomed. Eng.* **2000**, *17* (3), 363-365.

(87) Van Schaftingen, E.; Lederer, B.; Bartrons, R.; HERS, H. G. A Kinetic Study of Pyrophosphate: Fructose‐6‐Phosphate Phosphotransferase from Potato Tubers: Application to a Microassay of Fructose 2, 6‐Bisphosphate. *Eur. J. Biochem.* **1982**, *129* (1), 191-195.

(88) Hue, L.; Blackmore, P.; Shikama, H.; Robinson-Steiner, A.; Exton, J. Regulation of Fructose-2, 6-Bisphosphate Content in Rat Hepatocytes, Perfused Hearts, and Perfused Hindlimbs. *J. Biol. Chem.* **1982**, *257* (8), 4308-4313.

Chapter 2 Binuclear complexes as imaging agents for anionic guests

This Chapter describes the preparation of a series of Ln.NMM compounds, shown in Figure 2.1, can be used to explore their interactions with a series of phosphorylated glycolytic intermediates, particularly glucose-6-phosphate and fructose-1,6-bisphosphate. It also describes the visualisation of glucose metabolites using NMR and luminescence techniques.

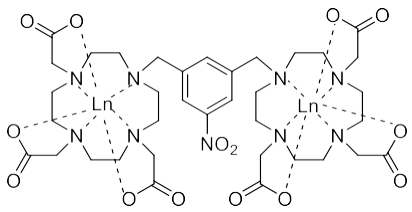


Figure 2.1 Binuclear nitro-m-xylyl complex (Ln.NMM).

2.1 Background

The previous gold standard for measuring glucose uptake is effective but highly sensitive and requires multiple washes.[1,2] We propose a new lanthanide complex that could image glycolysis products. Ln.NMM complexes have two binding sites,[3] and can bind to anionic guests. The potential guest candidates for Ln.NMM complexes include carboxylate groups or phosphate groups in glycolysis.

The glycolytic pathway contains an array of carboxylate and phosphate species, many of which can bind to the binuclear lanthanide complexes. Figure 2.2 shows the glycolytic pathway,[4] in which the potential guest species are glucose-6-phosphate (G6P) and fructose-1,6-bisphosphate (FBP).

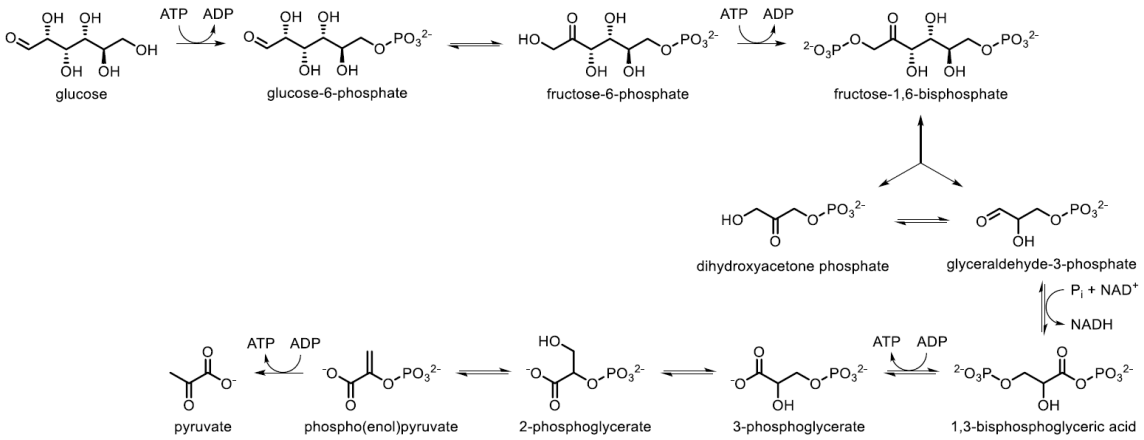


Figure 2.2 Molecules involved in the glycolytic pathway.[4]

2.2 Binuclear nitro-m-xylyl complex—Ln.NMM

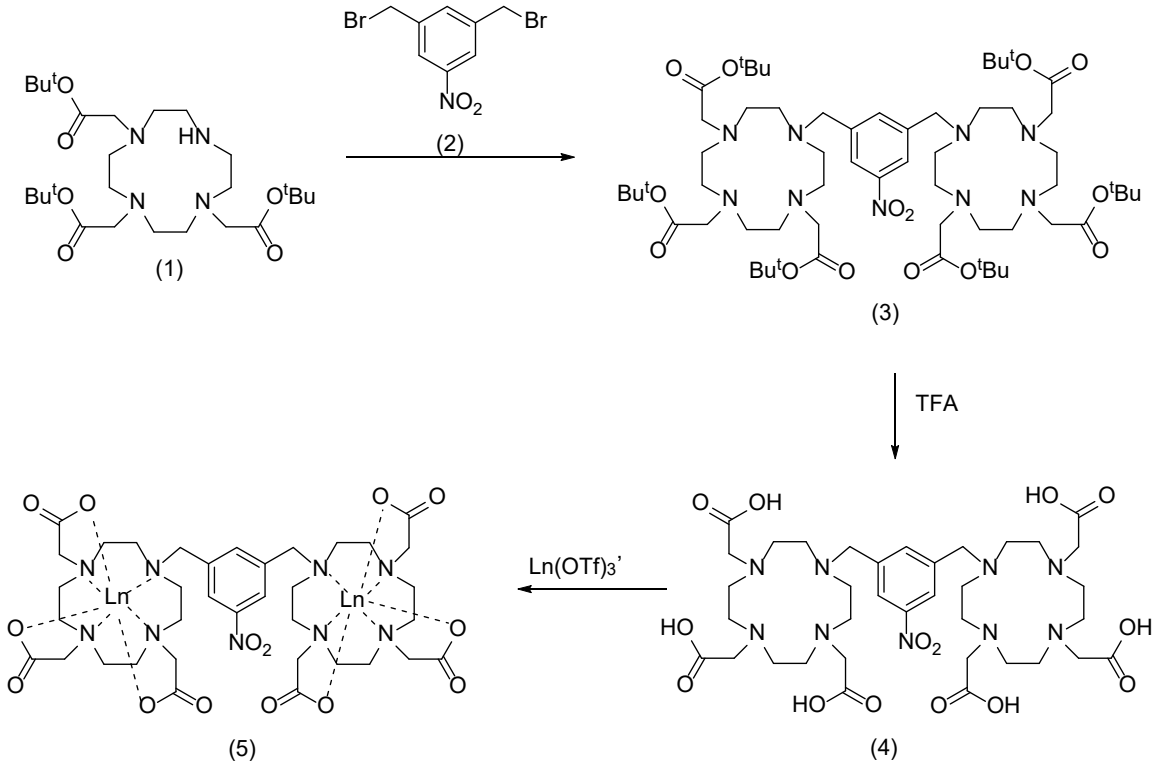
Faulkner et al. first developed the binuclear nitro-m-xylyl chelate displayed in Figure 2.1 in 2009, with the formation of the lanthanide complexes that possess kinetic stability, even in conditions that are highly acidic.[3]

Mononuclear DO3A derivative self-assembly complexes with carboxylate anions were used in the establishment of energy transfer procedures in near IR luminescence and for the efficient screening of possible sensitizers, transporting them to lanthanide centre proximity through an attached carboxylate.[5] Dicarboxylate anions were shown to undergo self- assembly with the binuclear nitro-m-xylyl complex in 2011. Specifically, strong binding is displayed by isophthalate, together with its water soluble analogue, dinicotinate.[6] Even in the presence of competitor anions like phosphate, which can hardly bind to the lanthanide complex. A guest's binding is not necessarily linked with water displacement.

The dramatic effects of remote substituents on anion affinity were demonstrated in 2013, when peptides were used with Ugi couplings for the extension of binuclear complexes, through the amino group on the bridging m-xylyl.[7] In the absence of bulky substituents, lanthanide binding sites occupy a wide range of conformational spaces. Nonetheless, with substituents becoming bulkier, limitations with regard to the available conformations were present, with major effects on isophthalate binding, with variations in affinities of up to seven orders of magnitude. There will always be increases in the affinity constant as a result of pre-organisational consequence, as long as the ideal binding conformer is included in the remaining conformational space. In the event that the ideal conformer fails, binding will not occur.

2.3 Synthesis of nitro-m-xylyl bridged binuclear complexes (Ln.NMM)

The synthesis of nitro-m-xylyl complex was undertaken in accordance with the multistep processes outlined in the literature.[3]



Scheme 2.1 Synthesis of nitro-m-xylyl bridged binuclear complexes (Ln.NMM).

Compound (1) was made from cyclen and was based on methods from the literature.[8] Bromination of the di-hydroxy species made use of PBr_3,[9] in the preparation of the nitro-m-xylyl bridging unit (2). This had been established as a bromination reaction, more effective than the method of Placidi *et al.*,[3] who made use of HBr and concentrated H_2SO_4. The coupling with compound (1) of the dibromo compound (2), was made in a substitution reaction in the presence of caesium carbonate. The reaction was carried out in acetonitrile and heated to reflux temperature for 48 hours to reach completion. Then, column chromatography was used to purify the crude product. After trituration in diethyl ether and removing the solvent, the nitrobenzyl hexaester compound (3) was formed as a yellow solid.

Using trifluoroacetic acid, the nitrobenzyl hexaester compound (3) can be transformed to the nitrobenzyl hexaacid compound (4). The reaction was in dichloromethane and was left to stir for 48 hours. After three to five washes and trituration in diethyl ether, the product was clean and yielded as a white or pale yellow solid.

The final step in making the complexation was done in several methods to achieve a satisfactory yield. Firstly, the most common complexation method was used. An excess of lanthanide triflate and the nitrobenzyl hexaacid compound (4) were dissolved in methanol, heated at 60 °C to reflux, and stirred for 48 hours. The excess of the lanthanide triflate was removed by adjusting the pH to 10 and filtering it out. An extra step to purify was by using the dialysis technique to remove the salt and leave an analytically pure lanthanide complex. This method was efficient for most of the complexes in our group.

During the process of obtaining europium or terbium complexes, considerable time was spent adjusting the standard method. Different solvent systems, temperatures, equivalents, and lanthanide salts were used to get the best yield of the europium and terbium complexes.

Different methods were compared with the standard one used in our group. It is found that using acetonitrile and heating the mixture at reflux temperature (90 °C) for 168 hours can achieve a higher yield. Under this method, yields of 36% for the europium complex and 32% for the terbium complex were obtained. The results show that this complex requires high temperatures and long reaction times to form due to the required activation energy.

2.4 Binding Studies

Research from our laboratory showed that using Eu.NMM and Tb.NMM could detect some glycolysis intermediates.[10] Based on binding studies of aryl dicarboxylate guests with Ln.NMM, a similar binding study with glucose and fructose, with Eu.NMM and Tb.NMM was performed. The binding was assessed by two methods: photophysical and ^{1}H-NMR experiments.

2.4.1 Photophysical titration experiment

Since bound and free species are likely to have different photophysical properties, the form and intensity of a luminescence spectrum can be used to obtain a binding isotherm, though it needs to be borne in mind that the observations reflect both the quantum yield and the speciation. In a similar way, changes to the luminescence lifetime can reflect binding.[11]

2.4.1.1 Eu.pDO3A with G6P

Despite the fact that the exploitation of cooperative effects in multinuclear lanthanide complexes will be the primary concern of this thesis, a study of mononuclear complexes was undertaken to better comprehend binuclear complex behaviour, as shown in Figure 2.3. The propargyl complex Eu.pDO3A, in contrast to Eu.NMM provides comparison points with other lanthanide complexes. As Eu.pDO3A has no chromophore and is mononuclear, it will not benefit from the chelate effect in the binding dynamics. This comparison helps assess how much the added arm improves the interaction, but it's important to consider the lower steric hindrance of the pendant group and its effect on the range of possible conformations.

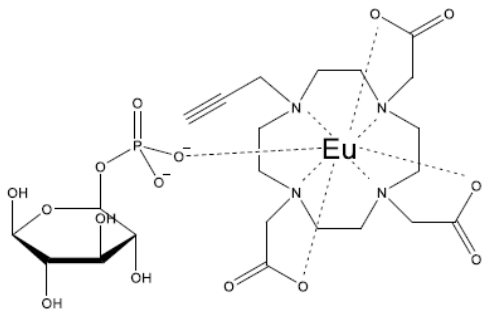
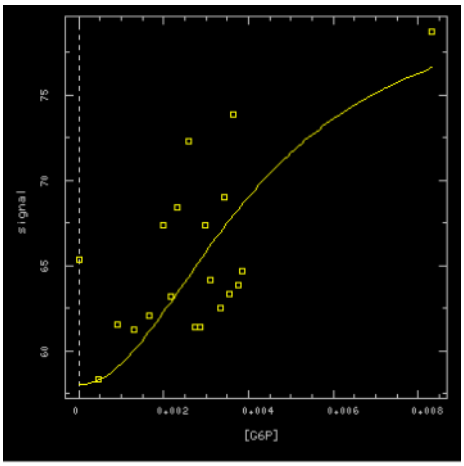


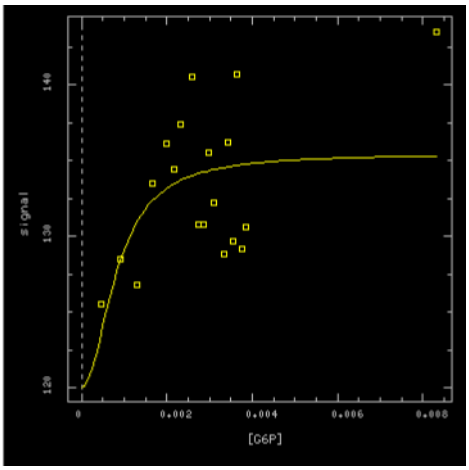
Figure 2.3 Binding model of G6P with Eu.pDO3A.

The self-assembly of glycolysis intermediate and propargyl complexes is influenced by the solvent system. Guest molecules will take the place of solvent molecules, so solvent choice should comprise a non-competitive molecule, and the pH should be similar to that of the human body, therefore PBS is an ideal choice.

An interesting outcome was observed for the titration of Eu.pDO3A with glucose-6- phosphate. The concentration of Ln^{3+} complexes in these systems were 10^{-3} M, which was maintained during the experiment. The concentration of glucose-6-phosphate was increased incrementally from 0 to 10 equivalents. The data was analysed by DynaFit software to reveal binding. The spectra below (Figure 2.4) show the effect of changing guest concentration on the integration of the J bands ΔJ = 1 or ΔJ = 2 for Eu.pDO3A. Through these spectra, we define the binding between the sugar and the propargyl complexes. The binding is not strong, therefore some points cannot perfectly fit the line.



(a) Eu.pDO3A ΔJ=1



(b) Eu.pDO3A Δ J=2

Figure 2.4 Binding curve for Eu. pDO3A with glucose-6-phosphate, secondary binding model.

2.4.1.2 Eu.NMM with G6P

After some positive results from the preliminary binding of Eu. pDO3A with glucose-6-phosphate (G6P) was confirmed, and the experiment was later continued with a luminescence binding titration study for Eu.NMM with G6P, shown in Figure 2.5.

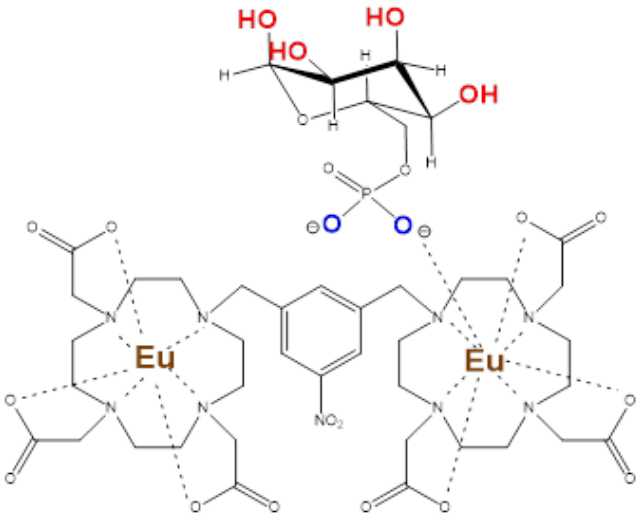


Figure 2.5 Binding model of Eu.NMM with G6P.

The luminescence spectrum below (Figure 2.6) shows how the Eu.NMM complex responds to increasing concentrations of glucose-6-phosphate (G6P) from 0 to 200 equivalents. When it comes to the key emission features for Eu^{3+} ions, the two characteristic peaks at around 595 nm ($\Delta J = 1$) and at around 615 nm ($\Delta J = 2$) are important. The peak at 595 nm ($\Delta J = 1$) corresponds to the magnetic dipole transition. The peak at 615 nm ($\Delta J = 2$) corresponds to the hypersensitive electric dipole transition, which means it is highly sensitive to changes in the coordination environment and symmetry.

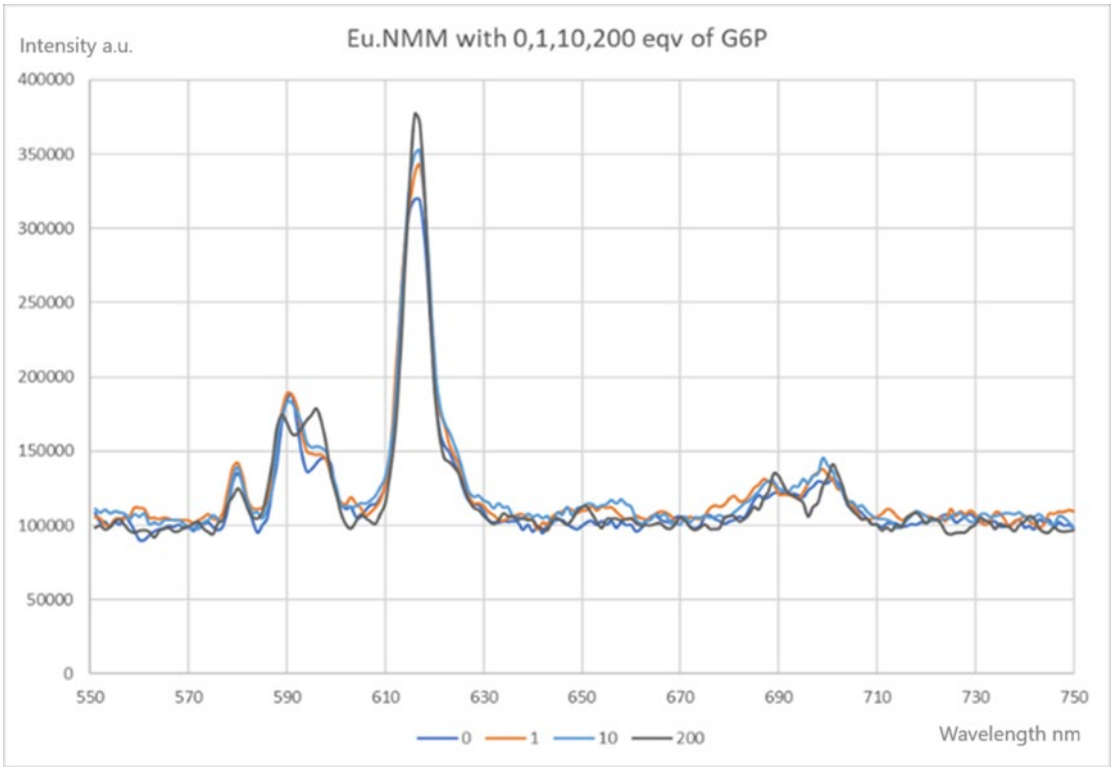


Figure 2.6 Luminescence titration spectrum of Eu.NMM with increasing G6P. (G6P = 0, 1, 10, 20, 200 eqv.). HEPES buffer (20 mM, pH 7.4); Eu.NMM (2.5 × 10^{-4} mol/L); 25 ℃.

When it comes to the observed trends with G6P titration, the peak at 615 nm (ΔJ = 2) exhibits a significant increase in intensity as the G6P concentration increases. From 0 → 1 → 10 → 200 eqv. of G6P, there is a steady and clearly visible enhancement, which strongly indicates G6P binding to Eu.NMM. G6P likely replaces quenching solvent molecules or introduces rigidity, enhancing emission. There is no peak shift that suggests binding affects intensity, not symmetry drastically, or that G6P binding does not distort the coordination sphere in a way that splits transitions.

Except for this dramatically increased peak, the peak at 595 nm (ΔJ = 1) also increases, but less significantly than ΔJ = 2. This is expected, as ΔJ = 1 is relatively insensitive to symmetry changes and is often used as a reference.

The other transitions at around 580–590 nm and 690 nm show small changes, likely noise or minor transitions. But there are no drastic shifts or intensity variations, indicating the binding event is localised around the primary Eu^{3+} site.

2.4.2 NMR binding study

The ^{1}H-NMR spectra of Eu.pDO3A and Eu.NMM changed upon the addition of 0, 1, 5 eq of G6P, shown in Figure 2.7&8. The photophysical and the ^{1}H-NMR study demonstrated a well-defined interaction between the sugar species and Eu^{3+} complexes. Furthermore, the changes in spectra suggest that moving from the free form to the bound form results in significant rigidification of the complex.

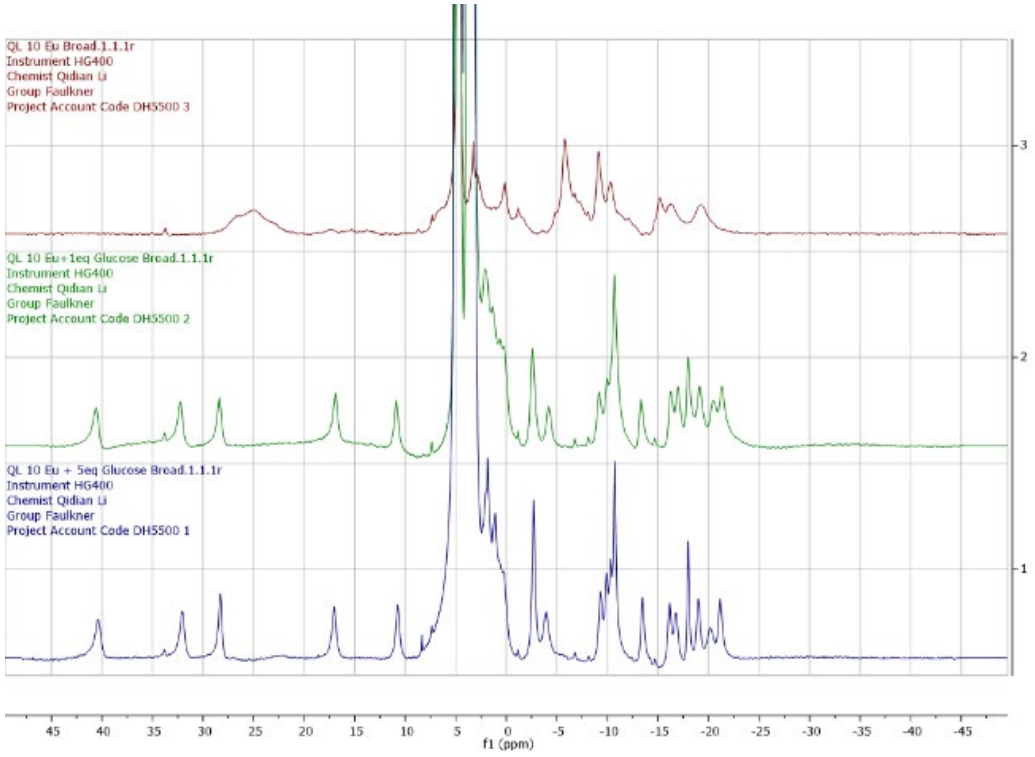


Figure 2.7 ^{1}H-NMR spectra of Eu.pDO3A with 0, 1, 5 eqv. of G6P.

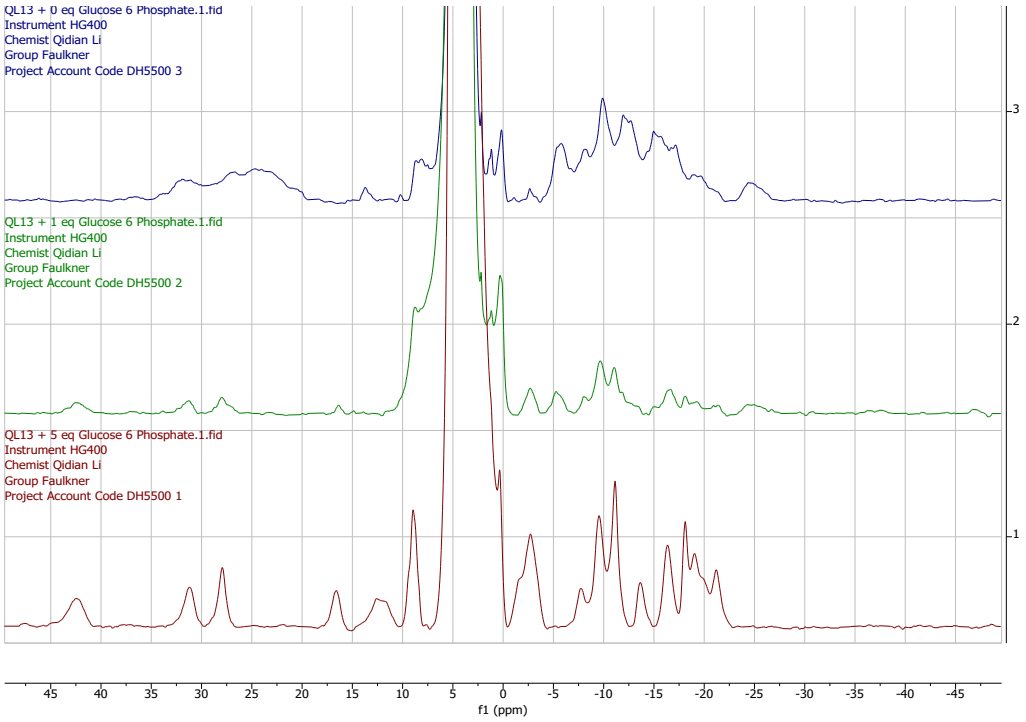


Figure 2.8 ^{1}H-NMR spectra of Eu.NMM with 0, 1,5 eq of G6P.

2.5 CEST experiments

The degree to which fructose-1,6-diphosphate binds to Ln.NMM complexes is investigated. The appropriateness of CEST methods for addressing these systems by the strength of binding is confirmed here. Chemical Exchange Saturation Transfer (CEST) imaging is an NMR imaging technique which exploits the exchange of protons or other NMR-active nuclei between bulk and a target molecule. For instance, in glucoCEST, the exchange of protons between bulk water and the hydroxyl groups on glucose can be exploited by saturating the water signal, thereby enhancing the hydroxyl proton signals. Such enhancement requires slow exchange between the two pools. Three factors influence the success of CEST experiments; the exchange rate k; the chemical shift between the interested -OH peak and the bulk water peak $\Delta\omega$ and the relaxation time. The k and $\Delta\omega$ values are important. To control the experiment, it can be altered through k and $\Delta\omega$.[12,13]

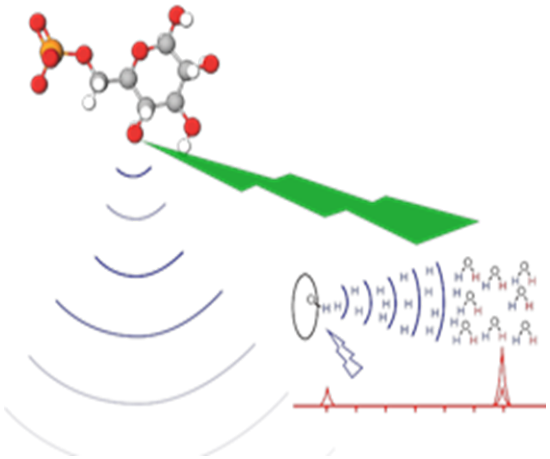


Figure 2.9 CEST experiment model.

In this work, EuNMM can give rise to a shifted proton signal for the bound G6P species, reasoning that this would shift the proton signal of the hydroxyl protons while simultaneously enhancing their relaxation rate. Figure 2.10 shows the spectrum obtained using a CEST pulse sequence and saturating the water peak. At 298k, this spectrum initially showed a degree of line broadening, with a clear shoulder on the water peak consistent with the hydroxyl protons. At lower temperatures, this shoulder resolved into multiple peaks corresponding to individual hydroxyl protons.

At the beginning, the experiment was conducted at 25 °C, as shown in Figure 2.10. The change in position of the peaks indicates the Eu.NMM can shift the OH peaks of G6P. As the concentration of the Eu.As NMM increases, the chemical shift difference changes, but the shift difference between the -OH and bulk water is not very large. There are two kinds of exchanges in the multiple equilibrium system: the hydroxyl group (OH) on glucose-6-phosphate

exchanges with bulk water, over which there is limited control, and the exchange between the bonded complexes and the bulk complexes.

Our hypothesis is that bound complexes and bulk complexes conflict with each other; they are in a fast exchange. The current problem is that the exchange rate k is too high, but the Δω is not high enough in our system. Δω is related to the paramagnetic field or the lanthanides. The stronger the paramagnetic field, the better the separation of the peaks. But the available NMR spectrometer field is fixed, so it is difficult to modify.

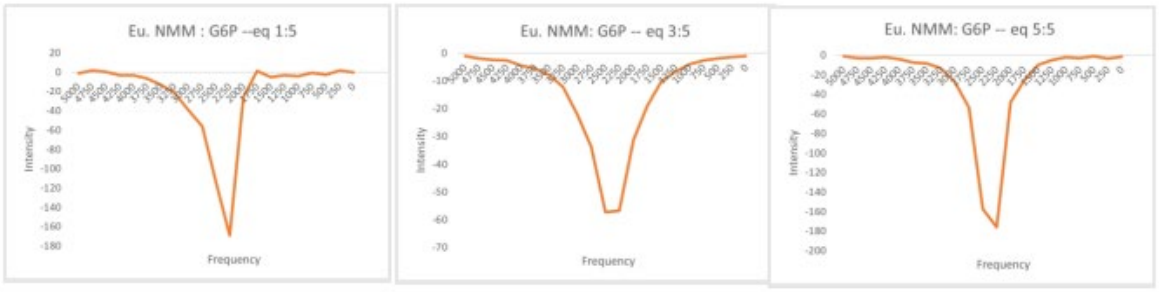


Figure 2.10 CEST spectra of G6P with increasing eq. of Eu.NMM NMR experiments were conducted in pH 7.4,10% D_2O: H_2O,25 ℃.

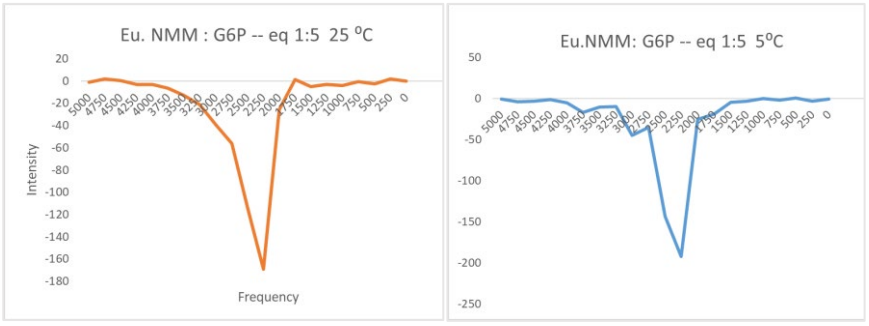


Figure 2.11 CEST spectra of G6P with increasing eq. of Eu.NMM NMR experiments were conducted in pH 7.4,10% D_2O: H_2O, at 25℃ and at 5℃.

The experiment was cooled down to 5 °C to slow down the rate of exchange and reduce k. This generated better results than at 25 °C. As Figure 2.11 shows, when compared with the spectrum at 25 °C, there were obvious chemical shifts of the -OH groups and bulk water. These results were the same for fructose-1,6-bisphosphate. But the problem is that when it comes to the in vivo imaging of the human body, the temperature is 37 °C. Therefore, different ways to slow down k needs to be investigated. Adjusting k to achieve a slow exchange range is necessary, but slowing it down too much is not ideal, as saturating the -OH peak to transfer magnetisation to the bulk water should occur continuously. So the exchange rate k should be faster than the relaxation time, to maintain saturation of the bulk water.

Eu.NMM complexes bind effectively to glucose phosphate, suggesting that the self-assembly approach might be effective for metabolic imaging. However, the CEST experiments carried out on these systems reveal that proton exchange occurs too rapidly to permit a ^{1}H CEST imaging experiment at physiological pH. The future work may prove possible to develop ^{31}P CEST approaches that exploit this self-assembly.

2.6 Conclusion

This chapter describes the investigation of lanthanide nitro-m-xylyl complexes (Ln.NMM) as responsive systems for the binding and potential imaging agents of glycolysis-related molecules, such as glucose-6-phosphate (G6P) and fructose-1,6-bisphosphate (FBP). The investigation was conducted by luminescence spectroscopy, NMR studies, and preliminary CEST measurements. The results showed that these multinuclear lanthanide complexes produce measurable and interpretable responses toward biologically relevant anionic guests.

Photophysical titration showed that increasing concentrations of G6P caused a substantial increase in the hypersensitive europium emission band. The increase in emission intensity is consistent with reduced non-radiative quenching. This effect arises from the displacement of coordinated solvent molecules and increased rigidity after guest binding.

^{1}H NMR titration studies provided further evidence for well-defined interactions between G6P and the europium complexes. Preliminary studies using Eu.pDO3A demonstrated that G6P could bind with each other. These studies provided a useful basis for comparison with the more structurally complex binuclear systems. The addition of G6P produced substantial spectral changes later in Eu.NMM. These changes indicated changes in the coordination and conformation of the complexes.

The CEST studies confirmed that interactions between G6P and Eu.NMM influences exchange processes between hydroxyl groups and bulk water. However, the experiments also revealed temperature limitations in achieving optimal CEST behaviour. Translating these systems to biologically relevant temperatures remains challenging and will require further optimisation.

Overall, this chapter demonstrates that multinuclear lanthanide complexes based on the Ln.NMM framework provides a promising platform for the recognition and sensing of glycolysis-related phosphate metabolites. The combined luminescence, NMR, and CEST studies showed that these systems respond to guest binding through changes in the coordination environment, hydration or rigidity. The results establish a foundation for the future development of metabolite imaging probes based on lanthanide nitro-m-xylyl complexes (Ln.NMM).

2.7 References

(1) Yamamoto, N.; Ueda-Wakagi, M.; Sato, T.; Kawasaki, K.; Sawada, K.; Kawabata, K.; Akagawa, M.; Ashida, H. Measurement of glucose uptake in cultured cells. *Curr. Protoc. Pharmacol.* **2015**, *71* (1), 12.14. 11-12.14. 26.

(2) Saito, K.; Lee, S.; Shiuchi, T.; Toda, C.; Kamijo, M.; Inagaki-Ohara, K.; Okamoto, S.; Minokoshi, Y. An enzymatic photometric assay for 2-deoxyglucose uptake in insulin-responsive tissues and 3T3-L1 adipocytes. *Anal. Biochem.* **2011**, *412* (1), 9-17.

(3) Placidi, M. P.; Natrajan, L. S.; Sykes, D.; Kenwright, A. M.; Faulkner, S. Bimetallic lanthanide complexes derived from macrocycle-appended *m*-xylyl derivatives: Synthesis and spectroscopic properties. *Helv. Chim. Acta.* **2009**, *92* (11), 2427–2438.

(4) Berg, J. M.; Tymoczko, J. L.; Stryer, L. *Biochemistry*; 5th ed.; W. H. Freeman and Company: New York, 2002.

(5) Faulkner, S.; Burton-Pye, B. P.; Khan, T.; Martin, L. R.; Wray, S. D.; Skabara, P. J. Interaction between tetrathiafulvalene carboxylic acid and ytterbium DO3A: solution state self-assembly of a ternary complex which is luminescent in the near IR. *Chem. Commun.* **2002**, (16), 1668-1669.

(6) Tilney, J. A.; Sørensen, T. J.; Burton-Pye, B. P.; Faulkner, S. Self-assembly between dicarboxylate ions and a binuclear europium complex: formation of stable adducts and heterometallic lanthanide complexes. *Dalton Trans.* **2011**, *40* (45), 12063-12066.

(7) Tropiano, M.; Blackburn, O. A.; Tilney, J. A.; Hill, L. R.; Placidi, M. P.; Aarons, R. J.; Sykes, D.; Jones, M. W.; Kenwright, A. M.; Snaith, J. S. Using remote substituents to control

solution structure and anion binding in lanthanide complexes. *Chem. Eur. J.* **2013**, *19* (49), 16566-16571.

(8) Dadabhoy, A.; Faulkner, S.; Sammes, P. G. Long wavelength sensitizers for europium (III) luminescence based on acridone derivatives. *J. Chem. Soc., Perkin Trans. 2* **2002**, (2), 348-357.

(9) Chhikara, B. S.; Kumar, N.; Tandon, V.; Mishra, A. K. Synthesis and evaluation of bifunctional chelating agents derived from bis (2-aminophenylthio) alkane for radioimaging with 99mTc. *Bioorg. Med. Chem.* **2005**, *13* (15), 4713-4720.

(10) Hill, L. *Binuclear Complexes as Quantitative Imaging Agents*; D.Phil. Thesis; University of Oxford: Oxford, U.K., 2018.

(11) Sørensen, T. J.; Hill, L. R.; Tilney, J. A.; Blackburn, O. A.; Jones, M. W.; Tropiano, M.; Faulkner, S. Self-Assembly between Dicarboxylate Ions and Dinuclear Lanthanide Complexes: A Surprisingly Complicated Problem. *Eur. J. Inorg. Chem.* **2014**, *2014* (15), 2520-2528.

(12) Ward, K.; Aletras, A.; Balaban, R. S. A new class of contrast agents for MRI based on proton chemical exchange dependent saturation transfer (CEST). *J. Magn. Reson.* **2000**, *143* (1), 79-87.

(13) Van Zijl, P. C.; Yadav, N. N. Chemical exchange saturation transfer (CEST): what is in a name and what isn't? *Magn. Reson. Med.* **2011**, *65* (4), 927-948.

Chapter 3 Self-assembly heterometallic complexes: controlling processes by competitive binding --- The interaction of homometallic binuclear nitro-m-xylyl complexes and the 8-coordinate aminoisophthalate complexes vs glucose phosphate

3.1 Eu.NMM + Tb.iphth / G6P competitive binding

We have explored the competitive binding system of Eu.NMM + Tb.iphth (Terbium isophthalate complex) / glucose-6-phosphate (G6P). This system allows us to explore the behaviour of a supramolecular assembly in which energy transfer between two lanthanide ions controls the colour of the emission. In such a system, disrupting the assembly will result in a colour change. As such, we resolved to explore how competitive binding of glucose phosphate influenced the photophysical and spectroscopic properties of the assembly.

3.2 The idea of Competitive Binding

The m-xylyl-linked binuclear lanthanide complexes first reported by Placidi *et al.* established the kinetic stability and well-defined photophysical behaviour of the Ln.NMM scaffold.[1] In the present work, this architecture is repurposed from a static luminescent system into a dynamic participant in competitive self-assembly, enabling guest-controlled intermetallic energy transfer.

The concept of competitive binding, also known as displacement assays, is utilised widely in biochemical sensing systems.[2] In lanthanide photophysics, it refers to the competition among different guests for a luminescent host lanthanide complex. Competitive displacement will generate measurable signals, such as luminescent emission intensity or spectral peak shifts, and thus provides a quantitative or qualitative method for detecting the guests.

One of the examples is demonstrated in the luminescent displacement assay developed by Gunnlaugsson *et al*..[3] In their system, the first step was to attach the Eu(III)-cyclen complexes to gold nanoparticles. The Eu(III) centre was initially non-emissive due to being quenched by water molecules, which are known to quench lanthanide luminescence through O–H vibration. After adding a sensitising antenna guest (1), water was displaced, and a ternary complex (AuNP-1.Eu-2) was formed, resulting in a sharp "turn-on" of the red Eu^{3+} emission. This luminescence served as the baseline signal for sensing.

The second step, the competitive binding step, was performed by adding the phosphate guest to the system above. The phosphate guest (2) would compete with the sensitising antenna guest (1) to bind to the Eu(III) centre. The phosphate guest had a binding constant that was high enough compared with that of the antenna guest. It occupied the space of the antenna guest one, disrupting energy transfer and quenching Eu(III) centre luminescence. The luminescence intensity from Eu(III) centre dropped, particularly in the hypersensitive $\Delta J = 2$ transition at 616 nm, which was used as a key reference peak for the binding event.

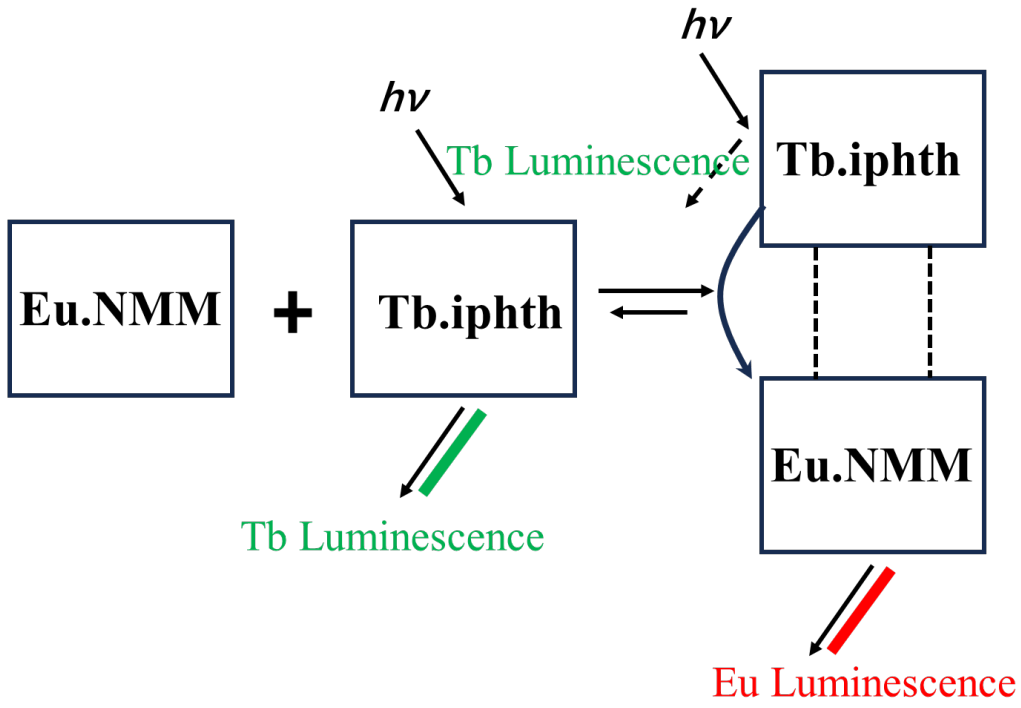


Figure 3.1 The proposed energy transfer for part 1: Direct excitation at the Tb^{3+} centre using 270 nm. Eu.NMM and Tb.iphth will form a self-assembled complex. Energy will be transferred from Tb^{3+} to Eu^{3+}, whereupon, Tb^{3+} luminescence will be quenched and Eu^{3+} luminescence will rise.

This displacement concept is the inspiration for the Eu.NMM + Tb.iphth /G6P system explored in this thesis. In the first step, shown in Figure 3.1, the host Eu.NMM and the guest (1) Tb.iphth form a Tb-Eu-Eu complex through self-assembly via bridging ligands, isophthalate. In this step, energy is transferred from Tb^{3+} (donor) to Eu^{3+} (acceptor). In the second step, shown in Figure 3.2, guest (2) glucose-6-phosphate (G6P) is introduced to the system, and competitive binding occurs. The G6P has the possibility to disrupt the self-assembly binding between Eu.NMM and Tb.iphth and block the energy transfer pathway. This results in changes in both the luminescent emission intensity and peak positions shifting, offering the luminescent signal that reflects the G6P concentration.

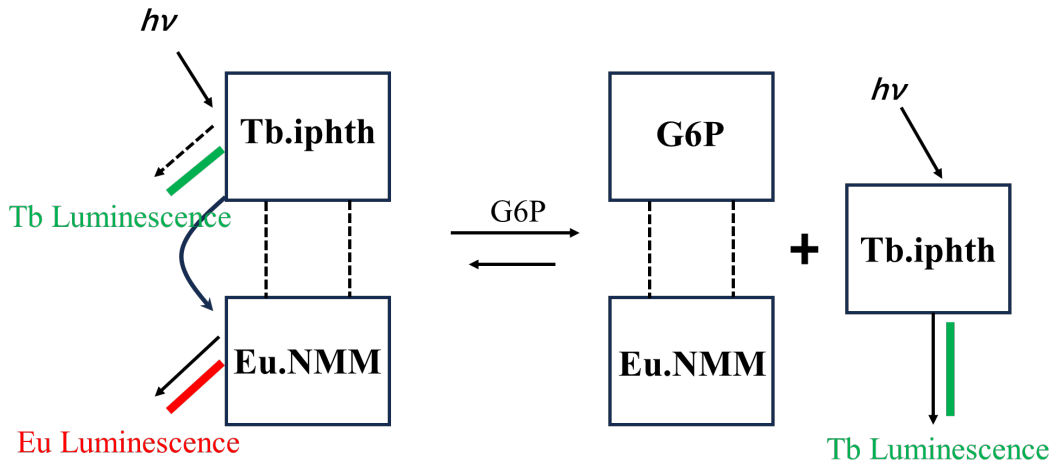


Figure 3.2 The proposed energy transfer for part 2: Direct excitation at the Tb^{3+} centre using 270 nm. G6P interrupt the 1:1 Eu.NMM + Tb.iphth complex, Eu^{3+} luminescence will disappear, and Tb^{3+} luminescence will be recovered.

Therefore, displacement assays can investigate the interactions between the guest and the metal centres of the host and convert binding events into optical outputs. Such systems are promising in the development of biological sensors, because in biological environments, the analyte-induced displacement can be linked to signaling pathways or metabolic activity.

3.3 Possible future applications

Using an analyte to control self-assembly is the basis of displacement assays. We intended that this work should provide proof of concept of the use of displacement in demonstrating the presence of an analyte. G6P serves as an example analyte, but it could be envisaged that this kind of approach could have much broader application. Since G6P is a key component of the glycolytic pathway, such tools might enable observation and understanding of glucose metabolism.

3.4 How did we choose these three candidates?

The plan to establish these three candidates originates from our previous work in 2011,[4] showing that Tb.iphth can bind well to Eu.NMM; the other part is from this work from Chapter 2, which shows that G6P can bind with Eu.NMM.

The work in 2015 investigated the binding behaviour between binuclear lanthanide complexes Eu.NMM and dicarboxylate guests such as isophthalate, dinicotinate and most importantly, aminoisophthalate-appended Tb.iphth complexes. There are some key findings in the work: Tb.iphth acts as a bidentate dicarboxylate-like linker, bridging the Eu.NMM host via the aminoisophthalate moiety; Binding of dicarboxylates is enthalpically driven and often causes an increase in emission intensity (due to removal of quenchers and increased rigidity); Eu^{3+} $\Delta J = 2$ transition is a useful probe for ligand environment changes; No significant lifetime change, which suggests that the lanthanide coordination sphere remains intact (outer-sphere association or weak perturbation of Eu^{3+} site). Emission enhancement may result from: Exclusion of outer-sphere quenchers; Increased chromophore density; Possible energy transfer effects not clearly resolved in this titration.

In this chapter, the key questions to be answered are the energy transfer process that was not established previously, specifically, the energy transfer between Eu.NMM and Tb.iphth. The hypothesis of energy transfer (ET) from terbium to europium within the Eu.NMM and Tb.iphth self-assembled system is supported by several key observations from previous work. Firstly, europium(III) cannot be excited at 488 nm; thus, any observed Eu^{3+} emission under this excitation condition must result from energy transfer originating from an excited terbium(III) donor. Secondly, complex formation will lead to increased rigidity and local chromophore

density, which are known as factors that improve energy transfer efficiency by better spatial alignment of donor and acceptor. Thirdly, although measured lifetimes of europium(III) change negligibly after self-assembly, the considerable increase in europium(III) emission intensity upon excitation at 488 nm implies strong evidence for Tb^{3+} to-Eu^{3+} energy transfer.

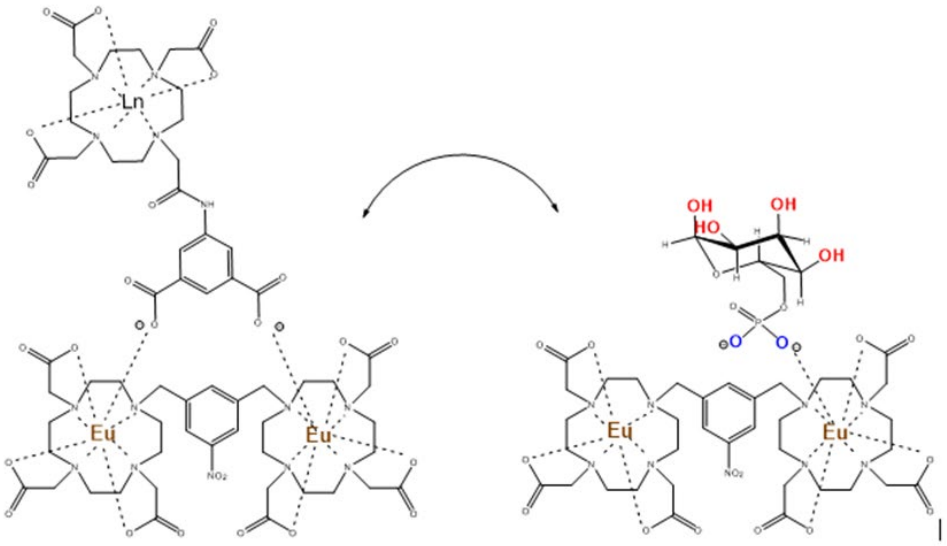
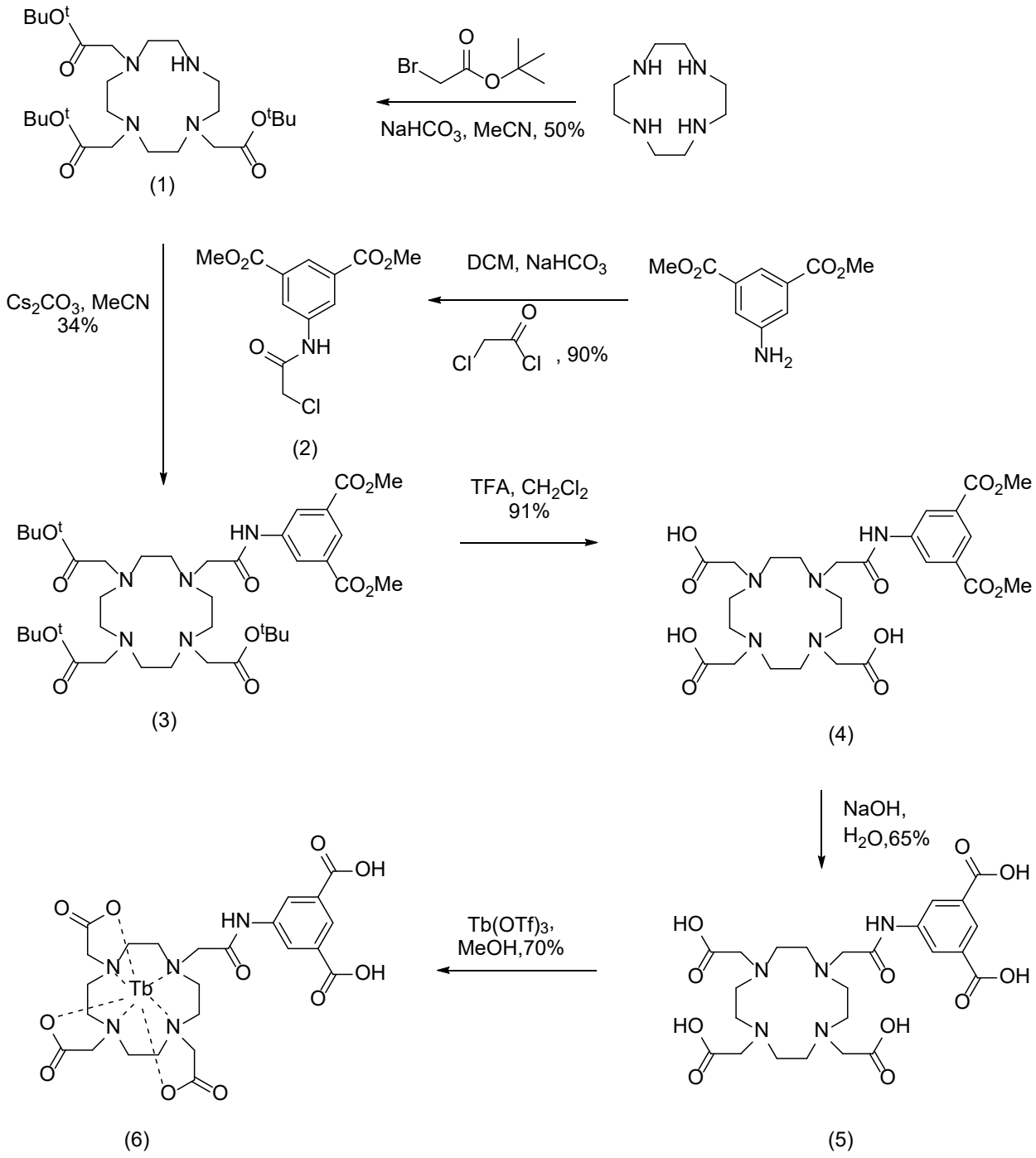


Figure 3.3 Competitive binding model of Eu.NMM + Tb.iphth / G6P.

3.5 Synthesis of Tb.iphth complex

Scheme 3.1 shows the route for the terbium isophthalate complex (Tb.iphth). The isophthalate unit provides a chromophore and a site for competitive binding. This synthesis is adapted from previous work and is detailed below.[5]



Scheme 3.1 Full synthesis route of terbium-isophthalate complex.[5]

3.6 Part 1: Experiment for Investigating the Energy Transfer between Eu.NMM and Tb.iphth.

Objective

This experiment is to investigate the feasibility and mechanism of lanthanide-to-lanthanide energy transfer within the heterometallic Eu.NMM and Tb.iphth system. The outcomes of this study will validate the role of supramolecular assembly in facilitating intermetallic energy transfer and lay the groundwork for potential displacement sensing applications in the second part.

Feasibility Conditions

The Eu.NMM + Tb.iphth system has potential for lanthanide-to-lanthanide energy transfer, particularly from terbium (donor) to europium (acceptor). We designed the experiment based on the following principles: Energy transfer feasibility from $Tb^{3+} \rightarrow Eu^{3+}$. For Tb^{3+}, the excited state is $^5D_4$, which is ~20,500 cm^{-1} or ~488 nm. For Eu^{3+}, the accepting state is $^5D_0$, which is ~17,300 cm^{-1} or ~580 nm. The energy gap between the Tb^{3+} donor and the Eu^{3+} acceptor is suitable for downhill energy transfer. The aminoisophthalate bridge in Tb·iphth binds into the binuclear Eu.NMM host, bringing Tb^{3+} close to Eu^{3+}. Upon excitation at 488 nm (selective for Tb^{3+}): if Eu^{3+} emission is observed, it confirms energy transfer from Tb^{3+} to Eu^{3+}. Upon excitation at 270 nm (chromophore): may sensitise both Tb^{3+} and Eu^{3+} via different pathways, making interpretation more complex.

Table 3.1 Excitation-Emission Measurements for Part 1.

Step	Objective	Details
a	Direct excitation of Tb^{3+} → Monitor for Eu^{3+} emission	λ<excitation> = 488 nm Look for $^5D_0 \rightarrow {}^7F_2$ at ~617 nm
b	Antenna excitation	λ<excitation> = 270 nm
c	Emission scan	λ<emission> = 450–750 nm

Experimental Confirmation to Verify Energy Transfer

To confirm the energy transfer from Tb^{3+} to Eu^{3+}, shown in Figure 3.4, luminescence emission spectra were recorded. The emergence of Eu^3-specific emission peaks, particularly the hypersensitive $^5D_0 \rightarrow {}^7F_2$ transition at approximately 617 nm upon direct Tb^{3+} excitation at 488 nm was taken as evidence of energy transfer.

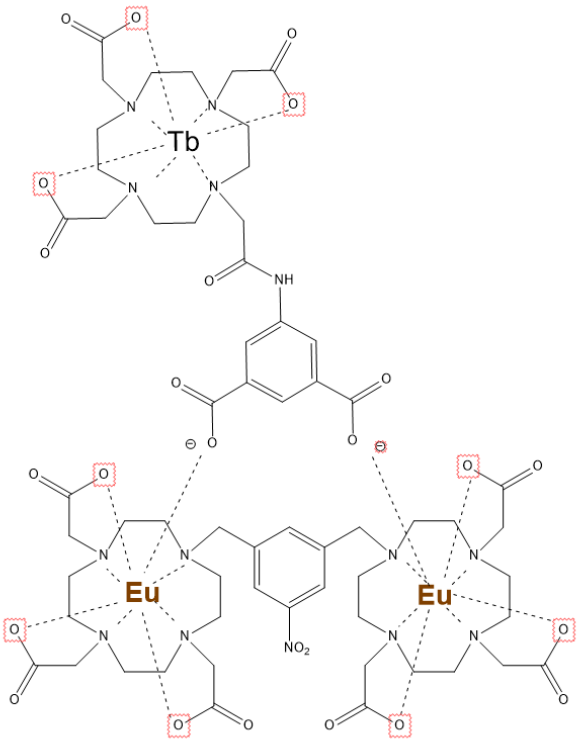


Figure 3.4 Binding model of Eu.NMM + Tb.iphth.

At the beginning of this investigation, we compared Eu.NMM, Tb.iphth and 1:1 Eu.NMM + Tb.iphth to establish the possibility of energy transfer between Eu.NMM and Tb.iphth, in which the europium centre acts as an acceptor from the terbium donor. Two wavelengths were used to excite the samples: excitation at 488 nm (Figure 3.5), which corresponded to direct excitation at the terbium centre, and excitation at 270 nm (Figure 3.7), which corresponded to excitation at the chromophore. Both these pathways can potentially lead to the formation of the terbium emissive state, but it is worth noting that the europium excited state manifold cannot be populated by excitation at 488 nm. As such, any europium emission observed following exciation at 488 nm must result from energy transfer from the terbium centre; by contrast excitation at 270 nm can give rise to europium centred emission as a consequence of two sensitization pathways: either via the aryl chromophore transferring energy directly to europium, or by the aryl chromophore transferring energy to the terbium centre, which can then act as a donor to europium.

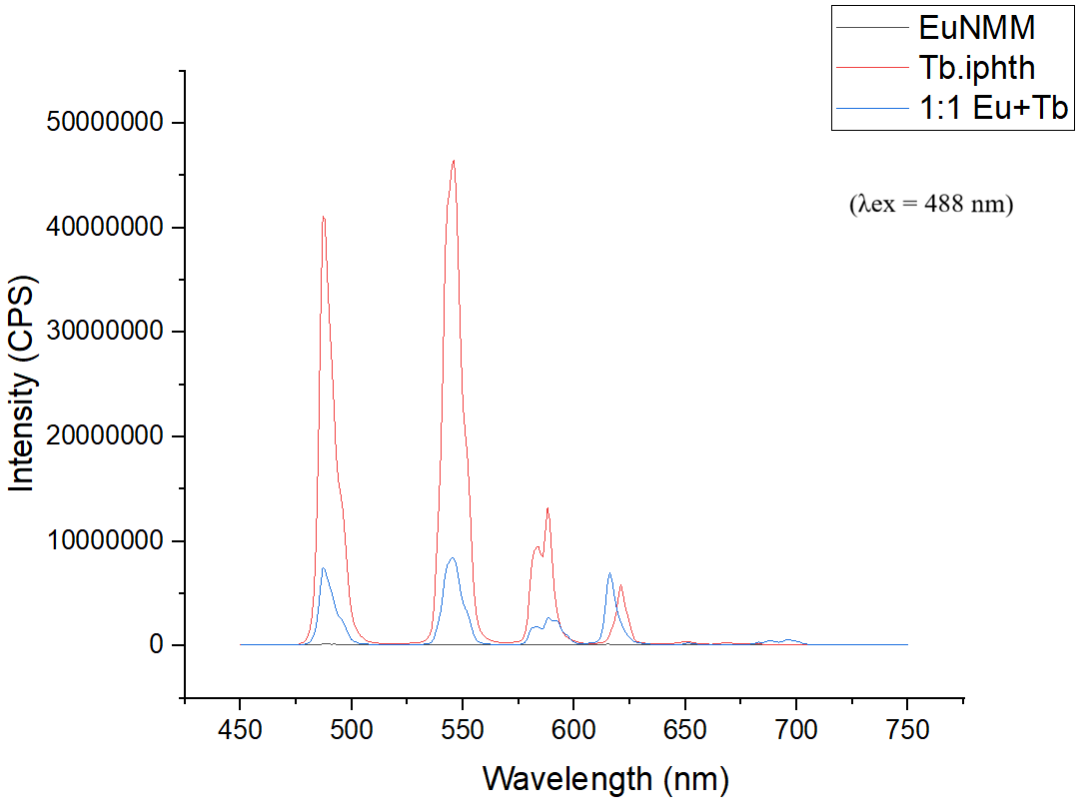


Figure 3.5 Comparison of the emission spectrum of the Eu.NMM, Tb.iphth and 1:1 Eu.NMM + Tb.iphth. Eu.NMM (black), Tb.iphth (red),1:1 Eu.NMM + Tb.iphth (blue). (λex = 488 nm). HEPES buffer (20 mM, pH 7.4); Eu.NMM (2.5 × 10^{-4} mol/L); Tb.iphth (2.5 × 10^{-4} mol/L), 25 ℃.

In the first group of samples, excitation was performed at 488 nm (Figure 3.5), which was direct excitation to the terbium centre. Under these conditions, Eu.NMM exhibited the lowest luminescence intensity (black line), which is consistent with the inherently lower emission of what is expected. Meanwhile, Tb.iphth exhibited the highest luminescence intensity (red line), with a strong terbium-centred emission observed. When Eu.NMM was mixed with Tb.iphth in a 1:1 ratio; a noticeable quenching of terbium emission occurred, resulting in a lower overall emission intensity compared with the pure Tb.iphth sample. This quenching effect indicates energy transfer from the terbium centre to the europium centre and appearance of Eu^{3+} emission.

As the europium and terbium ions reside in separate molecular species, the energy transfer is facilitated through self-assembly processes. A ternary Tb–Eu–Eu complex is formed in the 1:1 Eu.NMM + Tb.iphth mixture, where the isophthalate unit acts as a bridging ligand, coordinating both the terbium and europium centres to enable the energy transfer. Despite the change in intensity, the position of the peaks was also important. There was an obvious peak shift in the 610-625 nm region, which suggested that binding affected symmetry drastically. The binding distorted the coordination sphere, as the coordination of the isophthalate groups results in a change in the local crystal field at the lanthanide centre. A weak peak was observed at 617 nm ($^5D_0 \rightarrow {}^7F_2$) for pure Eu.NMM complex (black line); an intensive peak at 620 nm ($^5D_4 \rightarrow {}^7F_3$) for pure Tb.iphth complex (red line). Upon mixing Eu.NMM with Tb.iphth in a 1:1 ratio (blue line), the dominant emission peak shifted from 620 to 617 nm, accompanied by an increase in intensity at 617 nm compared with the 620 nm peak of pure Tb.iphth. This shift and enhancement indicate the formation of a new species and the occurrence of sensitized europium emission in the 1:1 Eu+Tb system. The key spectral assignments for the Eu-Tb system are summarised in Table 3.2. The energy-level diagram of the Eu+Tb system and the energy transfer from terbium to europium are summarised in Figure 3.6.

Table 3.2 Key spectral assignments for Eu-Tb system. [6]

Emitting Ion	Transition	Wavelength (approx.)	Note
Tb^{3+}	$^5D_4 \rightarrow {}^7F_6$	~487 nm	Blue-green emission
Tb^{3+}	$^5D_4 \rightarrow {}^7F_5$	~542 nm	Main Tb peak
Tb^{3+}	$^5D_4 \rightarrow {}^7F_3$	620 nm	Sensitive to binding
Eu^{3+}	$^5D_0 \rightarrow {}^7F_0$	~580 nm	Weak, sharp peak

Emitting Ion	Transition	Wavelength (approx.)	Note
Eu^{3+}	$^5D_0 \rightarrow {}^7F_1$	~590 nm	Magnetic dipole
Eu^{3+}	$^5D_0 \rightarrow {}^7F_2$	617 nm	Hypersensitive
Eu^{3+}	$^5D_0 \rightarrow {}^7F_4$	~700 nm	Minor line

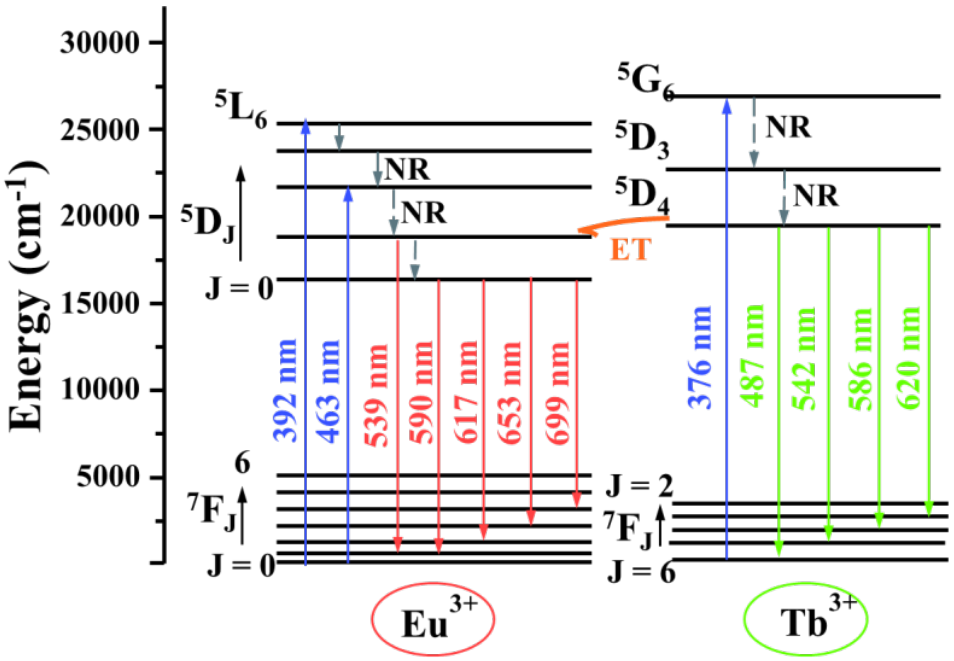


Figure 3.6 Energy transfer from terbium to europium.

Confirmation of sensitized europium emission upon terbium excitation at 488 nm indicates successful energy transfer from terbium to europium. This finding provides a basis for the next phase of investigation, involving the usage of glucose-6-phosphate (G6P) to establish a competitive binding system and further probe the dynamics of complex formation and energy transfer.

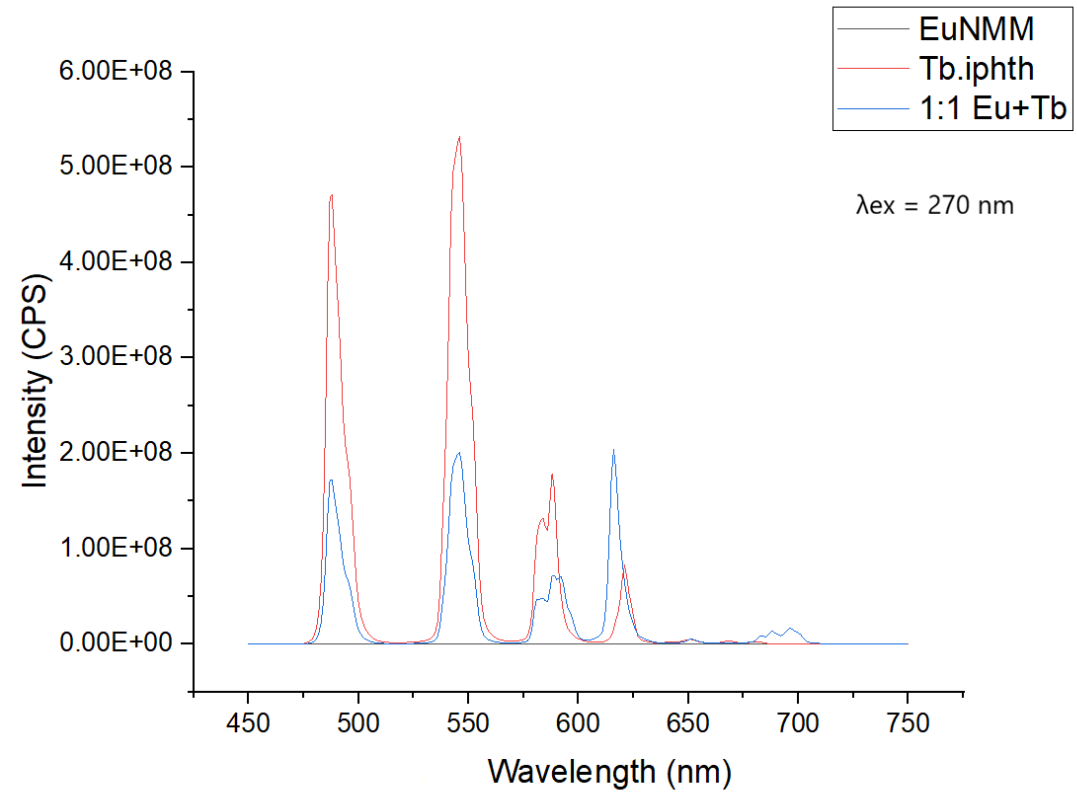


Figure 3.7 Comparison of the emission spectrum of the Eu.NMM, Tb.iphth and 1:1 Eu.NMM + Tb.iphth. Eu.NMM (black), Tb.iphth (red),1:1 Eu.NMM + Tb.iphth (blue). (λex = 270 nm). HEPES buffer (20 mM, pH 7.4); Eu.NMM (2.5 × 10^{-4} mol/L); Tb.iphth (2.5 × 10^{-4} mol/L), 25 ℃.

In the second set of samples, excitation was performed at 270 nm, shown in Figure 3.7. Under these conditions, Eu.NMM exhibited the lowest luminescence intensity (black line), while Tb.iphth showed the highest intensity (red line), and a strong terbium-centred emission was noted. Upon combining Eu.NMM with Tb.iphth in a 1:1 ratio, the overall emission intensity decreased compared with pure Tb.iphth. This quenching of terbium emission indicates energy transfer from the terbium centre to the europium centre. The overall trend observed with 270 nm excitation mirrors that found with 488 nm excitation, particularly in terms of reduction in terbium emission upon formation of the mixed Eu–Tb system.

Mechanisms

Two mechanisms may happen within the Eu.NMM and Tb.iphth to explain the observed luminescence behaviour. For excitation at 488 nm, which is direct and selective excitation to the terbium centre, the energy may transfer to the nearby Eu^{3+} centre through the self-assembled linker aminoisophthalate bridge. The first mechanism is a stepwise donor–acceptor energy transfer, driven by the spatial proximity. Secondly, for the excitation at 270 nm, which excites the aryl antenna, the energy is subsequently transferred to the terbium ion. Later, this excited terbium can transfer the energy to the europium centre. The second mechanism is an indirect two-step sensitization process employing the antenna-mediated step. Both energy transfer mechanisms lead to europium characteristic emission from $^5D_0 \rightarrow {}^7F_J$ transitions, notably at ~590 nm ($\Delta J = 1$) and ~617 nm ($\Delta J = 2$). Except for the main observation discussed above, the other results are summarised in the Table below.

Table 3.3 Observation table for Eu.NMM + Tb.iphth system.

Condition	Observation	Interpretation
Eu.NMM only at 488 nm	Nearly no emission	Confirms Eu^{3+} not excited directly at 488 nm
Tb.iphth only at 488 nm	Only Tb^{3+} emission	(Control)
1:1 Eu.NMM + Tb.iphth at 488 nm	Emission at ~617 nm	Eu^{3+} emission via ET from Tb^{3+}
Eu.NMM only at 270 nm	Weak Eu^{3+} emission	Eu^{3+} is naturally weak compared with Tb^{3+} emission
Tb.iphth only at 270 nm	Only Tb^{3+} emission	(Control)
1:1 Eu.NMM + Tb.iphth at 270 nm	Stronger Eu^{3+} emission vs excitation at 488nm	Possible dual sensitization or Tb→Eu ET

3.7 Part 2: Experiment for Competitive Binding Assay of EuNMM and Tb.iphth with G6P

Objective

To investigate the competitive binding behaviour of glucose-6-phosphate (G6P) in disrupting the supramolecular assembly between Eu.NMM and Tb.iphth, using luminescence spectroscopy to monitor changes in emission intensity and energy transfer.

Measurement Procedure

Emission spectra of all samples were recorded at the same two excitation wavelengths, as compared to Part 1, to investigate energy transfer and binding interactions. Initially, samples were excited at 488 nm to selectively target the terbium(III) centre, followed by excitation at 270 nm to excite the aryl chromophore and analyse antenna-mediated sensitisation. Spectral analysis should focus on changes in peak intensity and shifts to evaluate the formation or disruption of supramolecular assemblies and the occurrence of intermetallic energy transfer.

Experimental Confirmation to Verify Competitive Binding

To confirm the competitive binding of Eu.NMM +Tb.iphth/G6P, luminescence emission spectra were recorded. The emergence of the Eu^{3+} specific emission peak at 617 nm ($^5D_0 \rightarrow {}^7F_2$) and the disappearance of the Tb^{3+} specific emission peak at 620 nm ($^5D_4 \rightarrow {}^7F_3$) were taken as evidence of successful displacement.

To investigate competitive binding, two sets of samples were prepared: one containing 1 equivalent of G6P and the other containing 10 equivalents (Figure 3.8). All samples were excited at 488 nm under identical experimental conditions. Upon addition of 1 equivalent of G6P to the 1:1 Eu+Tb mixture, a decrease in luminescence intensity was found (blue line), while the emission peak positions remained unchanged compared with the 1:1 Eu+Tb sample (green line). This suggests that G6P began to compete with the Tb.iphth, partially disrupting the ternary Tb–Eu–Eu complex. However, as the original Tb–Eu–Eu complex remained the dominant species, the spectral profile, particularly the peak positions, was still largely preserved.

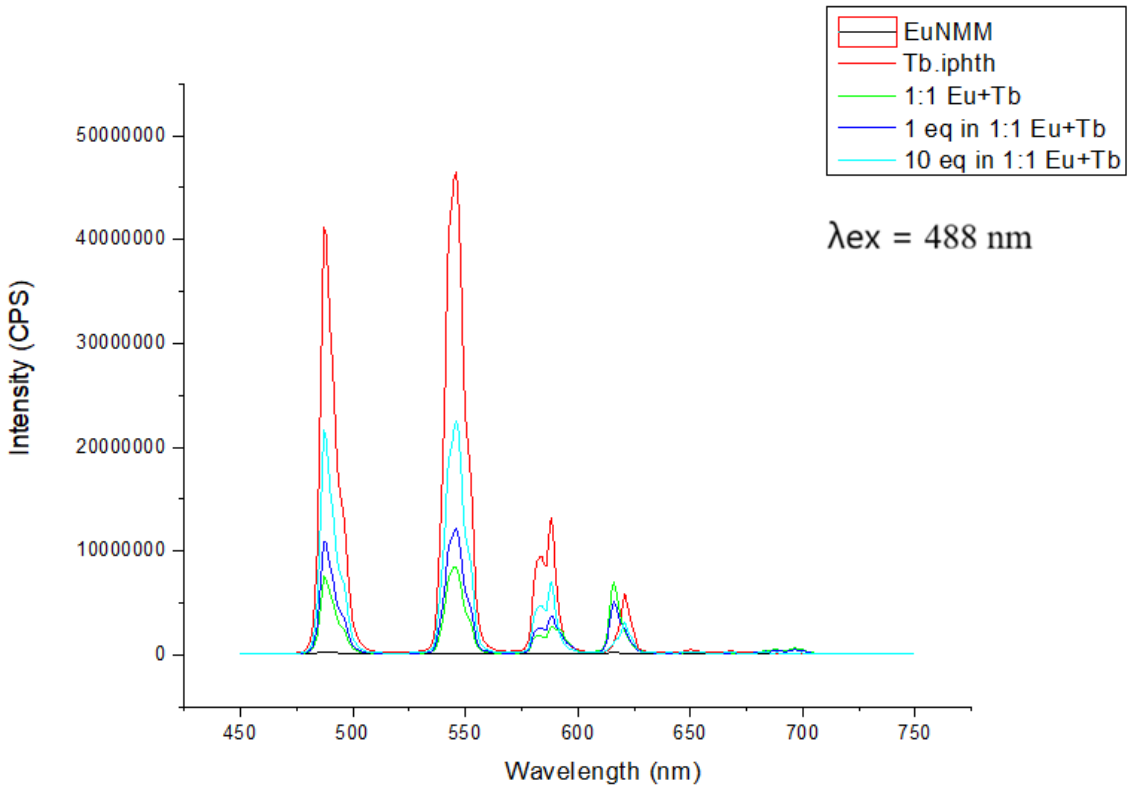


Figure 3.8 Comparison of the emission spectrum of the Eu.NMM + Tb.iphth/G6P. Eu.NMM (black); Tb.iphth (red);1:1 Eu.NMM + Tb.iphth (green); 1 eqv. of G6P in 1:1 Eu.NMM + Tb.iphth (blue); 10 eqv. of G6P in 1:1 Eu.NMM + Tb.iphth (sky blue).(λex = 488 nm). HEPES buffer (20 mM, pH 7.4); Eu.NMM (2.5 × 10^{-4} mol/L); Tb.iphth (2.5 × 10^{-4} mol/L), 25 ºC.

In contrast, the addition of 10 equivalents of G6P resulted in a more remarkable decrease in luminescence intensity (sky blue line) and noticeable shifts in the emission peaks in the 610–625 nm region. A more detailed comparison of peak shifts is shown in Figure 3.9. These peak positions matched those of the pure Tb.iphth complex, indicating that the ternary complex had been effectively disrupted. At this higher concentration, G6P outcompeted the isophthalate ligands for coordination to the lanthanide centres, leading to the release of free Tb.iphth as the predominant species in solution. The positions of the peaks in this 10 eqv. G6P sample were the same to pure Tb.iphth which indicates10 eqv. of G6P broke the system of 1:1 Eu+Tb and now the majority in the mixture was unbound Tb.iphth. For excitation at 270 nm (Figure 3.10 &11), similar trend appears compared with 488 nm (Figure 3.8 &9).

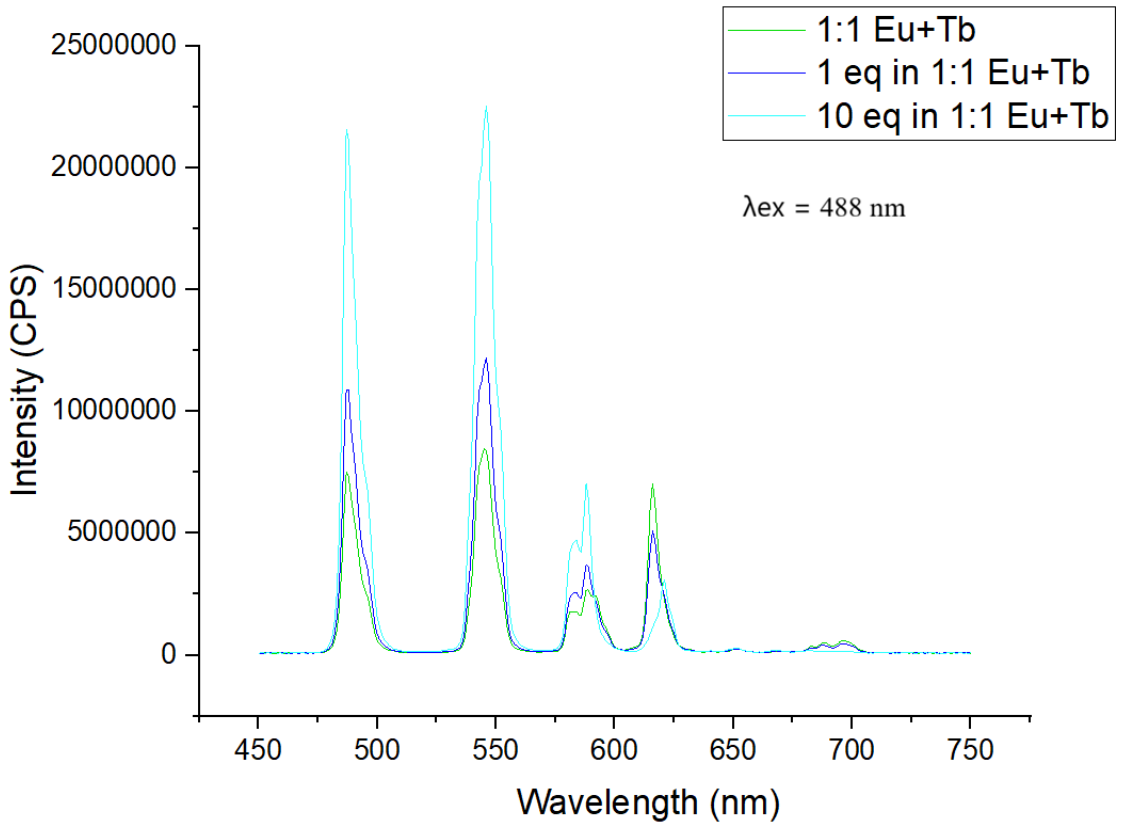


Figure 3.9 Comparison of the emission spectrum of the Eu.NMM + Tb.iphth/G6P. 1:1 Eu.NMM + Tb.iphth (green); 1 eqv. of G6P in 1:1 Eu.NMM + Tb.iphth (blue); 10 eqv. of G6P in 1:1 Eu.NMM + Tb.iphth (sky blue).(λex = 488 nm). HEPES buffer (20 mM, pH 7.4); Eu.NMM (2.5 × 10^{-4} mol/L); Tb.iphth (2.5 × 10^{-4} mol/L), 25 ºC.

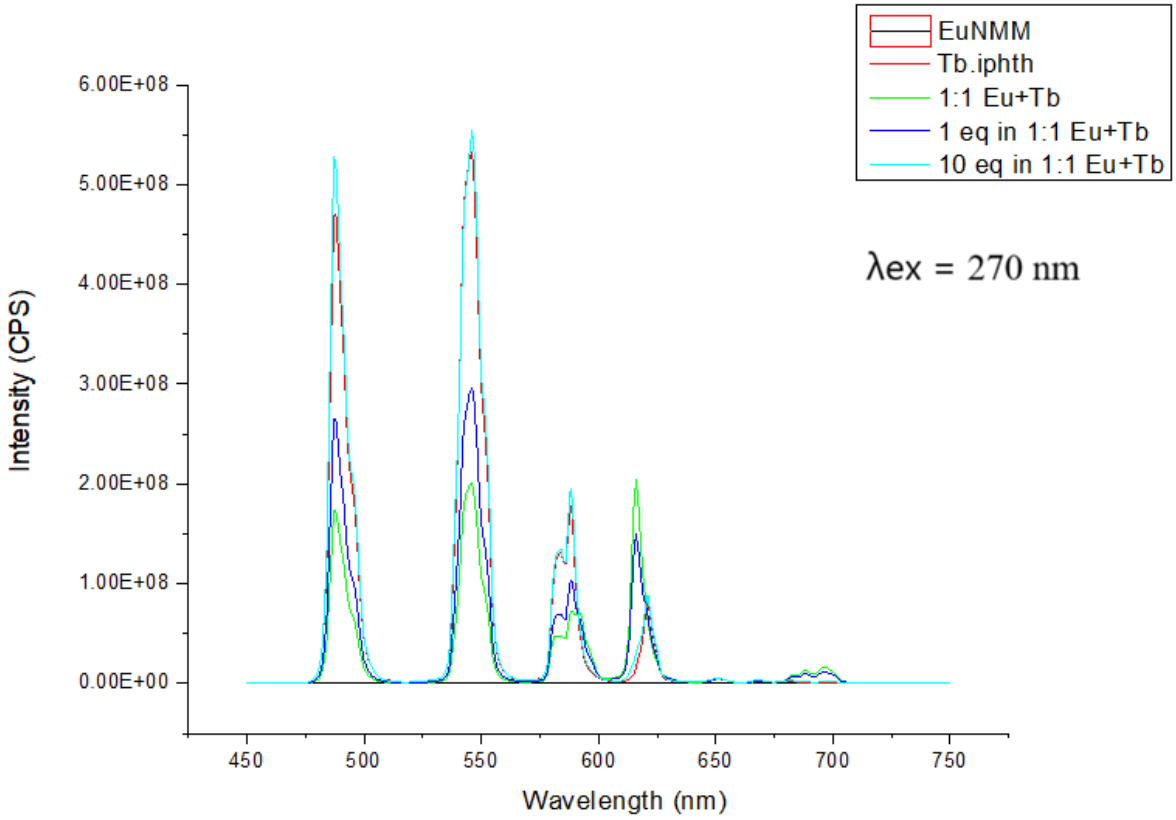


Figure 3.10 Comparison of the emission spectrum of the Eu.NMM + Tb.iphth/G6P. Eu.NMM (black); Tb.iphth (red);1:1 Eu.NMM + Tb.iphth (green); 1 eqv. of G6P in 1:1 Eu.NMM + Tb.iphth (blue); 10 eqv. of G6P in 1:1 Eu.NMM + Tb.iphth (sky blue).(λex = 270 nm). HEPES buffer (20 mM, pH 7.4); Eu.NMM (2.5 × 10^{-4} mol/L); Tb.iphth (2.5 × 10^{-4} mol/L), 25 ºC.

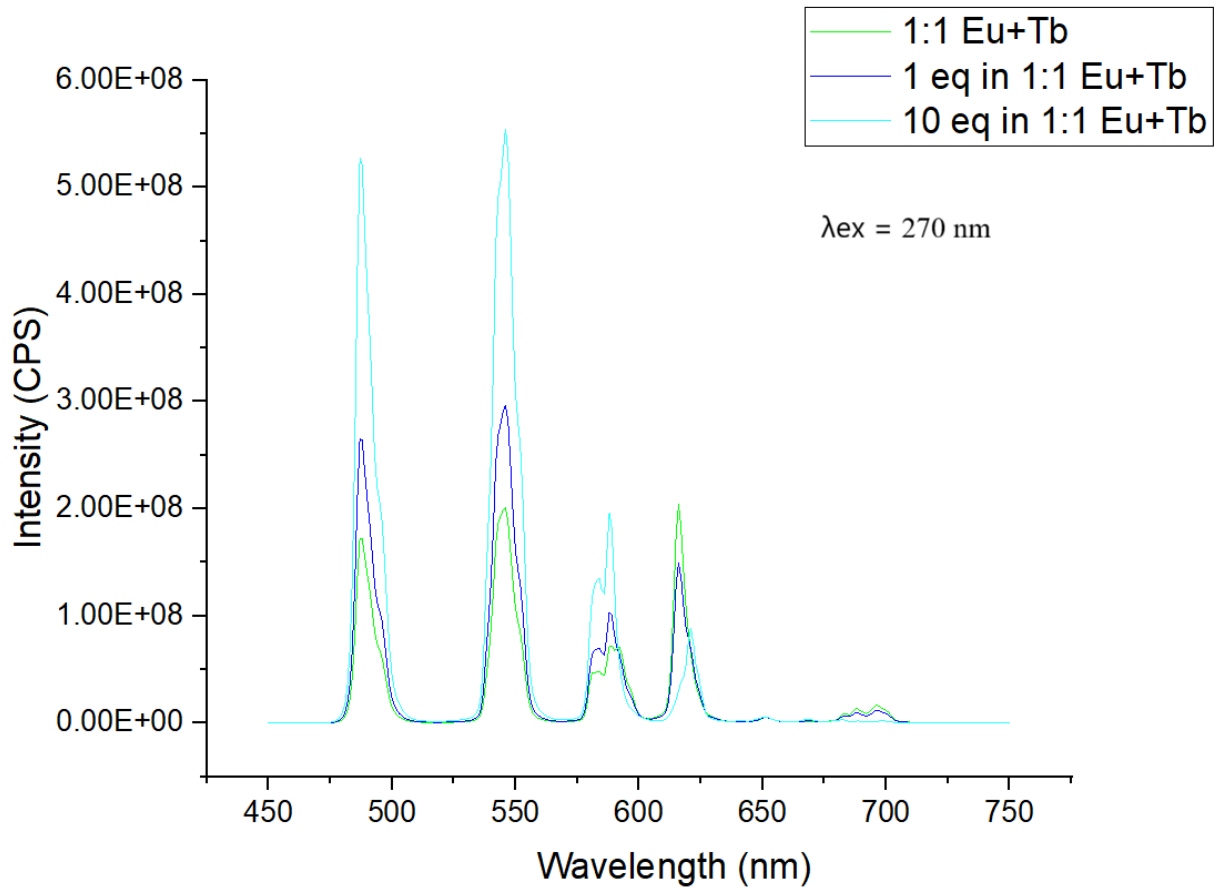


Figure 3.11 Comparison of the emission spectrum of the Eu.NMM + Tb.iphth/G6P. 1:1 Eu.NMM + Tb.iphth (green); 1 eqv. of G6P in 1:1 Eu.NMM + Tb.iphth (blue); 10 eqv. of G6P in 1:1 Eu.NMM + Tb.iphth (sky blue). (λex = 270 nm). HEPES buffer (20 mM, pH 7.4); Eu.NMM (2.5×10^{-4} mol/L); Tb.iphth (2.5×10^{-4} mol/L), 25 ºC.

In addition to the significant changes in spectral behaviour discussed above, another important change is summarised in Table 3.4. The terbium emission at 545 nm ($^5D_4 \rightarrow {}^7F_5$), the peak is the strongest in pure Tb.iphth form, after the addition of Eu.NMM, the emission is quenched. But after the G6P disrupts the Eu-Tb complex, the emission is recovered.

Table 3.4 Key assignments of Eu.NMM + Tb.iphth/G6.

Ion	Emission Wavelength (nm)	Assignment / Transition	Spectral Behaviour
Tb^{3+}	~545	$^5D_4 \rightarrow {}^7F_5$	Strong when unbound or after G6P disrupts the Eu–Tb complex (e.g., in 10 eqv. G6P)
Tb^{3+}	~620	$^5D_4 \rightarrow {}^7F_3$	Strong when unbound or after G6P disrupts the Eu–Tb complex (e.g., in 10 eqv. G6P)
Eu^{3+}	~617	$^5D_0 \rightarrow {}^7F_2$ (electric dipole, hypersensitive)	Strongest in 1:1 Eu + Tb due to Tb → Eu energy transfer; decreases with G6P addition

Mechanism of Energy Transfer and Disruption by G6P

The luminescent behaviour observed in the Eu.NMM and Tb.iphth system can be explained as two primary energy transfer mechanisms, and the addition of glucose-6-phosphate (G6P) as a competitive displacer—the supramolecular complex formed by mixing Eu.NMM and Tb.iphth in a 1:1 ratio is expected to support efficient energy transfer from Tb^{3+} to Eu^{3+}, either through direct donor–acceptor exchange or antenna-mediated pathways, depending on the excitation source. In both mechanisms, G6P will break the bridging coordination between Eu.NMM and Tb.iphth. This disrupts the energy transfer pathways and causes distinct spectral responses, allowing for the quantitative interpretation of the binding equilibrium. Except for the main observation discussed above, the other results are summarised in the table below.

Table 3.5 Observation table for Eu.NMM + Tb.iphth/G6P system.

Sample @ 488 nm	**Tb^{3+} Emission (~545 nm)**	**Tb^{3+} Emission (~620 nm)**	**Eu^{3+} Emission (~590 nm)**	**Eu^{3+} Emission (~617 nm)**	**Interpretation**
EuNMM only	Absent	Absent	Weak	Weak	Eu^{3+} not directly excitable at 488 nm
Tb.iphth only	Strong	Strong	Absent	Absent	Direct Tb^{3+} excitation; no Eu present
1:1 Eu + Tb	Quenched	Absent	Strong	Strong	Energy transfer from Tb^{3+} to Eu^{3+}
1 eqv. G6P in 1:1 Eu + Tb	Partially restored	Absent	Slightly decreased	Slightly decreased	Partial disruption of Eu–Tb assembly by G6P
10 eqv. G6P in 1:1 Eu + Tb	Strong	Strong	Nearly gone	Gone	Dissociation of complex; spectral profile resembles that of Tb.iphth

Saturation of G6P

To investigate at which concentration of glucose-6-phosphate (G6P) can fully disrupt the Eu.NMM–Tb.iphth assembly, a saturation titration experiment was performed. Emission spectra were recorded for a 1:1 mixture of Eu.NMM and Tb.iphth while incrementally increasing the concentration of G6P from 0 to 100 equivalents (Figure 3.12 & 13).

In all of the spectra, the 545 nm peak, which corresponds to the $^5D_4$ to $^7F_5$ transition of terbium(III), increases significantly from 0 to 1 eqv. of G6P, shown in Figure 3.12. This change shows disruption of the Eu–Tb supramolecular binding, leading to recovery of Tb^{3+} emission. From 2 to 10 equivalents of G6P, the emission intensity continues to increase, but at a slower

rate. This result means that G6P is gradually binding to the available Eu.NMM sites, breaking down the remaining assembled complexes.

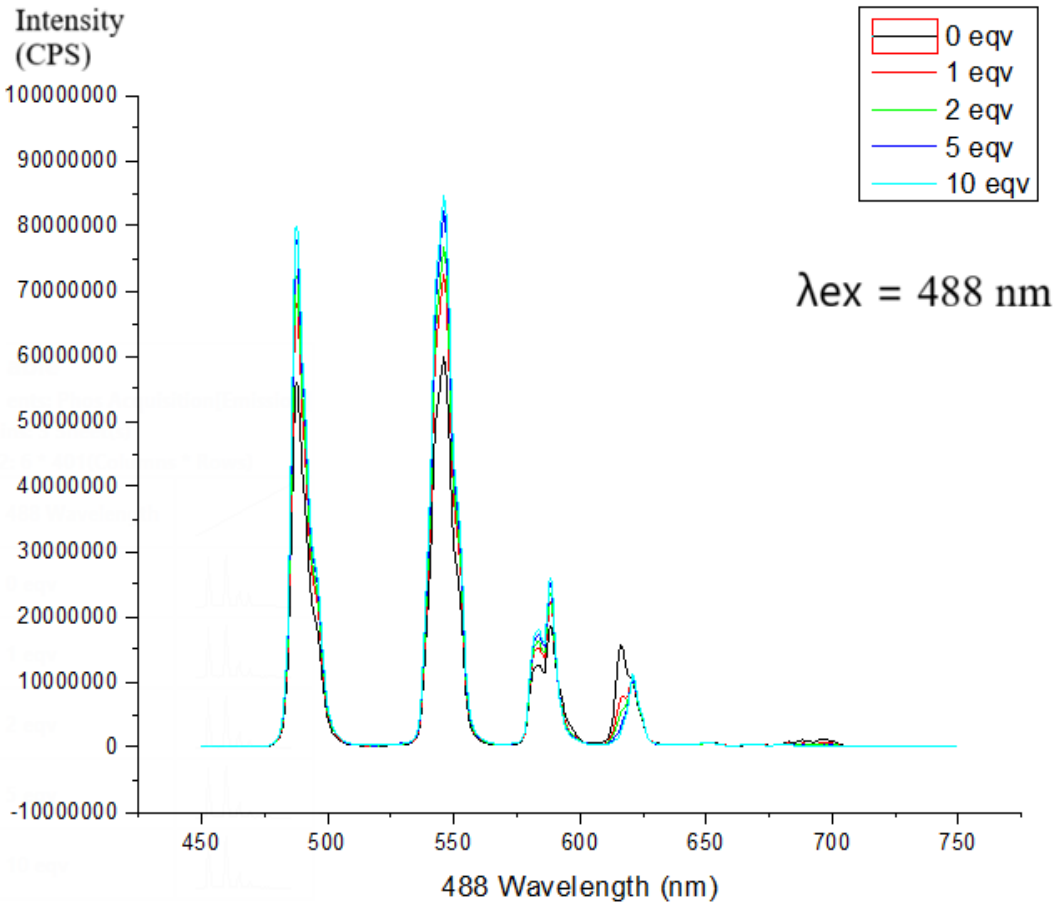


Figure 3.12 Comparison of the emission spectrum of the Eu.NMM + Tb.iphth/G6P. 1:1 Eu.NMM + Tb.iphth (black); 1 eqv. of G6P in 1:1 Eu.NMM + Tb.iphth (red); 10 eqv. of G6P in 1:1 Eu.NMM + Tb.iphth (sky blue). (λex = 488 nm). HEPES buffer (20 mM, pH 7.4); Eu.NMM (2.5 × 10^{-4} mol/L); Tb.iphth (2.5 × 10^{-4} mol/L), 25 ºC.

When the amount of G6P is further added to 50 and 100 equivalents, shown in Figure 3.13, the emission spectra remain similarly in both shape and intensity, indicating that saturation is achieved at approximately 50 eqv. of G6P.

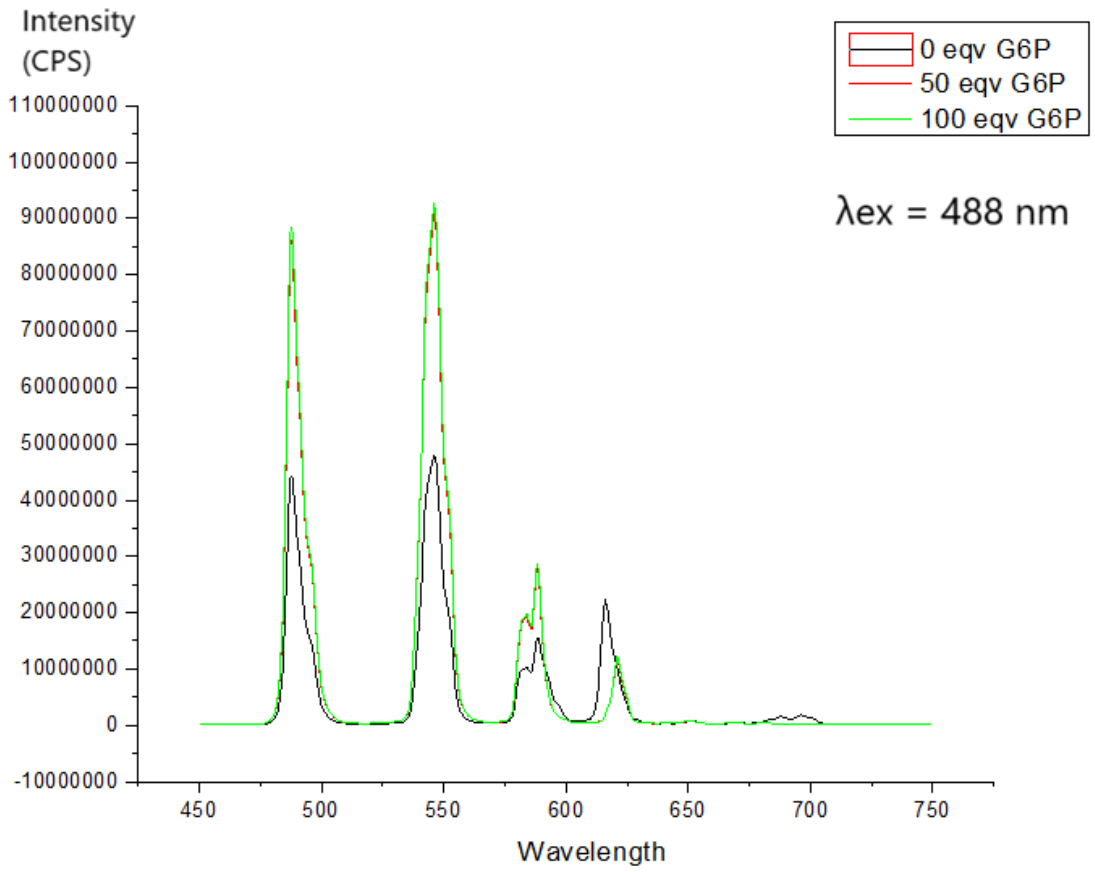


Figure 3.13 Comparison of the emission spectrum of the Eu.NMM + Tb.iphth/G6P. 1:1 Eu.NMM + Tb.iphth (black); 50 eqv. of G6P in 1:1 Eu.NMM + Tb.iphth (red); 100 eqv. of G6P in 1:1 Eu.NMM + Tb.iphth (blue). (λex = 488 nm). HEPES buffer (20 mM, pH 7.4); Eu.NMM (2.5×10^{-4} mol/L); Tb.iphth (2.5×10^{-4} mol/L), 25 ℃.

3.8 FBP for Competitive Binding

To extend the competitive binding study of the Eu.NMM–Tb.iphth system, we used another structurally similar guest fructose-1,6-bisphosphate (FBP), compared with glucose-6-phosphate (G6P). Both of them are the major intermediates in glycolysis, and both of them have phosphate groups which can fit into the lanthanide coordination sites. Furthermore, the bisphosphate structure in FBP may influence its binding affinity and displacement capability.

A series of emission spectra were collected using the 1:1 Eu.NMM + Tb.iphth complex as the host, with incremental additions of FBP ranging from 0.25 to 10 equivalents (Figure 3.14 & 15). Excitation wavelengths 270 nm was used to selectively probe direct terbium excitation and antenna-mediated sensitization, respectively.

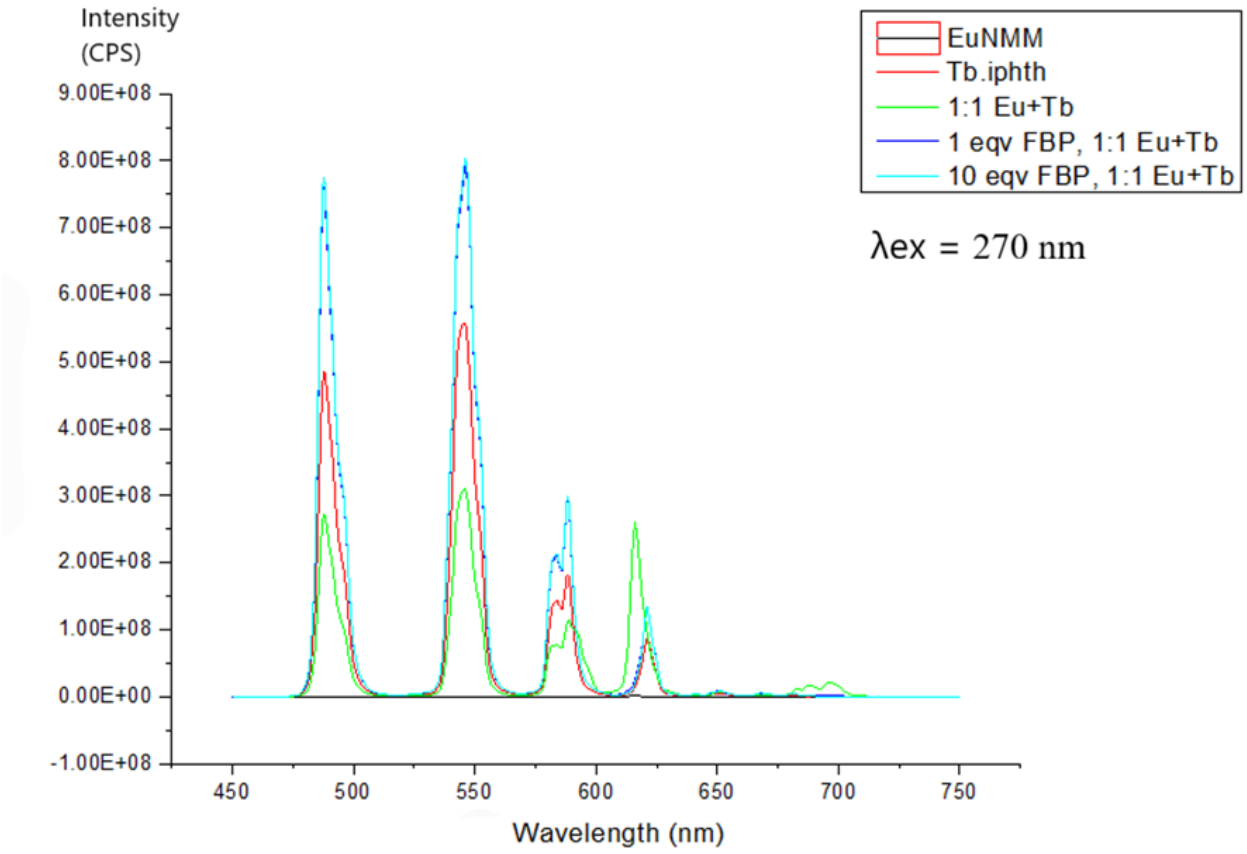


Figure 3.14 Comparison of the emission spectrum of the Eu.NMM + Tb.iphth/FBP. Eu.NMM (black); Tb.iphth (red); 1:1 Eu.NMM + Tb.iphth (green); 1 eqv. of FBP in 1:1 Eu.NMM + Tb.iphth (blue); 10 eqv. of FBP in 1:1 Eu.NMM + Tb.iphth (sky blue). (λex = 270 nm). HEPES buffer (20 mM, pH 7.4); Eu.NMM (2.5 × 10^{-4} mol/L); Tb.iphth (2.5 × 10^{-4} mol/L), 25 ℃.

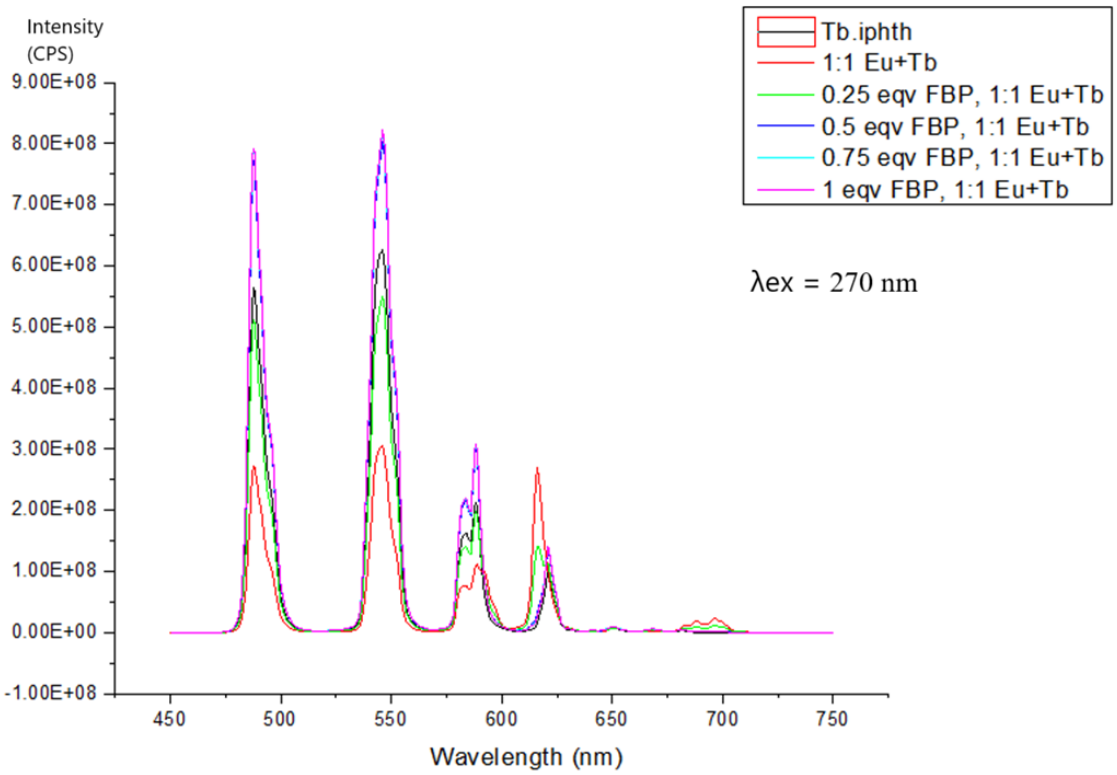


Figure 3.15 Comparison of the emission spectrum of the Eu.NMM + Tb.iphth/FBP. Tb.iphth (black); 1:1 Eu.NMM + Tb.iphth (red); 0.25 eqv. of FBP in 1:1 Eu.NMM + Tb.iphth (green); 1 eqv. of FBP in 1:1 Eu.NMM + Tb.iphth (plum). (λex = 270 nm). HEPES buffer (20 mM, pH 7.4); Eu.NMM (2.5 × 10^{-4} mol/L); Tb.iphth (2.5 × 10^{-4} mol/L), 25 ℃.

In contrast to G6P, the FBP-triggered spectral changes occurred more rapidly and reached saturation at significantly lower concentrations. The luminescence intensity of the displacement system reached saturation after adding a small amount of FBP, and further addition of FBP led to a minimal increase. This rapid saturation suggests that FBP have a stronger binding affinity to the lanthanide complex, due to the additional phosphate and its bidentate coordination sites.

3.9 Gd.NMM for Competitive Binding with G6P

To further understand the mechanism of energy transfer and displacement in the Eu.NMM–Tb.iphth system, we continued a control study with Gd.NMM to replace the luminescent Eu.NMM. Gadolinium(III), unlike Eu^{3+} and Tb^{3+}, does not exhibit observable f–f emission under typical photophysical conditions due to its electronic configuration ($^8S_{7/2}$ ground state). As Gd^{3+} cannot accept energy resonantly from Tb^{3+} nor emit luminescence, it could introduce quenching pathways through ligand assembly.

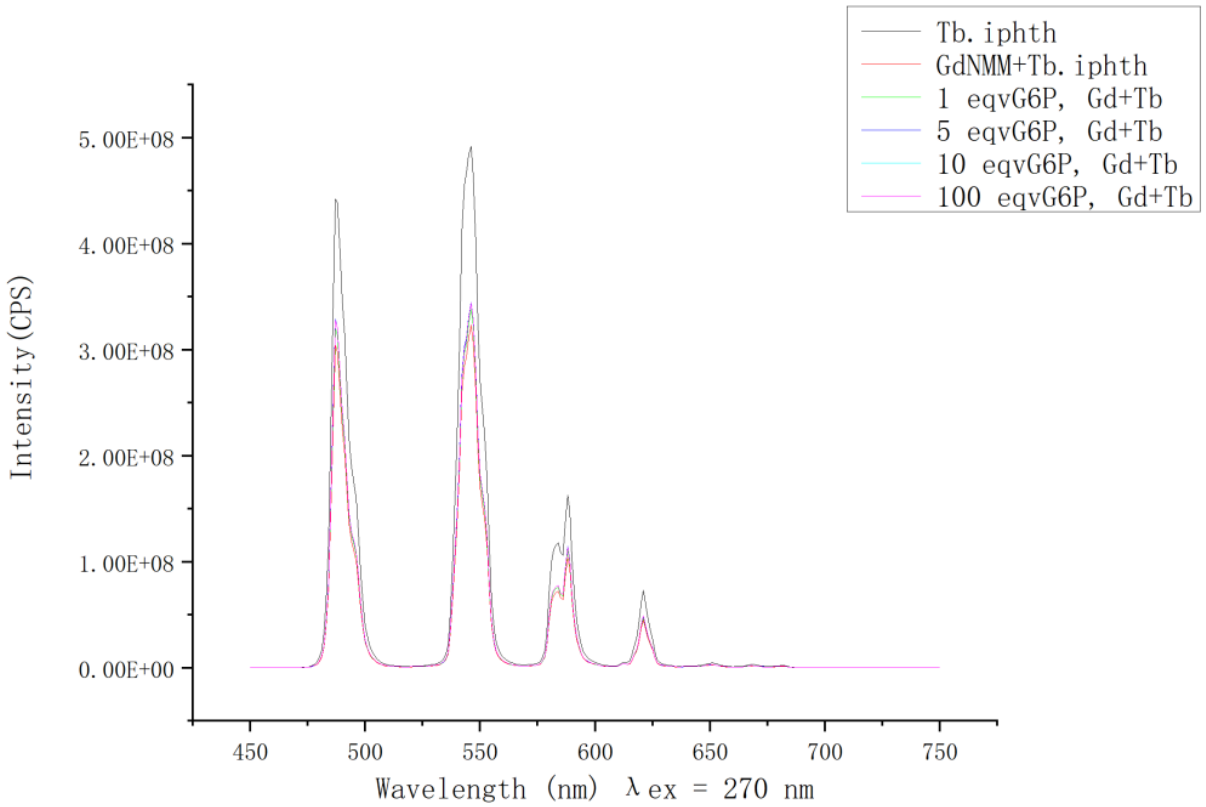


Figure 3.16 Comparison of the emission spectrum of the Gd.NMM + Tb.iphth/G6P. Tb.iphth (black); 1:1 Gd.NMM + Tb.iphth (red); 100 eqv. of G6P in 1:1 Gd.NMM + Tb.iphth (plum). (λex = 270 nm). HEPES buffer (20 mM, pH 7.4); Gd.NMM (2.5 × 10^{-4} mol/L); Tb.iphth (2.5 × 10^{-4} mol/L), 25 ºC.

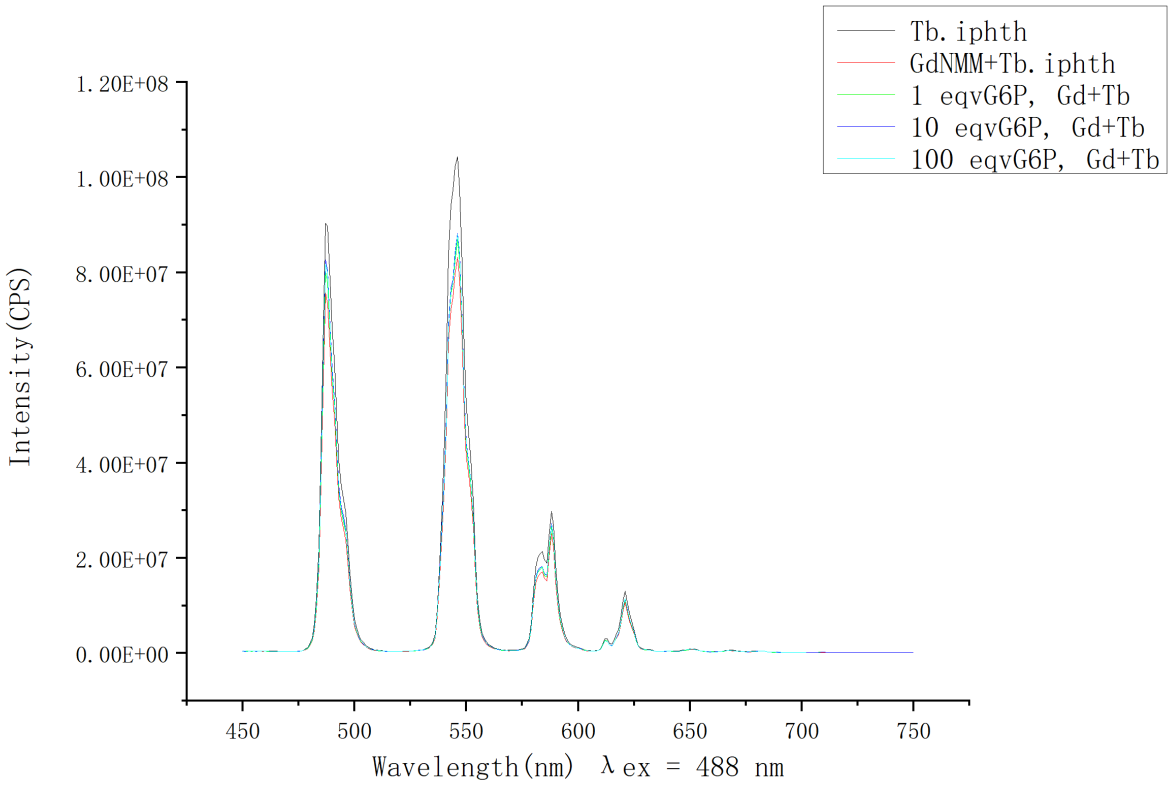


Figure 3.17 Comparison of the emission spectrum of the Gd.NMM + Tb.iphth/G6P. Tb.iphth (black); 1:1 Gd.NMM + Tb.iphth (red); 100 eqv. of G6P in 1:1 Gd.NMM + Tb.iphth (sky blue). (λex = 488 nm). HEPES buffer (20 mM, pH 7.4); Gd.NMM (2.5 × 10^{-4} mol/L); Tb.iphth (2.5 × 10^{-4} mol/L), 25 ℃.

Emission spectra were recorded under both 488 nm (selective Tb excitation) and 270 nm (antenna excitation) to monitor any changes in Tb^{3+} emission and to assess whether Gd.NMM could facilitate or interfere with energy transfer processes (Figure 3.16 & 17).

Interestingly, in the 1:1 mixture of Gd.NMM and Tb.iphth system, there is a notable decrease in Tb^{3+} emission intensity, which differs from the expected result. As Gd^{3+} cannot accept energy resonantly from Tb^{3+} nor emit luminescence, this indicates that Gd.NMM quenches the Tb.iphth luminescence through energy transfer from the aromatic ring from Tb.iphth to Gd.NMM. The schematic below shows how this energy transfer happens. When 270 nm

excitation wavelength is used (Figure 3-18 left half), the fluorophore absorbs the energy and which is subsequently transferred to the Gd.NMM complex via the nitro (-NO_2) group. This interaction leads to approximately a 30% decrease in terbium emission, indicating quenching happens.

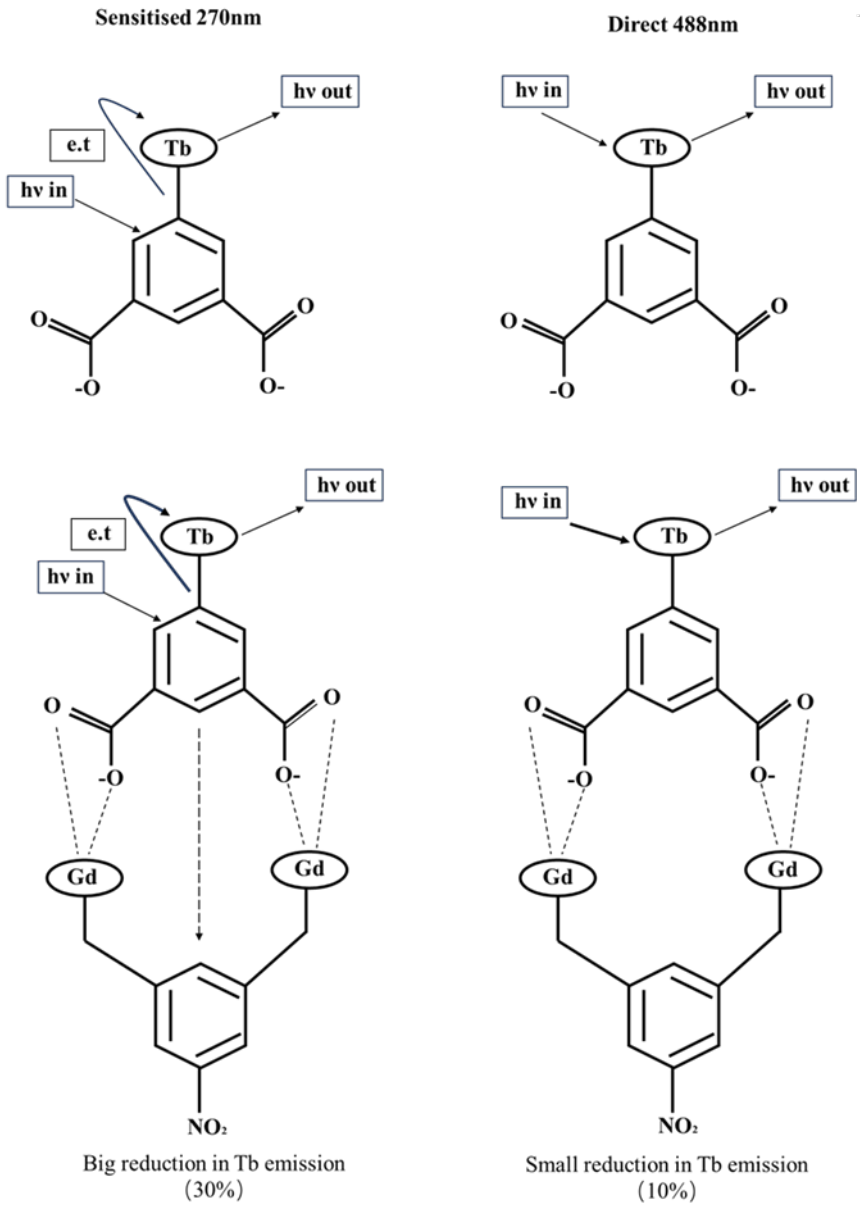


Figure 3.18 Mechanism of energy transfer in a 1:1 mixture of Gd.NMM and Tb.iphth system. (λex = 270 & 488 nm).

In contrast, when 488 nm excitation wavelength is used for the direct excitation at the Tb (Figure 3.18 right half), energy remains predominantly localized at the terbium site, leading to only a slight reduction in luminescence intensity, further addition of G6P to the Gd.NMM + Tb.iphth system did not restore Tb^{3+} emission, in contrast to the Eu.NMM. In the NMM system, where G6P competes with the bridging ligand and restores Tb^{3+} emission by breaking the energy-transfer pathway, no such recovery occurred here. This suggests that Gd.NMM may disrupt the luminescent geometry or increase non-radiative decay channels in a way that G6P cannot reverse. A proposed mechanism is shown below to illustrate the addition of G6P into Gd.NMM + Tb.iphth system and Eu.NMM + Tb.iphth system.

Overall, the use of Gd.NMM confirms that Gd^{3+} does not participate in energy transfer, and quenching observed in Gd–Tb mixtures arises from non-luminescent interactions rather than optical absorption or antenna competition.

This experiment suggests that emission switching in Eu.NMM-Tb.iphth systems are lanthanide-specific, and the luminescent outcome is tied to the photophysical properties of Eu^{3+} and Tb^{3+} ions. The Table below shows how these two dynamic binding behaviour differ (Table 3.6). Although Gd.NMM is structurally similar to Eu.NMM, the binding behaviour is different after the addition of G6P to form a G6P-Gd.NMM-Tb.iphth complex. Unlike the Eu.NMM-Tb.iphth system, Tb^{3+} emission can be recovered after the addition of G6P, with G6P-Gd.NMM-Tb.iphth provides a valuable non-emissive system for understanding the competitive binding mechanism observed in this study. The schematic mechanism graph below shows how these two dynamic binding behaviour may differ (Figure 3.19).

System	Emission Behaviour	Effect of G6P Addition	Interpretation
Tb.iphth only	Strong Tb^{3+} emission at ~545 nm	No significant change	Tb^{3+} emission intact; no binding competition
Eu.NMM + Tb.iphth (1:1)	Tb emission quenched; Eu emission enhanced	G6P disrupts assembly; Tb emission restored; Eu quenched	Energy transfer Tb → Eu confirmed; G6P breaks the supramolecular complex
Gd.NMM + Tb.iphth (1:1)	Tb emission reduced (quenched)	G6P does not restore Tb emission	Gd^{3+} acts as non-emissive quencher; no energy transfer or recovery

Table 3.6 Comparison of Gd.NMM and Eu.NMM in Competitive Binding with Tb.iphth and G6P.

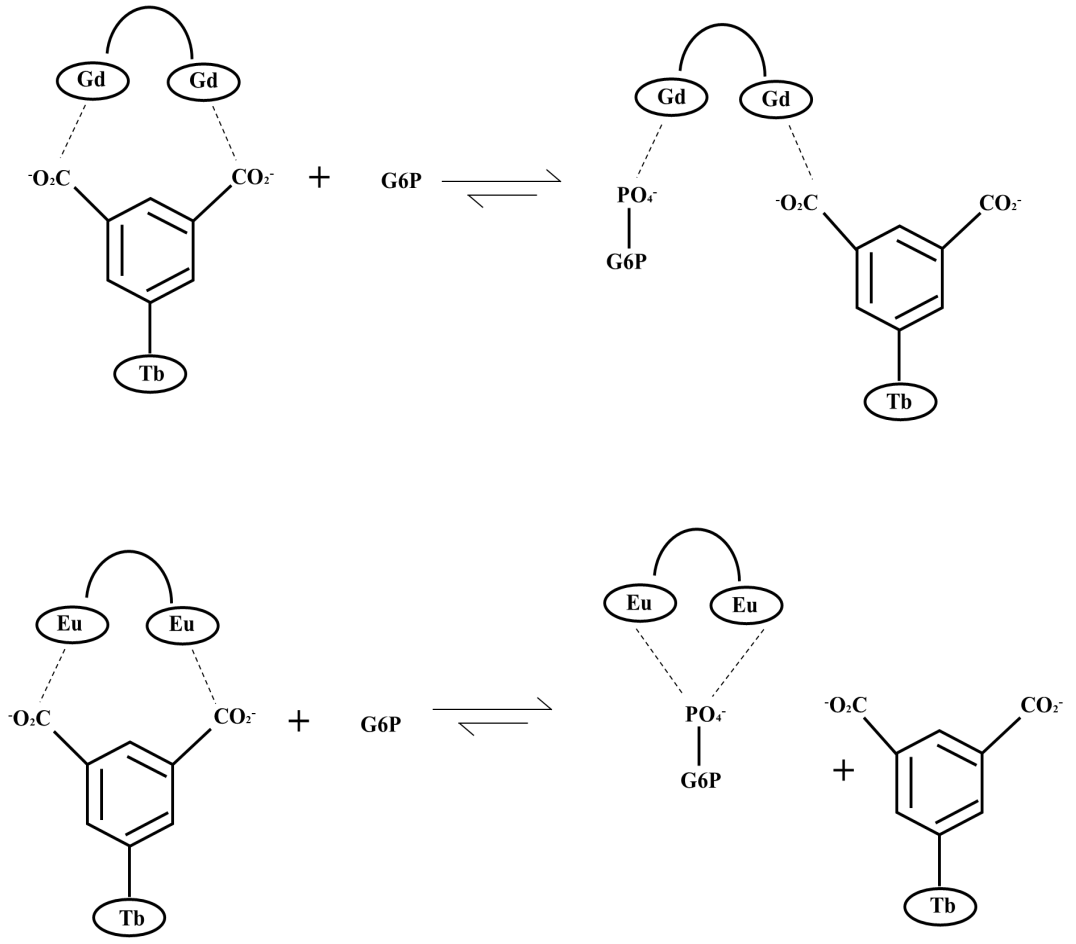


Figure 3.19 Comparison of the dynamic binding behaviour of Gd.NMM and Eu.NMM in Ln.NMM + Tb.iphth/G6P system.

3.10 Comparative Binding Behaviour of FBP and G6P in the Gd.NMM – Tb.iphth System

To investigate the influence of phosphate-containing analytes on the luminescence and binding properties of the Gd.NMM–Tb.iphth system, both glucose-6-phosphate (G6P) and fructose-1,6-bisphosphate (FBP) were used as potential displacing guests. For the Eu.NMM–Tb.iphth system, both of the G6P and FBP had similar responses, but some different results were observed here. Two titration groups are present here: under excitation at 270 nm and 488 nm (Figures 3-20 & 21). After adding a minimum amount of FBP (0.25 eqv.), saturation is achieved.

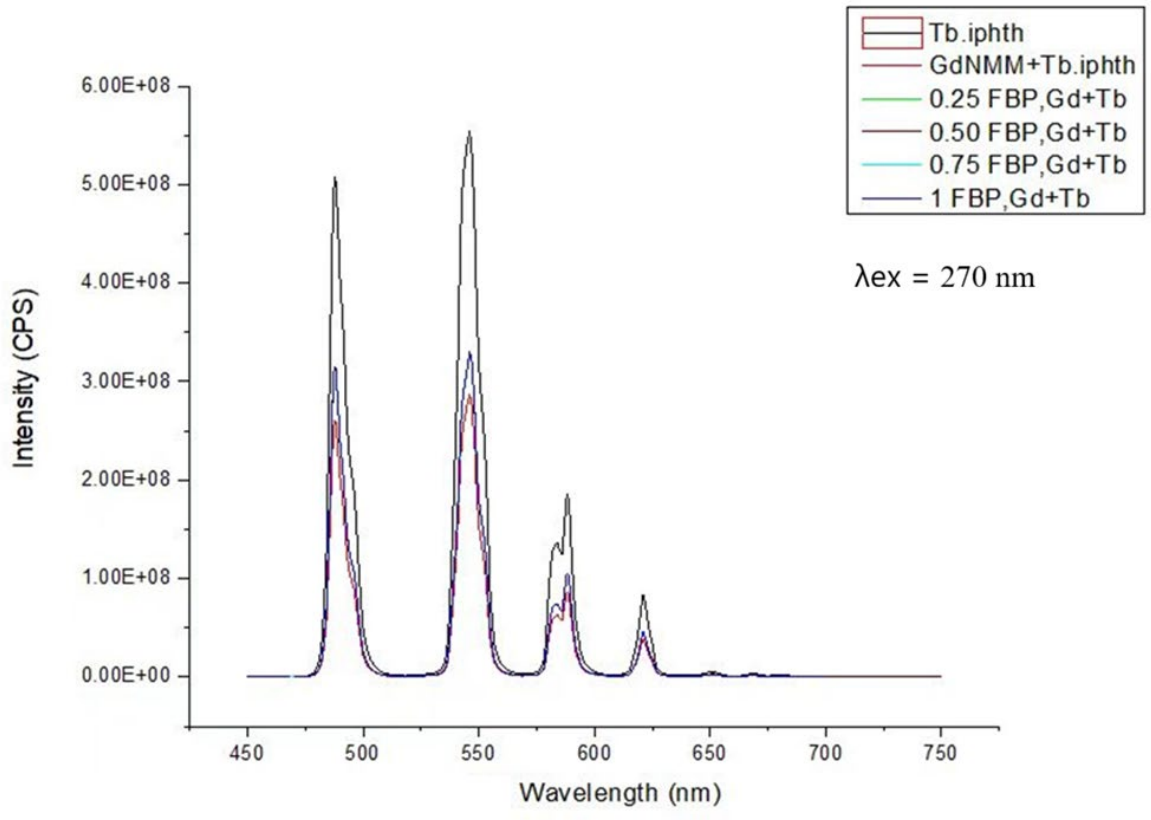


Figure 3.20 Comparison of the emission spectrum of the Gd.NMM + Tb.iphth/FBP. Tb.iphth (black); 1:1 Gd.NMM + Tb.iphth (red); 1 eqv. of FBP in 1:1 Gd.NMM + Tb.iphth (dark blue). (λex = 270 nm). HEPES buffer (20 mM, pH 7.4); Gd.NMM (2.5 × 10^{-4} mol/L); Tb.iphth (2.5 × 10^{-4} mol/L), 25 ºC.

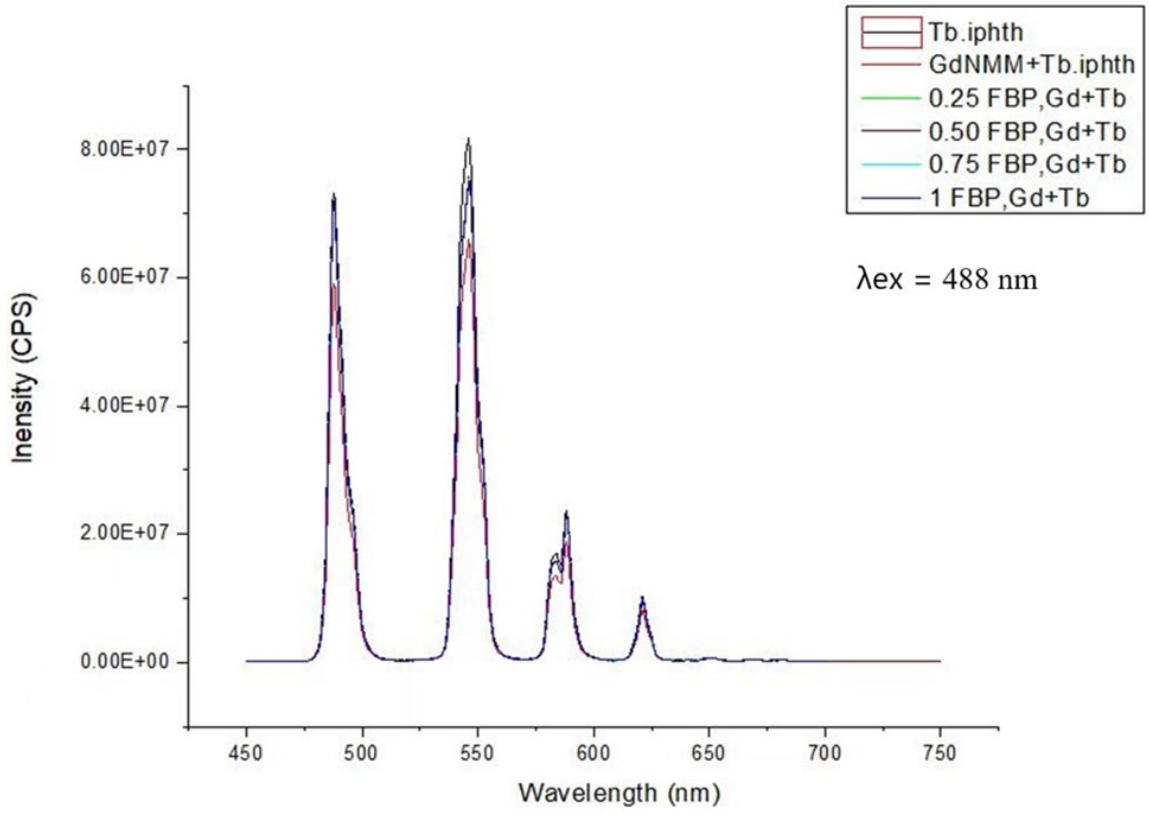


Figure 3.21 Comparison of the emission spectrum of the Gd.NMM + Tb.iphth/FBP. Tb.iphth (black); 1:1 Gd.NMM + Tb.iphth (red); 1 eqv. of FBP in 1:1 Gd.NMM + Tb.iphth (dark blue). (λex = 488 nm). HEPES buffer (20 mM, pH 7.4); Gd.NMM (2.5 × 10^{-4} mol/L); Tb.iphth (2.5 × 10^{-4} mol/L), 25 ºC.

In contrast, FBP demonstrated a markedly different response. Upon the addition of just 0.25 equivalents of FBP, a significant enhancement in Tb^{3+} emission was observed, and this intensity plateaued with further FBP addition. The rapid saturation of the emission response suggests that FBP binds strongly and selectively to the supramolecular complex, likely through multidentate interactions enabled by its bisphosphate structure. The Table below shows how these two dynamic binding behaviour differ (Table 3.7).

Table 3.7 Comparison Summary: Why FBP ≠ G6P

Feature	**G6P**	**FBP**
Number of phosphate groups	1	2 (bisphosphate)
Structural complexity	Monophosphate sugar	Bisphosphate sugar with more donor sites
Response in Gd–Tb system	No change in Tb emission (even at 100 eqv.)	Strong increase in Tb emission at 0.25 eqv.
Binding strength (relative)	Weak	Strong
Effect on quenching	None	Partially reverses Gd-induced quenching

The schematic mechanism graph below shows how these two dynamic binding behaviours differ. For G6P as a monophosphate sugar, it is more likely to form a G6P-Gd.NMM-Tb.iphth complex, which will stop the recovery of Tb^{3+} emission. For FBP as a bisphosphate sugar with more donor sites, it is more likely to bind strongly with Gd.NMM and leave Tb.iphth, helping the Tb^{3+} emission rise.

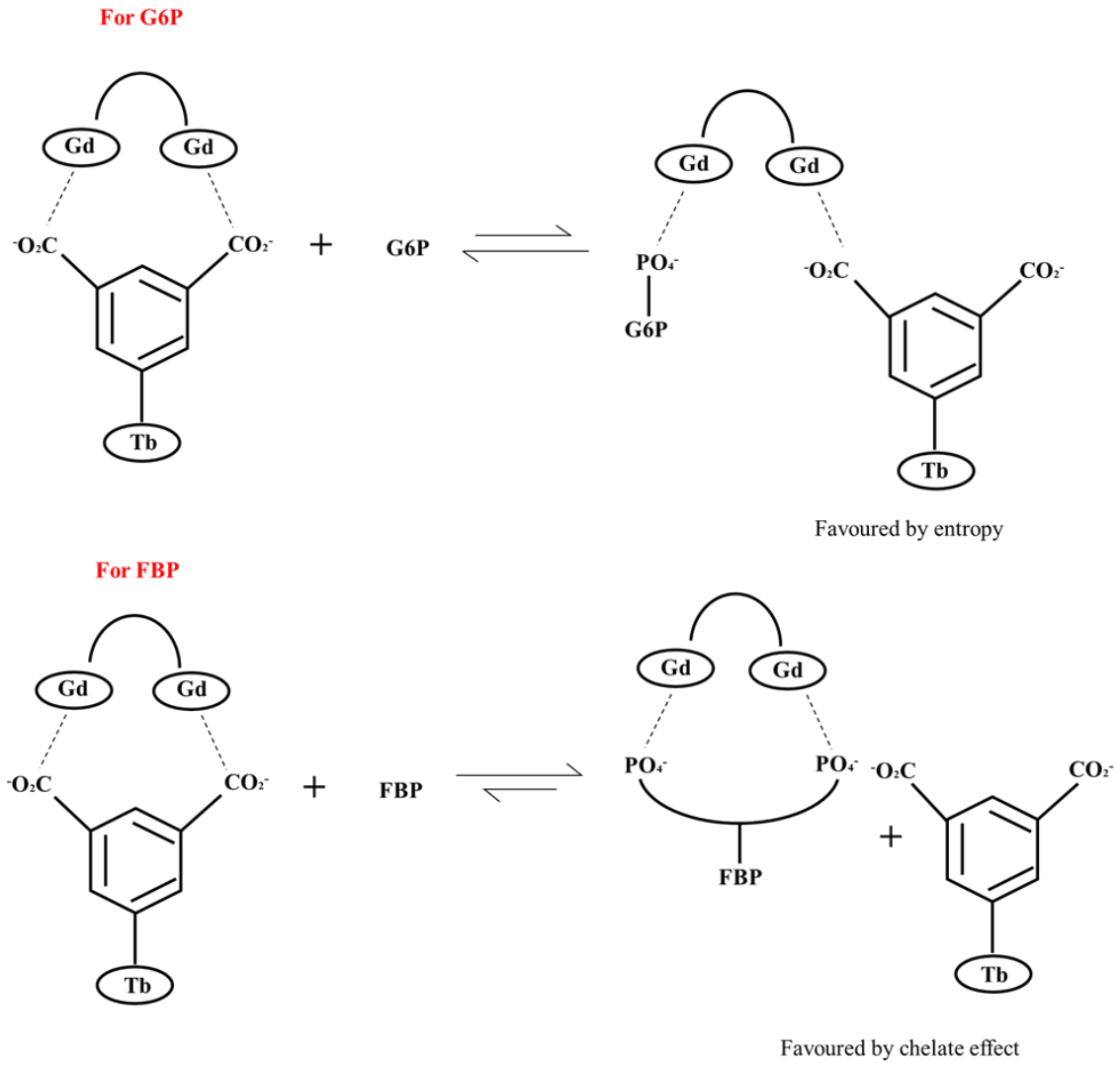


Figure 3.22 Comparison of the dynamic binding behaviours of G6P and FBP in Gd.NMM + Tb.iphth system.

The contrasting result demonstrates the importance of the analyte structure and the binding model in luminescence responses. FBP, with its two phosphate groups and higher denticity, acts as a more effective competitive displacer than G6P. Its ability to de-quench in a Gd-containing system further emphasizes its ability in analyte-induced coordination rearrangement. Moreover, in Gd.NMM, FBP and G6P behave differently, whereas in Eu.NMM, they behave similarly. The increased charge density for gadolinium ions likely results in stronger binding to the gadolinium complex than was previously observed for the europium complex, since the gadolinium ions are stronger Lewis acids and better electron pair acceptors. Furthermore, since

G6P can only act as a monodentate ligand, binding to only one gadolinium centre, it would be expected to compete unfavourably with the bidentate isophthalate in cases where isophthalate is more strongly bound. This may also reflect a structural discontinuity across the Ln.NMM series: structural breaks are often observed in families of lanthanide complexes around the middle of the series, since larger lanthanide ions can accommodate higher coordination numbers. The decrease in calculated q values between the Eu^{3+} and Tb^{3+} complexes may support this hypothesis,[1] and it seems likely that a structural break is occurring between europium and gadolinium NMM.

3.11 Conclusion

This chapter described how competitive binding can change the self-assembly between multinuclear lanthanide complexes. In this study, the Eu.NMM and Tb.iphth mixture were introduced with a guest molecule such as glucose-6-phosphate (G6P) and fructose-1,6-bisphosphate (FBP). The results showed that guest binding could disrupt the supramolecular assembly and change the energy transfer between terbium and europium.

Luminescence experiments confirmed that energy transfer from Tb^{3+} to Eu^{3+} occurred in the Eu.NMM–Tb.iphth assembly. In this mixture, terbium emission decreased and europium emission increased. These results showed that the two lanthanide were communicating with each other. The isophthalate group in Tb.iphth brings terbium and europium closer, enabling energy transfer.

It has been shown that glucose-6-phosphate could be used as competitive displacer in the system described above. As more G6P was added, the Eu.NMM–Tb.iphth assembly gradually broke apart. This caused terbium emission to recover and europium emission to decrease. At high G6P concentrations, the spectra became similar to free Tb.iphth. These changes showed that G6P disrupted the bridge between terbium and europium, thereby blocking the terbium to europium energy transfer.

Studies with fructose-1,6-bisphosphate showed stronger binding compared with glucose-6-phosphate. FBP caused spectral changes at much lower concentrations. This behaviour was likely due to its two phosphate groups, which allowed stronger interactions with the lanthanide centres. These results showed that the system could respond differently to different phosphate-containing metabolites.

Control experiments using Gd.NMM helped explain the mechanism of the system. Gadolinium cannot take part in Tb to Eu energy transfer. Although Gd.NMM still reduced terbium emission, adding G6P did not restore the emission strongly. These results suggested that the behaviour of the Eu.NMM–Tb.iphth system mainly came from reversible Tb to Eu energy transfer rather than simple quenching effects.

Overall, this chapter showed that competitive binding can control supramolecular lanthanide assemblies and change energy transfer pathways in solution. The Eu.NMM–Tb.iphth system provides an important example of a responsive luminescent sensing system based on lanthanide self-assembly and displacement-driven photophysical changes.

3.12 References

(1) Placidi, M. P.; Natrajan, L. S.; Sykes, D.; Kenwright, A. M.; Faulkner, S. Bimetallic lanthanide complexes derived from macrocycle-appended *m*-xylyl derivatives: Synthesis and spectroscopic properties. *Helv. Chim. Acta.* **2009**, *92* (11), 2427–2438.

(2) Pollard, T. D. A guide to simple and informative binding assays. *Molecular biology of the cell* **2010**, *21* (23), 4061-4067.

(3) Bonnet, C. S.; Massue, J.; Quinn, S. J.; Gunnlaugsson, T. Lanthanide luminescent gold nanoparticles: pH-driven self-assembly formation between Eu (III)-cyclen conjugated AuNPs and sensitising β-diketonate antenna in water. *Organic & Biomolecular Chemistry* **2009**, *7* (15), 3074-3078.

(4) Tilney, J. A.; Sørensen, T. J.; Burton-Pye, B. P.; Faulkner, S. Self-assembly between dicarboxylate ions and a binuclear europium complex: formation of stable adducts and heterometallic lanthanide complexes. *Dalton transactions* **2011**, *40* (45), 12063-12066.

(5) Faulkner, S.; Matthews, J. Fluorescent complexes for biomedical applications. *Comprehensive Coordination Chemistry II* **2004**, *9*, 913-944.

(6) Hänninen, P.; Härmä, H. *Lanthanide luminescence: photophysical, analytical and biological aspects*; Springer Science & Business Media, 2011.

Chapter 4 The exploration of a new Glucose Imaging Probe - Synthesis of a new kinetically stable 7- and 8-coordinate heterometallic complexes and their interactions with anionic guests

This Chapter describes the preparation, synthesis, and photophysical investigation of a novel heterometallic lanthanide complex, shown in Figure 4.1, which has two potential binding sites: one can form 8-coordinate complexes, while the other is 7-coordinate. Based on this design, the resulting 7-coordinate pocket can have interactions with the anionic glycolytic-intermediate guests, especially glucose-6-phosphate (G6P). The Eu/Tb pair can be used as a ratiometric sensor for guests by emitting different luminescence responses. Our objective is to examine and evaluate the ratio of Eu and Tb luminescence in the presence and absence of glucose phosphate.

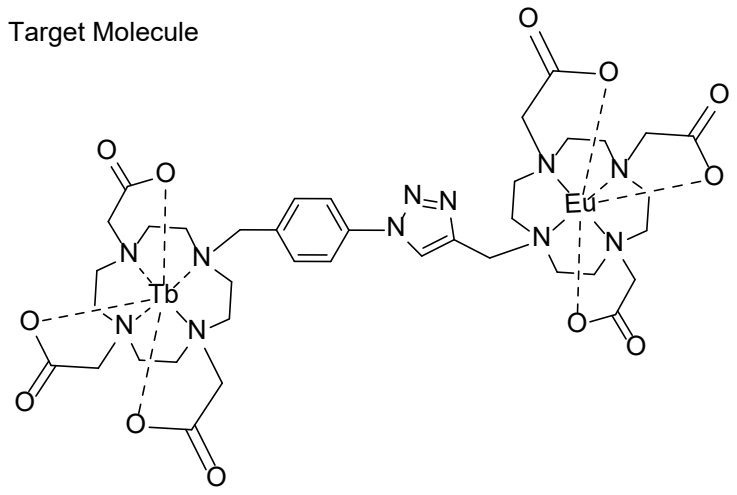


Figure 4.1 7 - and 8-coordinate heterometallic complex.

4.1 Background and Rationale

The design of this molecule is based on the former group member's work in our group. In 2015, Tropiano *et al.* introduced azidophenacyl-DO3A complexes as kinetically stable building

blocks for click chemistry, shown in Figure 4.2, enabling heterometallic arrays, which is the structural base of the design.[1] In 2017, Routledge *et al.* extended the work to the application of this molecule for cyanide sensing, shown in Figure 4.3, using the carbonyl group to form a cyanohydrin and quench the lanthanide emission.[2]

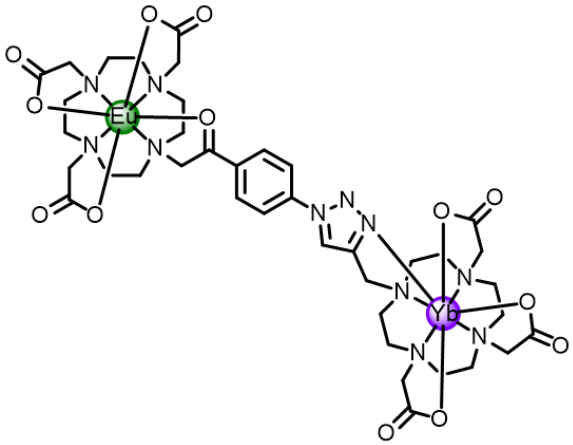


Figure 4.2 Azidophenacyl-DO3A complex established by Tropiano et al.[1]

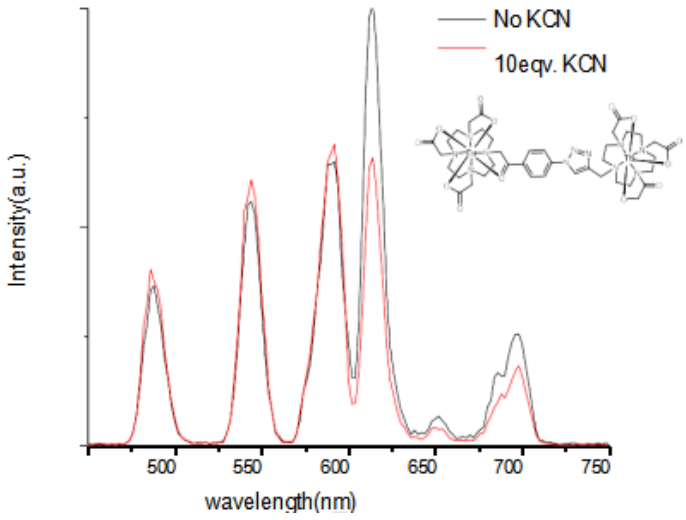


Figure 4.3 Changes in the azidophenacyl-DO3A complex emission spectra in H_2O upon addition of KCN by Routledge et al.. Start of titration (black), end of titration (red; 2 eq.).[2]

Both of their works use the same molecular framework, so the syntheses are similar. Precursors are the alkyne- and azide-appended DO3A lanthanide complexes. Click chemistry (CuAAC) is used to couple the two lanthanide complexes, generating dual-metal arrays with complementary emission profiles. In Routledge's work, the dual-emission profiles are successfully utilised as ratiometric luminescence detection, with one lanthanide acting as the "detection channel" and the other as the "reference channel".[2]

Refining these approaches, a novel molecule was designed for ratiometric detection of anionic sugar carboxylate and phosphates, as shown in Figure 4.4. The framework of the molecule is kept the same; however, the carbonyl group from the left side will be removed to present bound metal ion ready to form complexes with anionic guests. After the removal, the metal in this pocket adopts a seven-coordinate instead of an eight-coordination, bringing it closer to the benzene ring and introducing a vacant site. Furthermore, it removes the through-bond pathway that permits Dexter exchange, enforcing Forster energy transfer hrough space.

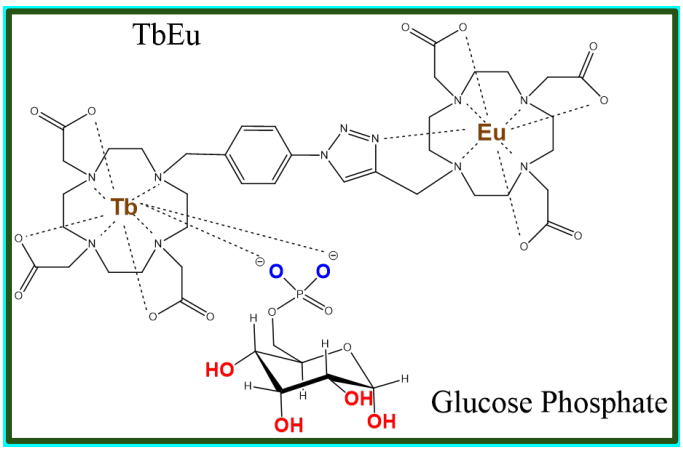


Figure 4.4 The proposal of binding between the 7- and 8-coordinate TbEu heterometallic complex and glucose phosphate system.

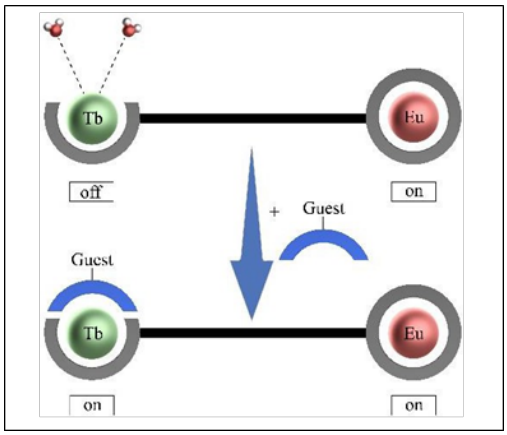


Figure 4.5 The proposal of Eu and Tb luminescence in the presence and absence of the guest.

In the original proposal hypothesis, shown in Figure 4.5, this 7-coordinate site will selectively bind anionic guests (phosphates and carboxylates) while the other, fully saturated site remains unaffected. In a monometallic complex, lanthanide luminescence is sensitised by a single antenna that corresponds to the analyte's presence in the solution. However, it is hard to calculate the analyte's concentration precisely without first knowing the concentration of the complex. However, in a heterometallic system, the addition of the analyte may affect only one Lanthanide ion and leave the other lanthanide ion unchanged, acting as a "reference channel" and remaining "switched on". However, the results turned out to be more complicated than expected, shown in Figure 4.6, indicating that the molecule behaves more complexly than the proposal and deserves further investigation.

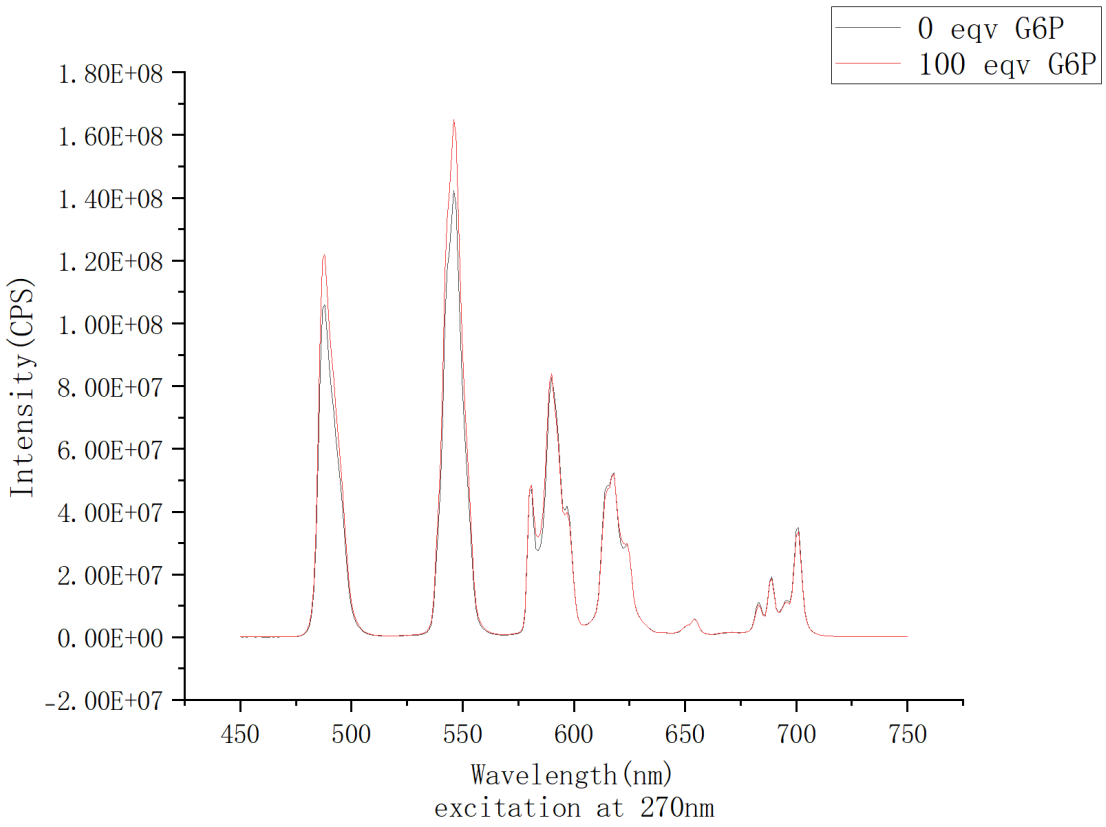
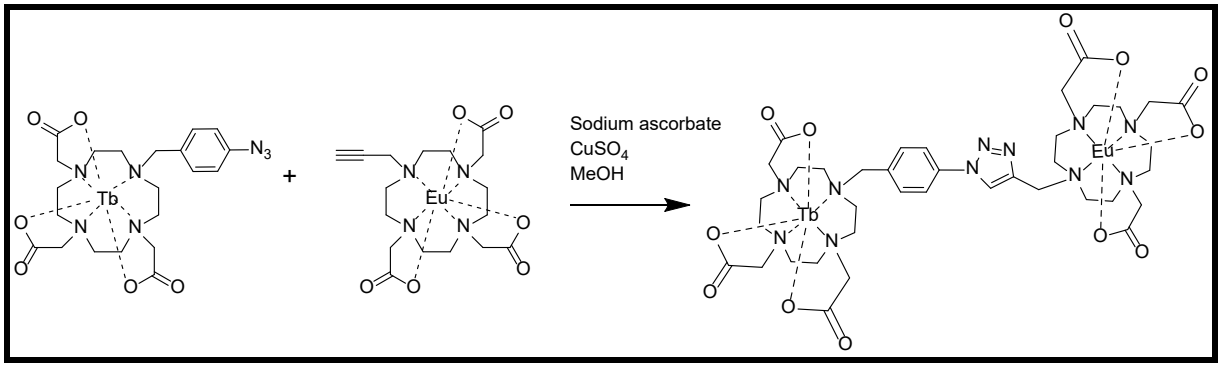


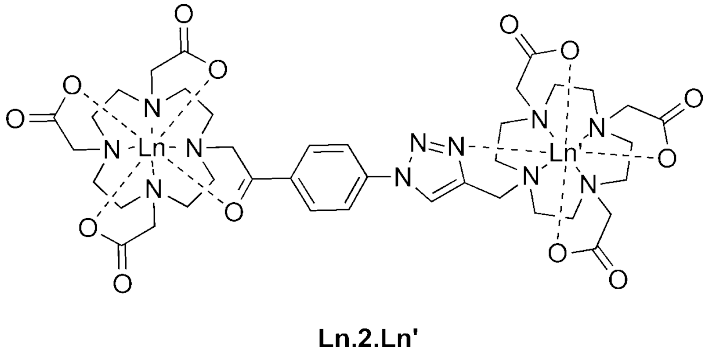
Figure 4.6 Changes in the 7- and 8-coordinate TbEu heterometallic complex emission spectra upon addition of Glucose-6-Phosphate. Start of titration (black), end of titration (red; 100 eq.). Both spectra were recorded following excitation at 270 nm. HEPES buffer (20 mM, pH 7.4); TbEu heterometallic complex (2.5 × 10^{-4} mol/L); 25 ℃.

4.2 Synthesis of a new Tb-Eu bimetallic complex

The synthesis of this Tb-Eu bimetallic molecule has not been reported previously, shown in Scheme 4.1. Tropiano's synthesis of the phenacyl analogue, shown in Figure 4.7, which employed azide-alkyne click chemistry to link two complexes, and we adapted this process to synthesize the new system. To achieve this goal, (4-azidobenzyl) DO3A was prepared before using Click chemistry to link its complexes to complexes of propargylDO3A.



Scheme 4.1 Synthesis of the Tb-Eu bimetallic complex using click reaction.



Ln.2.Ln'

Figure 4.7 Azidophenacyl-DO3A complex established by Tropiano et al..[1]

The synthesis has three parts. The two motifs should be prepared first, and the final step of the click reaction can achieve the desired final product. One of these motifs is a well-established propargyl complex,[3] while the other is a novel azidophenacyl-DO3A complex, the preparation of which required additional effort.

4.2.1 Azidobenzyl-DO3A complex

Developing new lanthanide complexes helps advance analyte-probing systems with different structures. To synthesize heterometallic lanthanide complexes efficiently, click chemistry was

chosen to connect two complexes together. Since alkyl complexes have been previously explored, it is worthwhile to focus on a new type that contains an azide group.

In sensing applications, the presence of target molecules is usually detected through changes in luminescence, which are easy to observe. To design these azide-containing complexes, a chromophore has to be involved to enhance the lanthanide's luminescence. This also helps in studying their photophysical properties.

The ligands chosen for this study needed to be simple to synthesise and remain stable under various conditions. Based on these needs, azidobenzylDO3A complexes were selected, shown in Figure 4.8. This structure also satisfies the proposal that forming a 7-coordinate pocket can facilitate interaction with the anionic glycolytic intermediate guests.

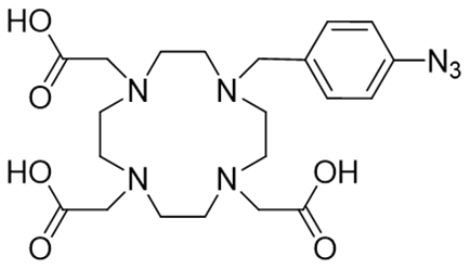
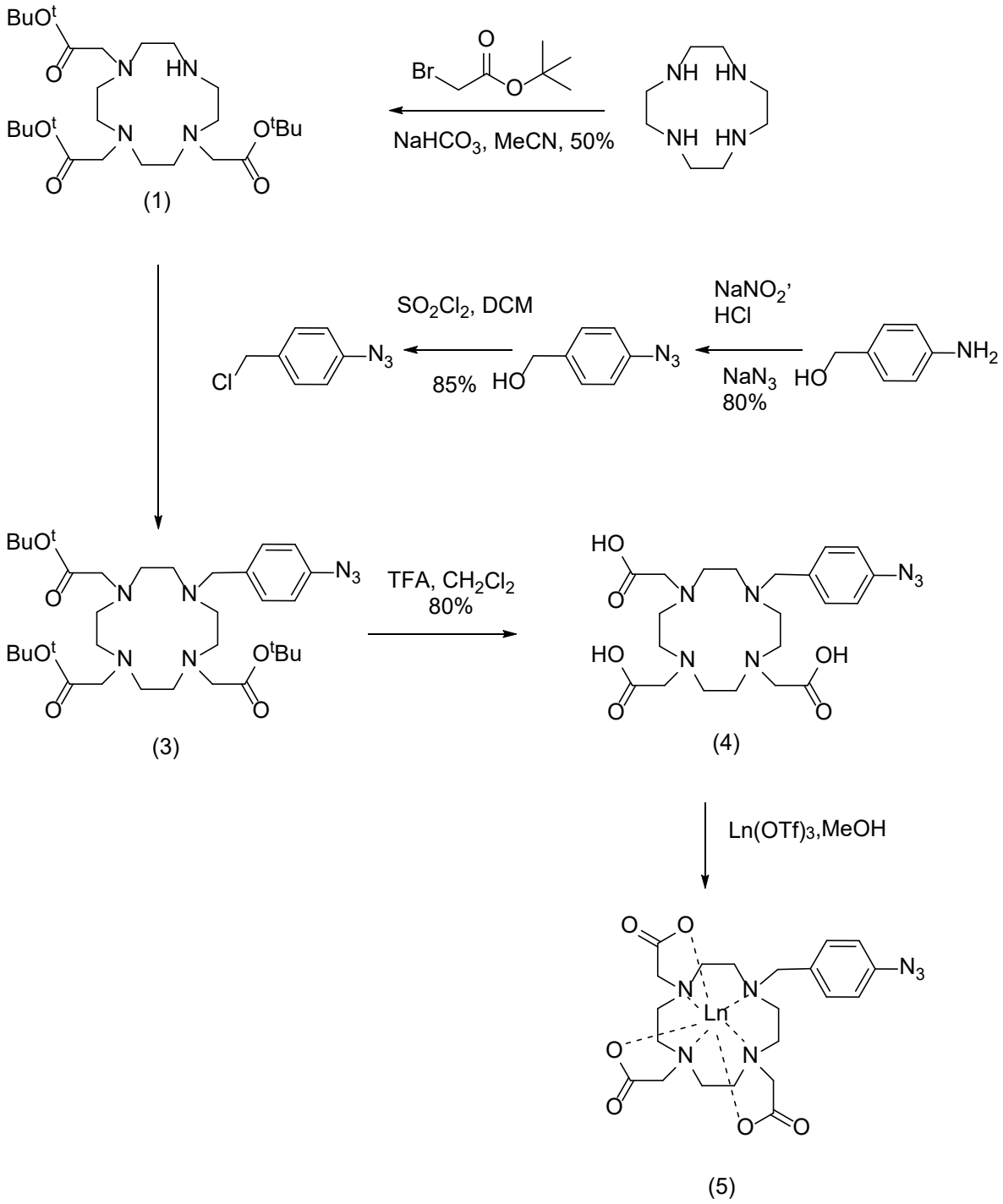


Figure 4.8 AzidobenzylDO3A Ligand.

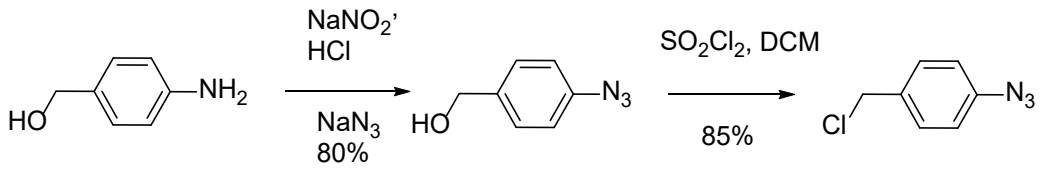


Scheme 4.2 Full synthesis route of Azidobenzyl-DO3A complex.

The pendent azide, 4-azidochloromethylbenzene, was obtained according to the synthetic methodology reported by Zhou *et al.*.[4] The novel azidobenzyl-DO3A complex, isolated as a

pink-white material, was found to be stable at ambient temperature, a property essential for progression to subsequent synthetic steps.

4-Azidochloromethylbenzene was synthesised from aminobenzylalcohol as shown in the Scheme 4.3.[4] Using the conventional NaN_3 and $NaNO_2$ conditions, the primary amine was converted into the aromatic azide. The reaction was accomplished rapidly in high yield, and the product, azidophenylmethanol, was obtained after the extraction with ether and flash chromatography. The chlorination of 4-azidophenylmethanol was performed with an excess amount of thionyl chloride in DCM. This step was stirred at room temperature overnight, and the final product was obtained after purification with flash chromatography. 4-Azidophenylmethanol was converted to azidochloromethylbenzene in a yield of 90 %.



Scheme 4.3 Synthesis route of azidochloromethylbenzene. [4]

Azidochloromethylbenzene was reacted with the tert-butyl-protected triester in the presence of potassium carbonate and KI, giving the crude protected ligand (3). The crude protected product was purified by flash column chromatography on silica gel. The removal of the tert-butyl protecting groups was carried out with trifluoroacetic acid in dichloromethane. The deprotected ligand was mixed with the corresponding lanthanide triflate salt in methanol, which was heated to 60 °C for 48 hours. To remove the excess lanthanide ions, sodium hydroxide was used to

form the lanthanide hydroxide precipitates. The desired complexes were finally examined by ^{1}H-NMR spectroscopy and IR spectroscopy and mass spectrometry.

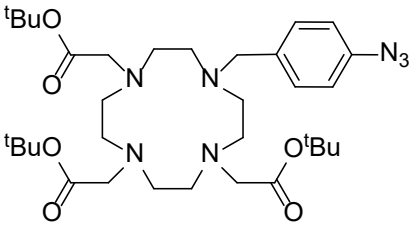


Figure 4.9 Protected azidobenzylDO3A ligand.

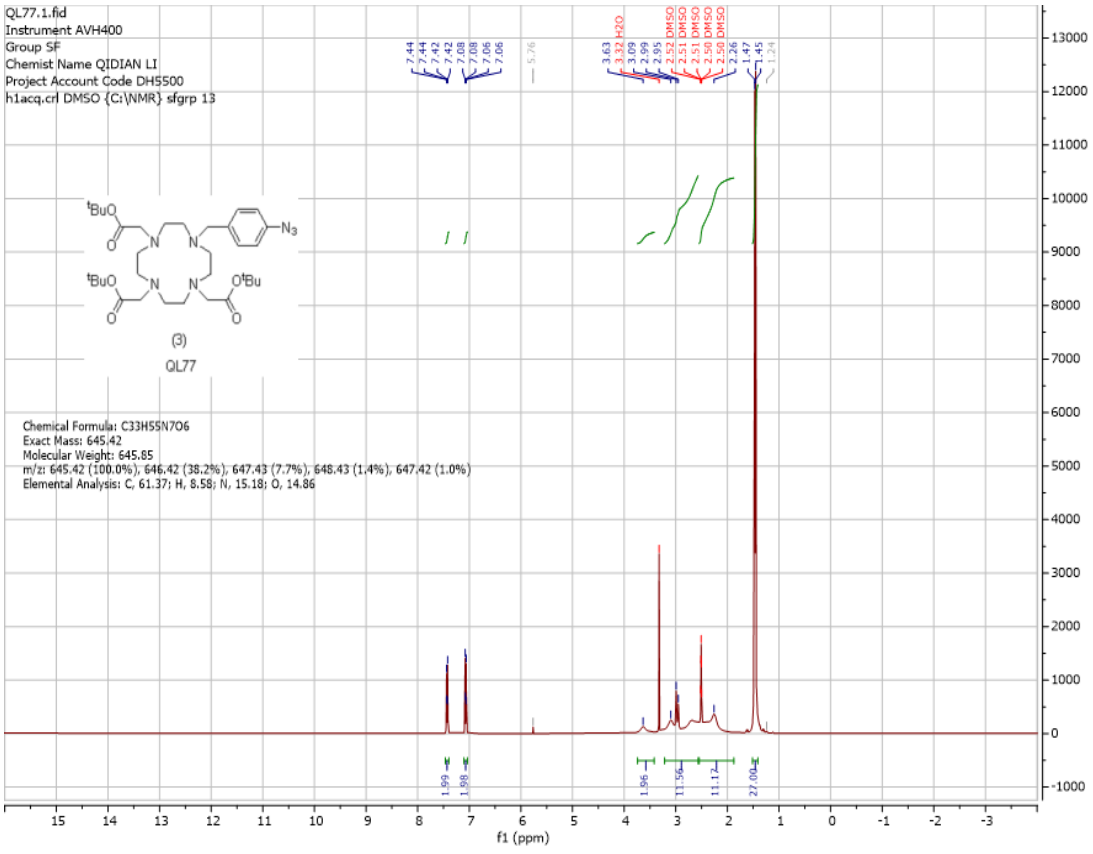


Figure 4.10 The ^{1}H-NMR spectrum of the protected azidobenzylDO3A ligand in DMSO at RT.

The ^{1}H-NMR spectrum confirms that this compound contains both the azidobenzyl group and the DO3A sub-unit, shown in Figure 4.10. The peaks between 7 and 7.5 ppm are characteristic of a para-substituted aromatic compound, while the broadened singlet around 3.5 ppm corresponds to the benzylic CH_2 protons. The protons of the cyclen ring and the NCH_2 protons

on the other pendent arms are observed as a broad multiplet between 2 and 3.5 ppm, while the t-butyl protons are observed around 1.45 ppm. It is noteworthy that the linewidths for the aryl protons and the t-butyl protons are much sharper than the others. This reflects fluxionality in the cyclen ring and motion of the pendent arms.

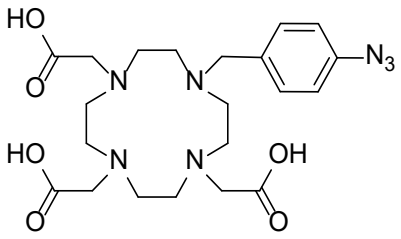


Figure 4.11 Deprotected azidobenzylDO3A ligand.

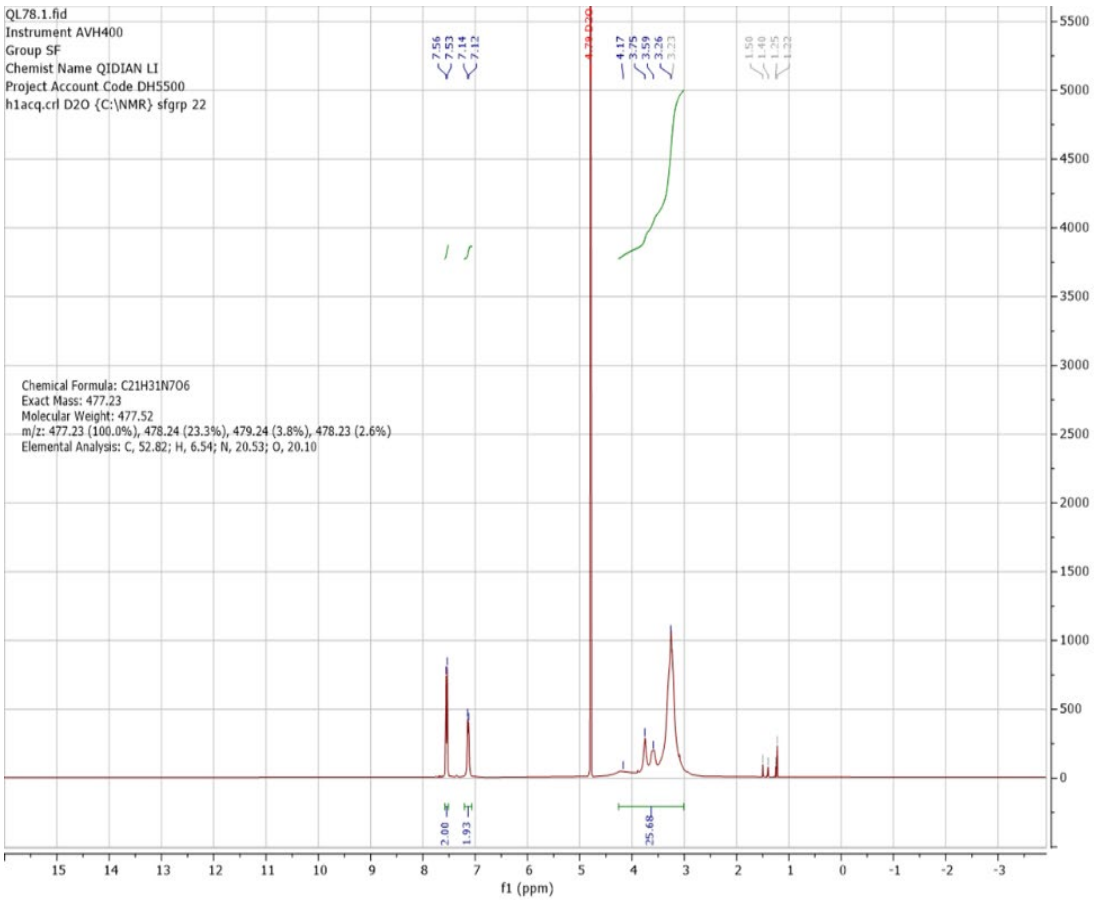


Figure 4.12 The ^{1}H-NMR spectrum of the deprotected azidobenzylDO3A ligand in D_2O at RT.

Following cleavage of the t-butyl esters by reaction with trifluoroacetic acid, the ^{1}H- NMR spectrum changes, reflecting loss of the t-butyl groups, shown in Figure 4.12. While the remaining peaks are observed with similar chemical shifts to those seen before, with the protected ligand, the cyclen protons appear sharper after hydrolysis, suggesting that protonation of some of the amine groups results in a more open structure, in which faster exchange occurs between isomers.

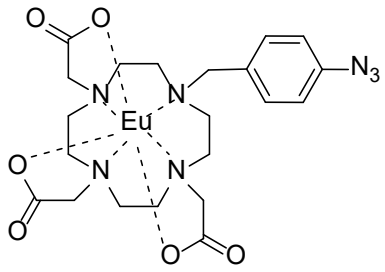


Figure 4.13 Eu-Azidobenzyl-DO3A complex.

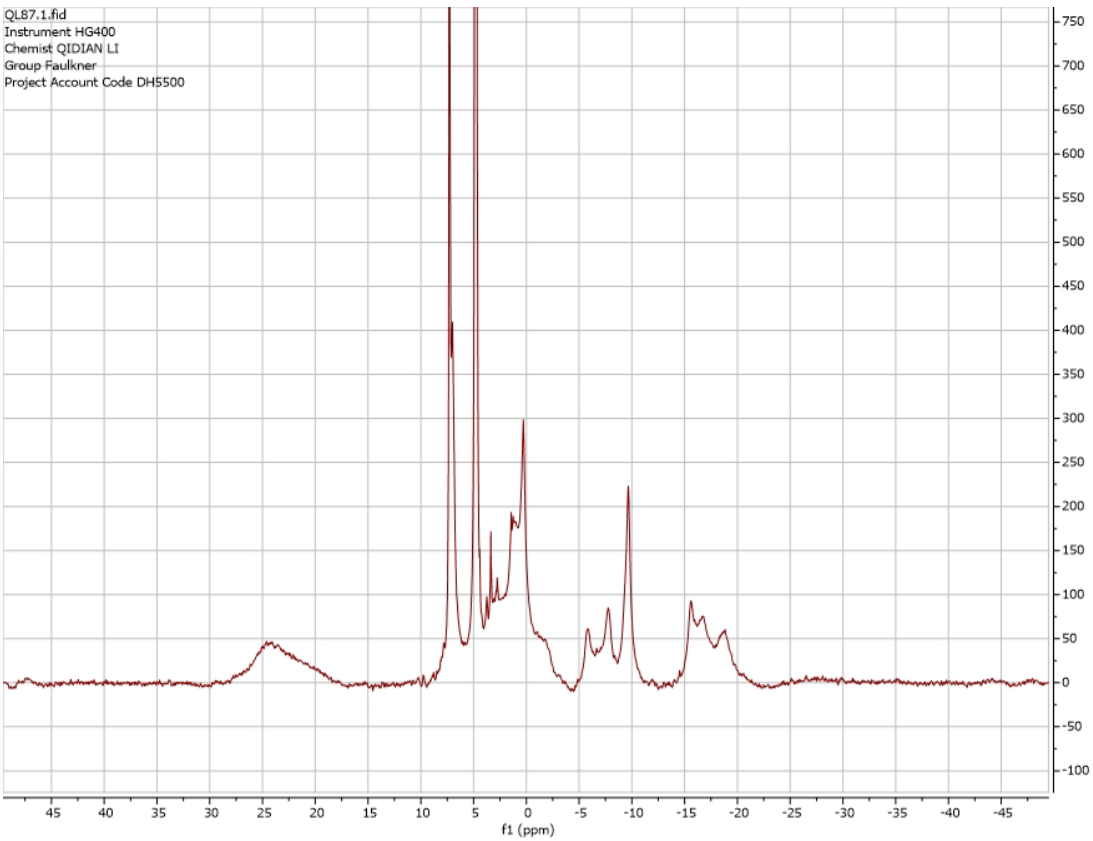


Figure 4.14 The ^{1}H-NMR spectrum of Eu-Azidobenzyl-DO3A complex in D_2O at RT.

The ^{1}H-NMR spectrum of the Eu-Azidobenzyl-DO3A complex exhibited typical broad shifted resonances due to the paramagnetic nature of lanthanide ion, shown in Figure 4.14. The signal at 25 ppm can be assigned to the axial protons on the macrocycle backbone. The broad peaks observed in this spectrum are consistent with exchange between diastereoisomers of the ligand skeleton on the timescale of the NMR experiment. Such fluxional behaviour is relatively common for heptadentate DO3A-derived systems. In this case it results in much broader lines than would be associated with common octandetnate ligands such. Furthermore, the observed chemical shifts reflect a population weighted average of the shifts that would be associated with the SAP and TSAP isomers. For instance, the broad feature around 25 ppm represents exchange between axial ring protons on the SAP and TSAP forms as a consequence of interconversion between the isomers. Given that the peaks for SAP isomers would be expected to be in the range between 25 and 35 ppm, while those for TSAP would be expected to be in the range between 10 and 20 ppm. On this basis, it seems reasonable to assume that both SAP and TSAP are present.

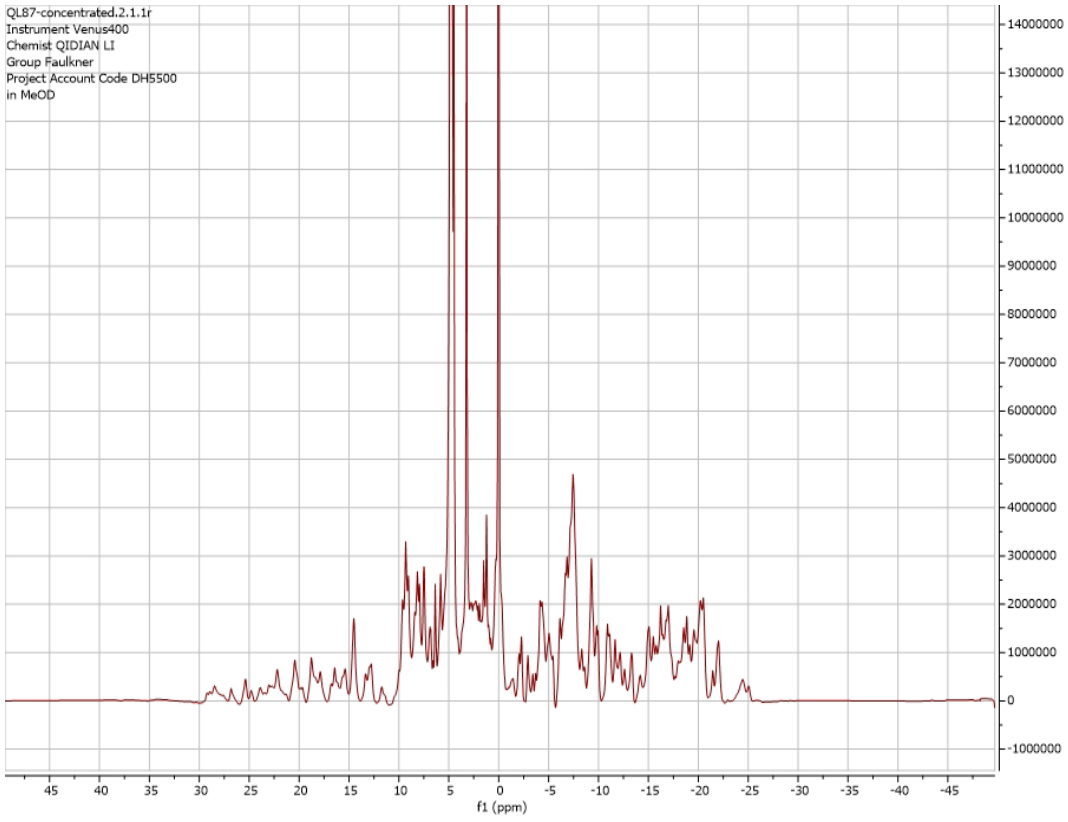


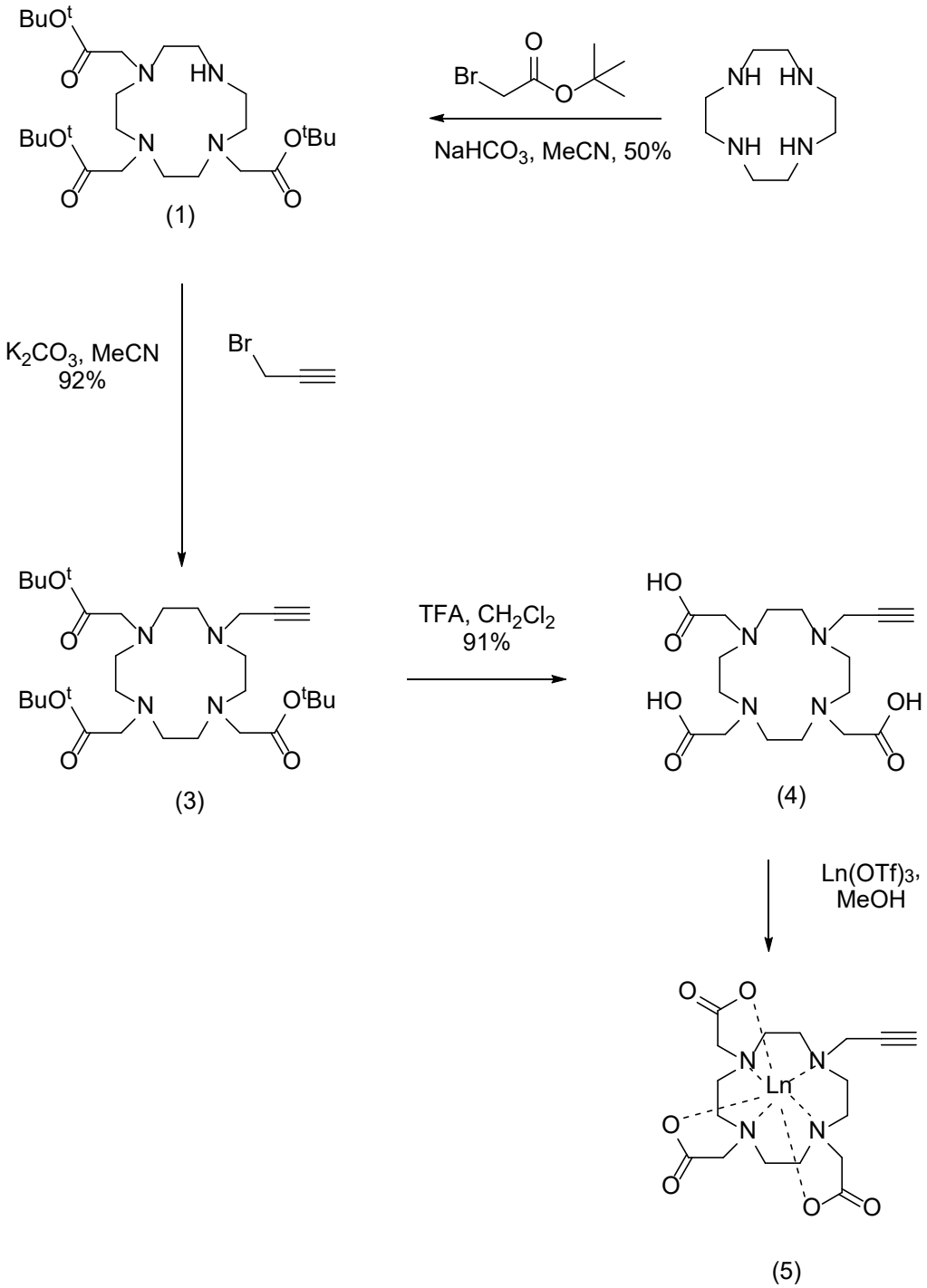
Figure 4.15 The ^{1}H-NMR spectrum of Eu-Azidobenzyl-DO3A complex in MeOD at RT.

When using MeOD as the NMR solvent, compared with the spectrum in D_2O, slower exchange between isomers is observed as seen in Figure 4.15. This spectrum appears to show many resonances, corresponding to both the SAP and TSAP forms. Since the spectrum shows many resonances, it is possible that the complex is aggregating in methanol. The high concentration used to obtain this spectrum would support such a hypothesis, which is necessary to explain the large number of axial ring protons observed. Without aggregation, it is expected to see four resonances for the SAP ring protons and four for the TSAP ring protons. However, in aggregate, each complex can act as a chiral auxiliary for other complexes, giving rise to a range of possible diastereoisomers and to a large number of resonances that would be consistent with the observed spectrum. Aggregation of DO3A derivatives, and of other coordinatively unsaturated lanthanide complexes, has previously been proposed to be mediated by MeOD.

4.2.2 Propargyl-DO3A complex

The synthesis of propargyl-DO3A lanthanide complexes was performed using a reported method, shown in Scheme 4.4.[3] Initially, the triester was synthesised by alkylating cyclen with tert-butyl bromoacetate in acetonitrile using potassium carbonate. Later, the unreacted tertiary amine group was alkylated with propargyl bromide. Compound (3) was obtained in good yield and confirmed by ^{1}H NMR spectroscopy. The tert-butyl protecting group was removed by acid, yielding the propargyl carboxylic acid ligand. In the final step, the propargyl carboxylic acid ligand was mixed with lanthanide triflates in methanol to synthesise the desired lanthanide complex. The ^{1}H-NMR spectra of Eu-propargyl complex and Tb-propargyl complex support the idea that propargylDO3A forms seven-coordination (heptadentate), non-symmetrical complexes. The signals from the axial protons are all different and appear to form a broad peak,

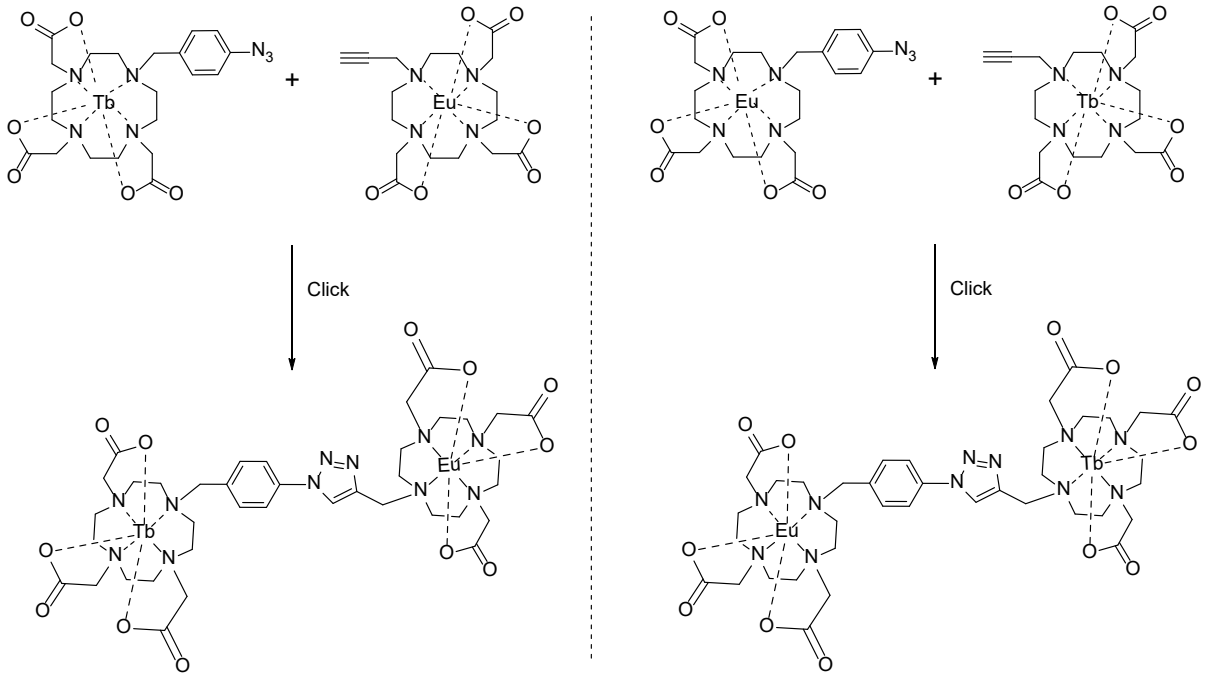
which suggests that the molecule is rotating, allowing the complex to change between different isomer forms. This is expected because the propargyl group does not directly bind to the lanthanide ion. Since this isomer switching has already been well studied, this chapter won't go into more detail.



Scheme 4.4 Synthetic scheme for the lanthanide complexes containing propargyl arms.[3]

4.2.3 Click Chemistry to access Heterometallic Arrays

The alkynyl group would easily conduct [3+2] cycloaddition with the azido group in the presence of azidophenacylDO3A complexes, producing pure heterometallic complexes that have high selectivity, shown in Scheme 4.5. Using CuAAC reactions, a variety of heterometallic lanthanide complexes were produced and characterised via NMR spectroscopy and luminescence spectroscopy.



Scheme 4.5 Synthetic procedure for the TbEu complex and EuTb complex.

The complexes were linked together by using standard CuAAC click chemistry.[5] The two precursors and copper(II) sulfate were mixed in methanol. The Cu(I) catalyst was then formed in the reaction mixture by reducing copper(II) with sodium ascorbate. Initial reactions using equimolar amounts of azide and alkyne resulted in poor conversion; therefore, an excess of the alkyne component was introduced to drive the reaction toward completion. Various polar

solvents and alternative Cu(I) sources were also tested, but none of them improved the yield of the desired product.

Purification of the target complex was achieved by dialysis using a 1000 MWCO cellulose membrane, effectively removing unreacted lanthanide precursors and residual copper species, both of which can strongly quench lanthanide luminescence. Attempts to characterise the final product by mass spectrometry were unsuccessful, as ionisation consistently led to demetallation of the lanthanide centres.

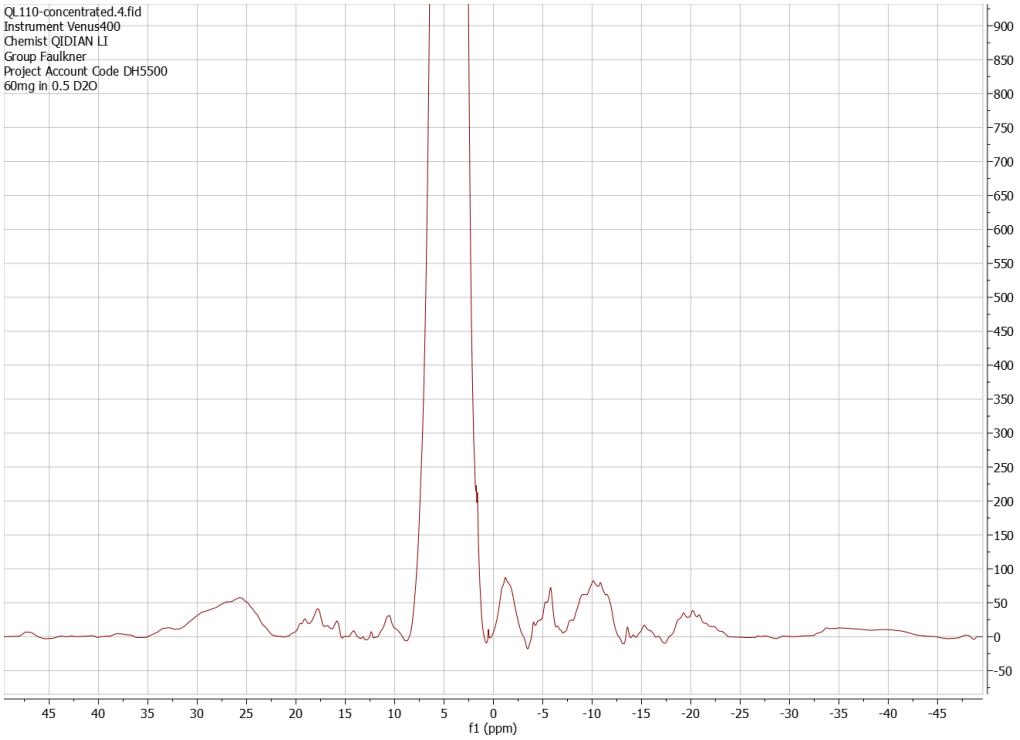


Figure 4.16 The ^{1}H-NMR spectrum of TbEu complex in MeOD at RT.

The spectrum of the click product TbEu complex clearly shows peaks in the 10-20 ppm region (Figure 4.16), corresponding to axial ring protons associated with the europium binding site. The broader, less well-resolved, feature observed between 25 and 35 ppm corresponds to the

SAP isomer, and it may be noted that the breadth of these signals is suggestive of more rapid exchange in the SAP isomer.

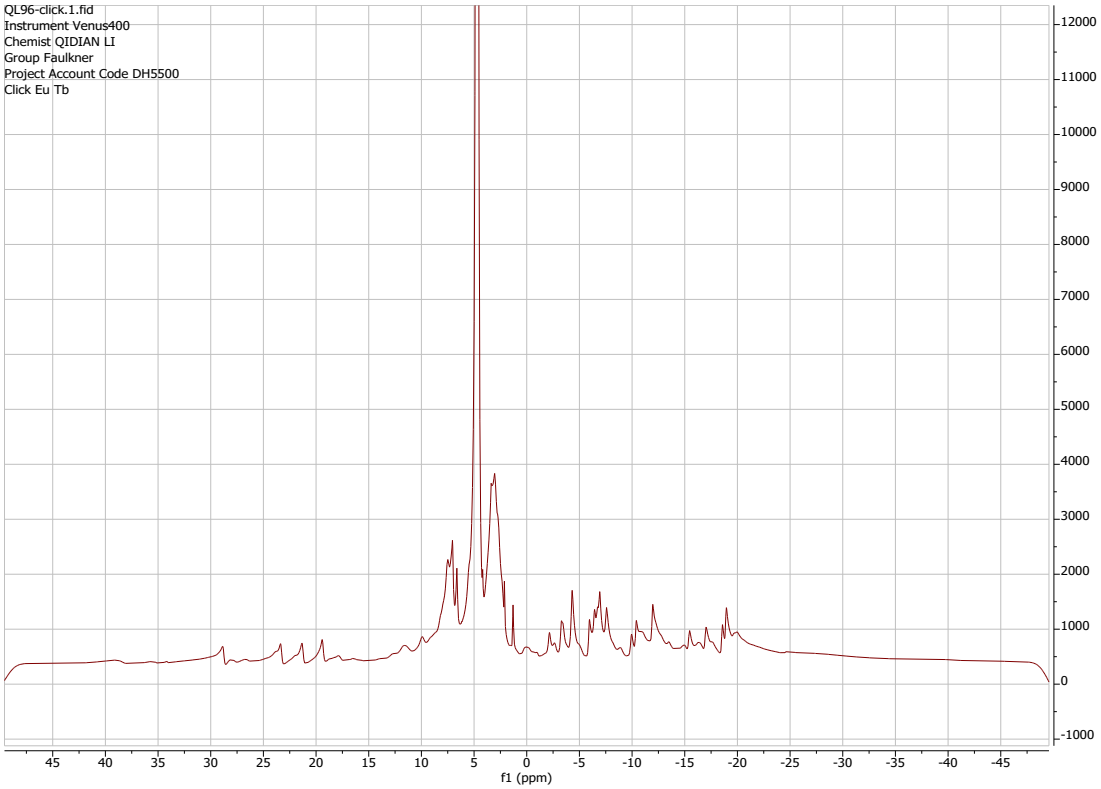


Figure 4.17 The [1]H-NMR spectrum of EuTb complex in MeOD at RT.

The [1]H-NMR spectra of the reversed EuTb complex, shown in Figure 4.17, which are much sharper and dominated by peaks that have shifts intermediate between those expected for SAP and those for TSAP isomers, e.g. the axial ring protons between 20 and 30 ppm. This suggests rapid exchange between stereoisomers at the europium-binding site.

4.3 Photophysical Properties

The TbEu UV–Vis absorption spectrum (Figure 4.18) shows a broad absorption that decreases steadily from ~215 nm to ~395 nm. There are no sharp peaks — instead, there is a continuous tailing-off of absorption intensity with increasing wavelength. The strong absorption in the 215–270 nm region likely arises from the organic ligands used to coordinate Tb^{3+} and Eu^{3+}. These transitions are typically: $\pi \rightarrow \pi^*$; $n \rightarrow \pi^*$. Since there is no absorbance tailing into the visible region, any luminescence from Tb^{3+} or Eu^{3+} is not due to direct light absorption by the metal ions but rather through sensitization via the ligand (antenna effect).

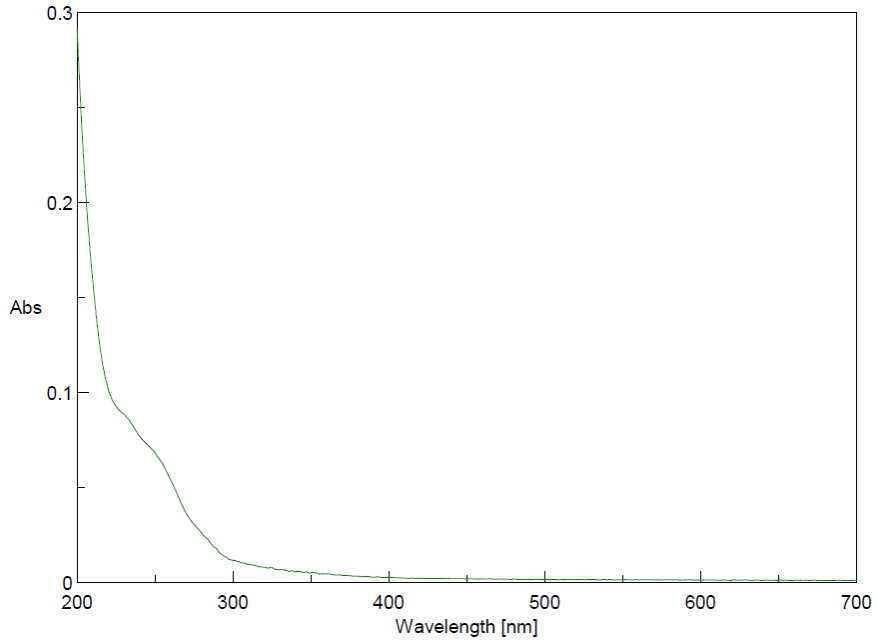


Figure 4.18 UV–Vis absorption spectrum of the TbEu complex.

The EuTb UV–Vis absorption spectrum (Figure 4.19) shows a broad absorption band with intensity sharply decreasing from ~0.25 at 215 nm to near-zero at 300–320 nm. The EuTb complex strongly absorbs in the deep UV (215–280 nm) due to ligand-centred transitions. After 300 nm, absorbance is minimal, indicating no direct f-f transitions or charge-transfer bands.

The spectral profile supports a ligand-sensitized luminescence mechanism, consistent with common photophysical behaviour of lanthanide complexes.

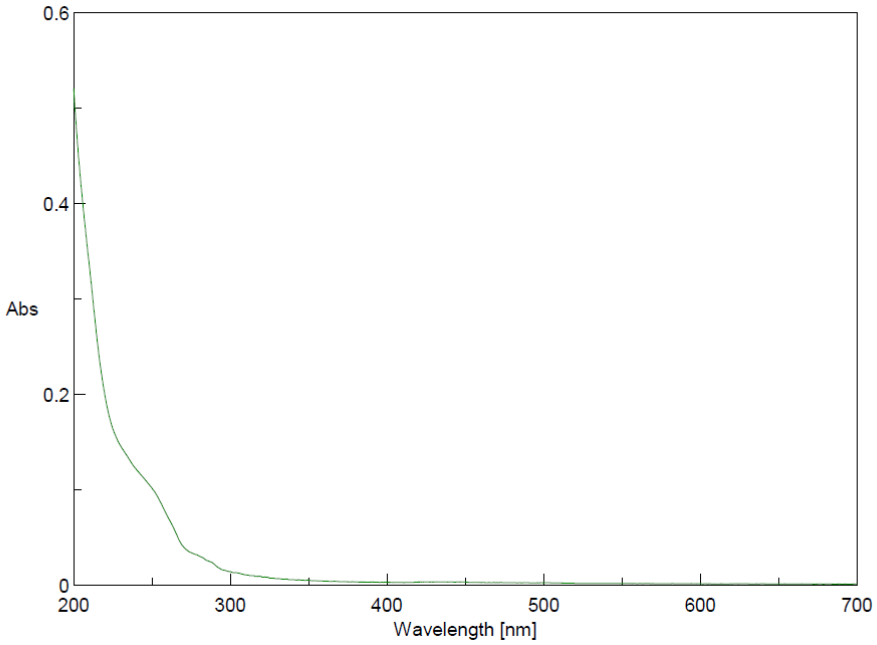


Figure 4.19 UV–Vis absorption spectrum of the EuTb complex.

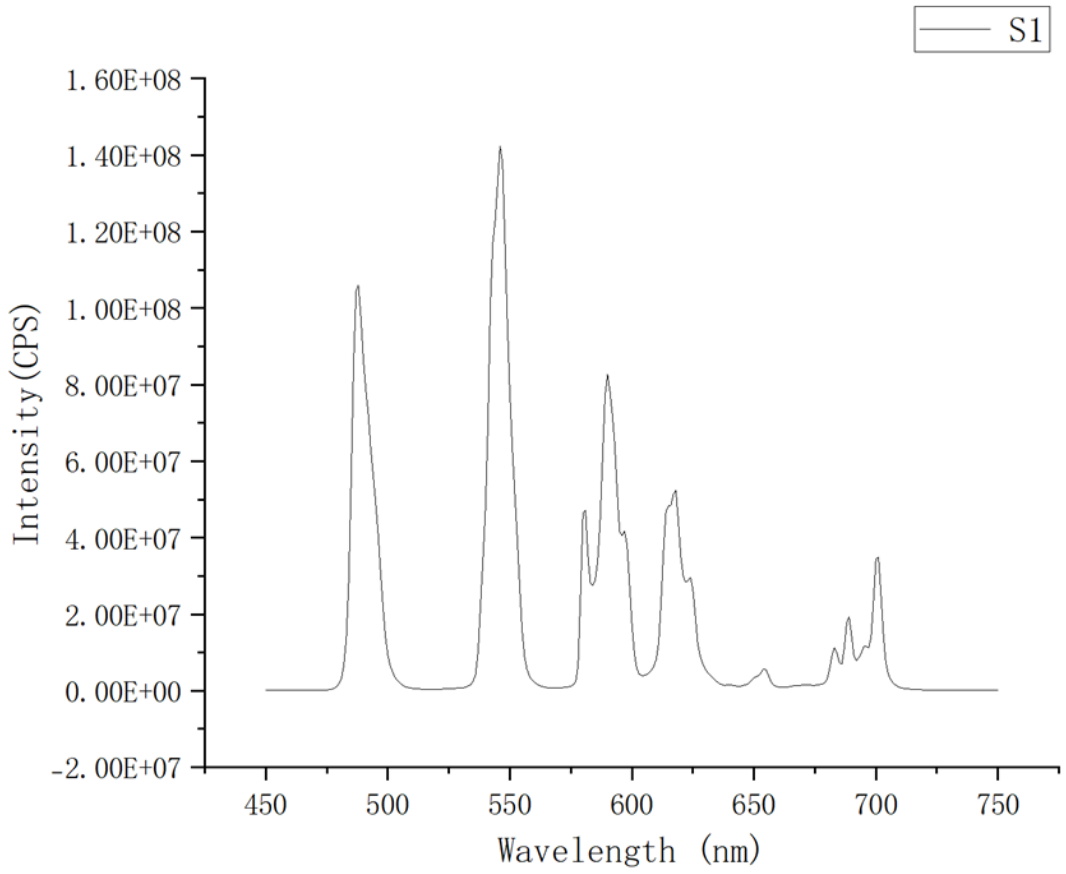


Figure 4.20 Emission spectrum of the TbEu complex (no guest). HEPES buffer (20 mM, pH 7.4); TbEu heterometallic complex (2.5 × 10^{-4} mol/L); 25 ºC.

The Tb–Eu complex shows characteristic dual luminescence from both Tb^{3+} (green) and Eu^{3+} (red) upon excitation at 270 nm, with strong emission bands at around 545 nm for Tb and 615 nm for Eu, shown in Figure 4.20. In this system, the ligand functions as an effective antenna, sensitising both Tb^{3+} and Eu^{3+}, and enabling partial energy transfer from Tb to Eu. As a result, both metal centres emit appreciably, indicating that the energy transfer is efficient but not complete, with Tb emission still present rather than fully quenched. Overall, the spectrum reflects a carefully designed heterometallic complex with well-controlled and tunable photophysical behaviour.

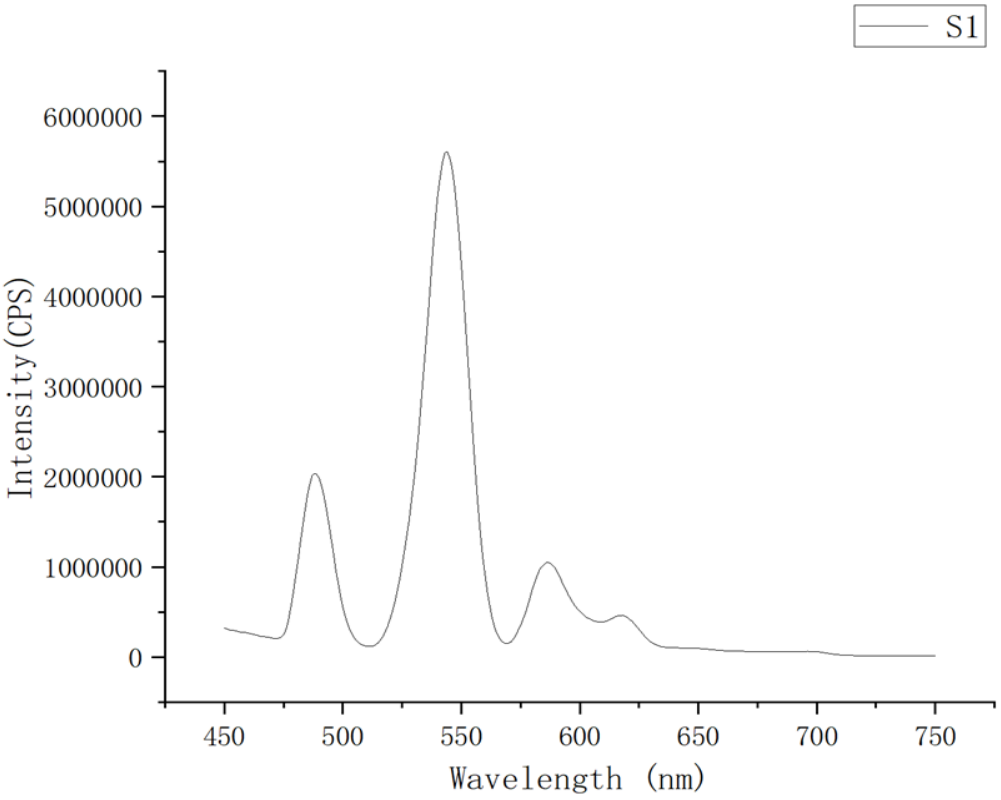


Figure 4.21. Emission spectrum of the EuTb complex (no guest). Baseline emission of the EuTb heterometallic complex in HEPES (λex = 270 nm). HEPES buffer (20 mM, pH 7.4); EuTb heterometallic complex (2.5 × 10^{-4} mol/L); 25 ℃.

In the case of the Tb-Eu complex, where the Tb is in the left isolated DO3A site and the europium is in the propargyl site, the azide-bound site. Direct conjugation exists between the azide-chromophore and the Eu. This results in a spectrum showing numerous europium peaks due to efficient energy transfer from the azide chromophore. In the case of the Eu-Tb complex, the emission spectrum is shown in Figure 4.21. The Eu is not directly conjugated to the azide-chromophore; instead, energy transfer is more efficient to the Tb centre azide-bound site. This results in low-intensity europium peaks by comparison with strong terbium peaks as a consequence of efficient energy transfer to terbium and less efficient energy transfer to

europium. Taken together, these spectra show that energy transfer to the site in which a triazole binds the metal is more efficient than energy transfer to the isolated DO3A site. This is unsurprising, given that the former can result in energy transfer through Dexter exchange, while the latter must rely on relatively inefficient Forster energy transfer.

4.4 Binding Studies with Anionic Guests

4.4.1 Interaction with Glucose-6-Phosphate

The luminescence binding study shows different behaviours at three excitation wavelengths (λ_{ex} = 398 nm, 270 nm, 488 nm). The titrations under three excitation wavelengths are given below and analysed separately. Three main peaks of the TbEu complex emission spectra, especially the trend in their intensity changes, are given greater consideration.

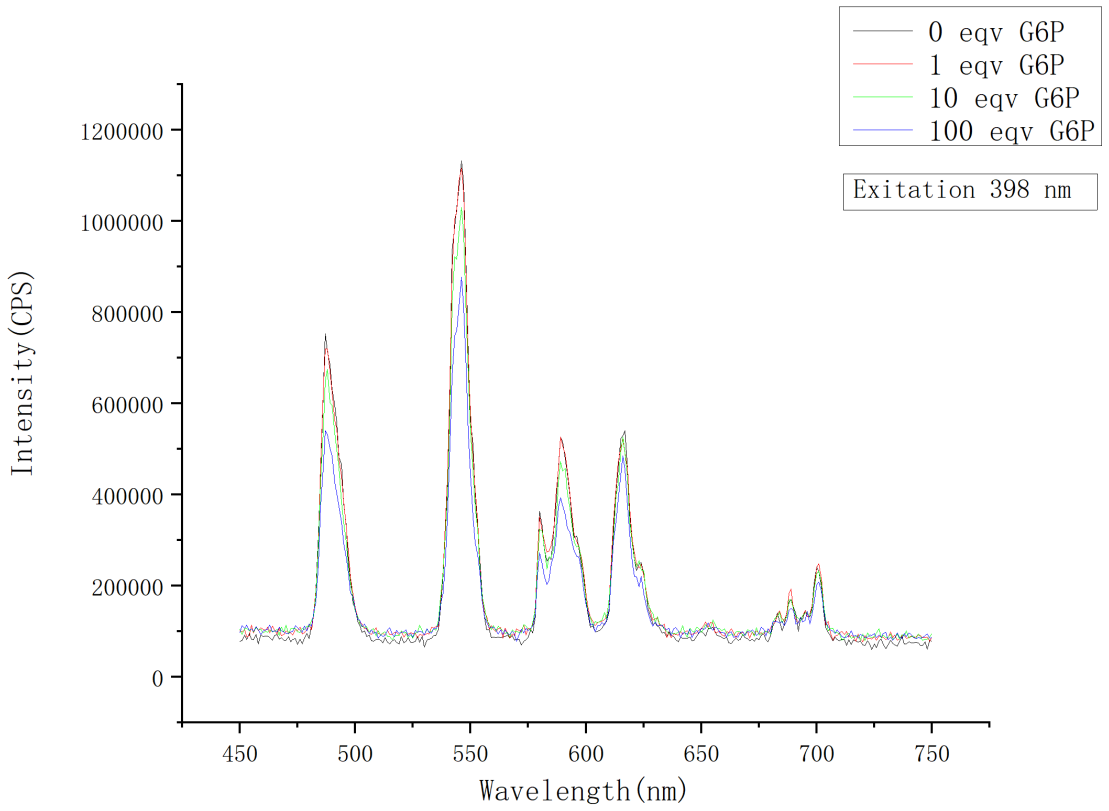


Figure 4.22 Overlay TbEu complex emission spectra before and after G6P addition. Emission spectra showing ratiometric response of Tb/Eu luminescence upon addition of G6P. (λex = 398 nm). HEPES buffer (20 mM, pH 7.4); TbEu heterometallic complex (2.5 × 10^{-4} mol/L); 25 ℃.

This set of emission spectra shows the titration of the TbEu complex with 0, 1, 10, and 100 eqv. of G6P (Figure 4.22). 398 nm excitation gives rise to europium emission following direct excitation of Eu^{3+} ($^7F_0$-$^5D_6$). However, in this system, terbium is also excited, likely via sensitisation through energy transfer in the upper manifold. Three main peaks are chosen in the spectra: 488 nm and 545 nm represents Tb^{3+} emission, 690 nm represents Eu^{3+} emission.

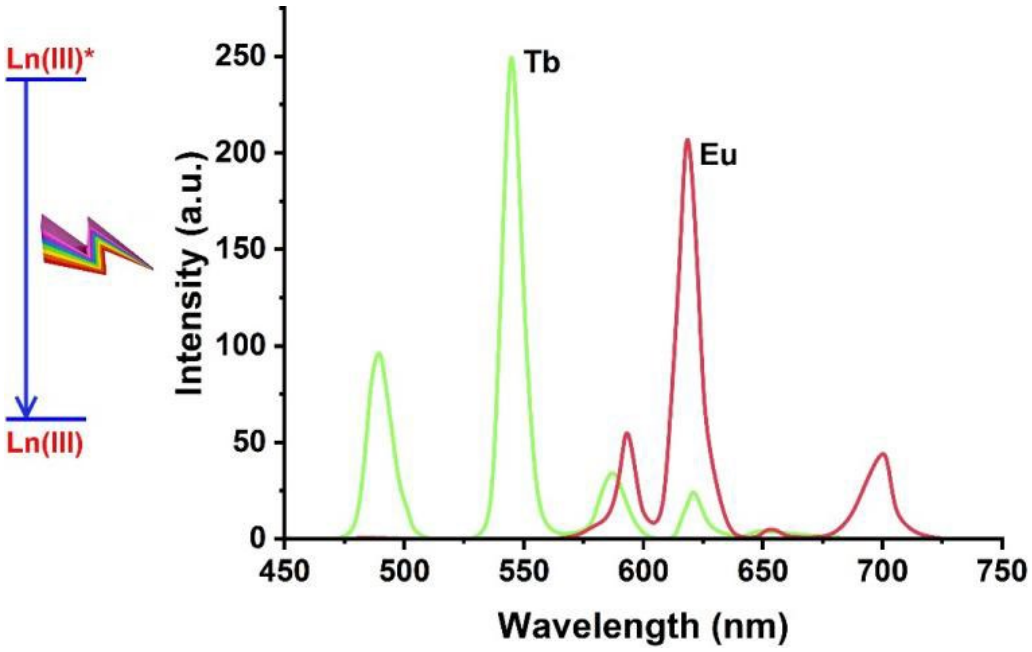


Figure 4.23 Tb^{3+} emission vs Eu^{3+} emission.

Adding G6P disturbs the energy transfer, conceivably by altering the conformation of the complex as a whole to limit through-space interactions. From Figure 4.24, the trendline of Tb emission peaks decreases after the addition of more G6P, while the Eu emission peak remains relatively stable.

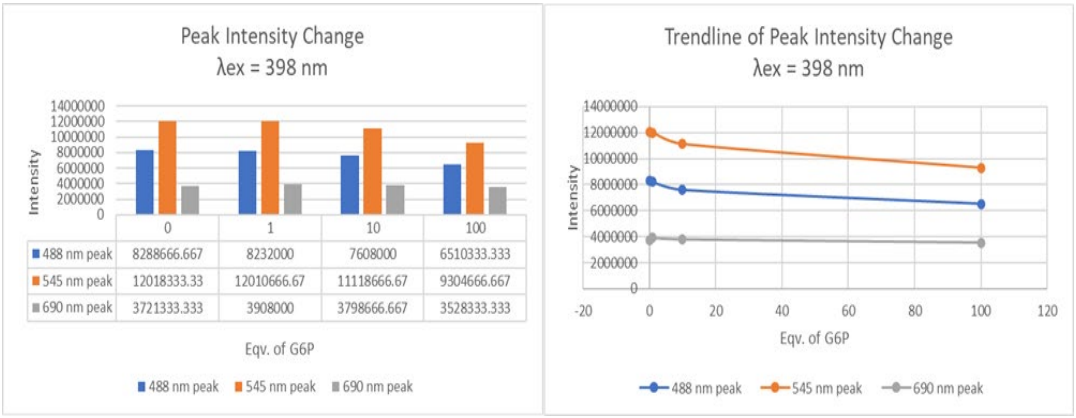


Figure 4.24 The trend of the three main peaks of the TbEu complex emission spectra after 100 eqv. G6P addition. (λex = 398 nm).

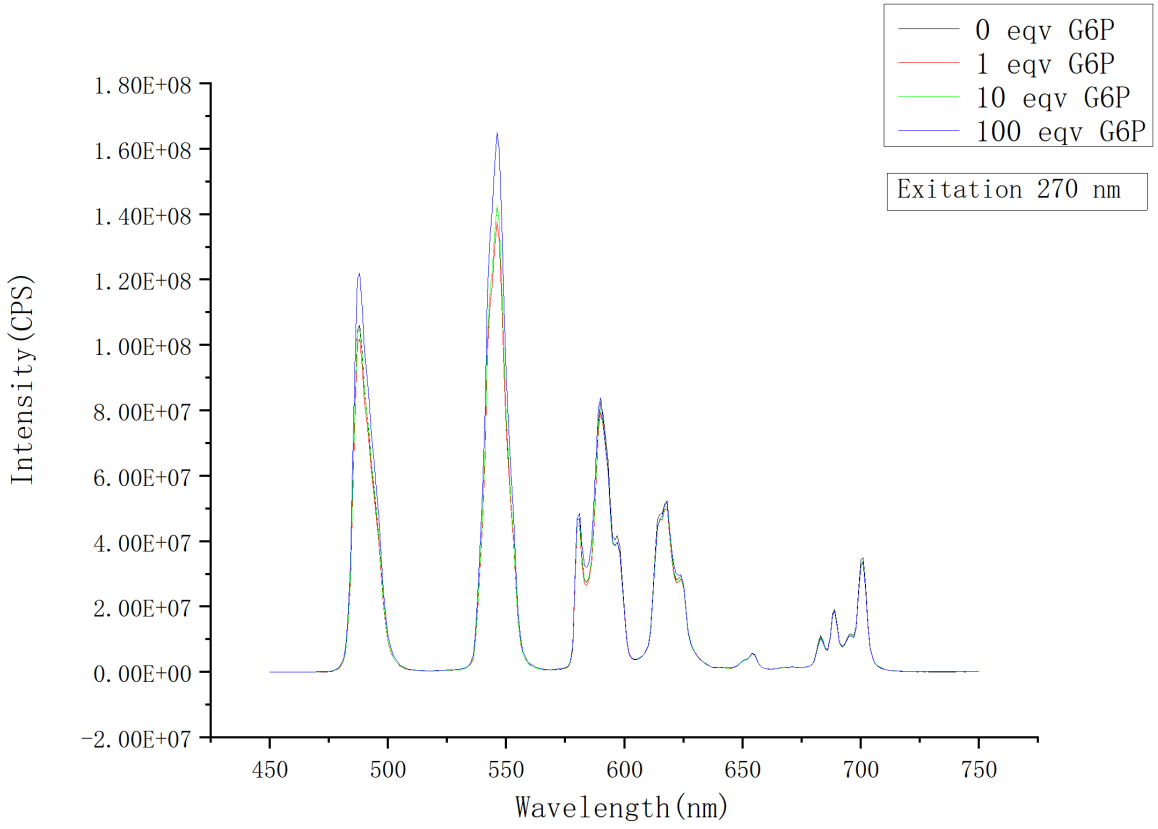


Figure 4.25 Overlay TbEu complex emission spectra before and after G6P addition. Emission spectra showing ratiometric response of Tb/Eu luminescence upon addition of G6P. (λex = 270 nm). HEPES buffer (20 mM, pH 7.4); TbEu heterometallic complex (2.5 × 10^{-4} mol/L); 25 ℃.

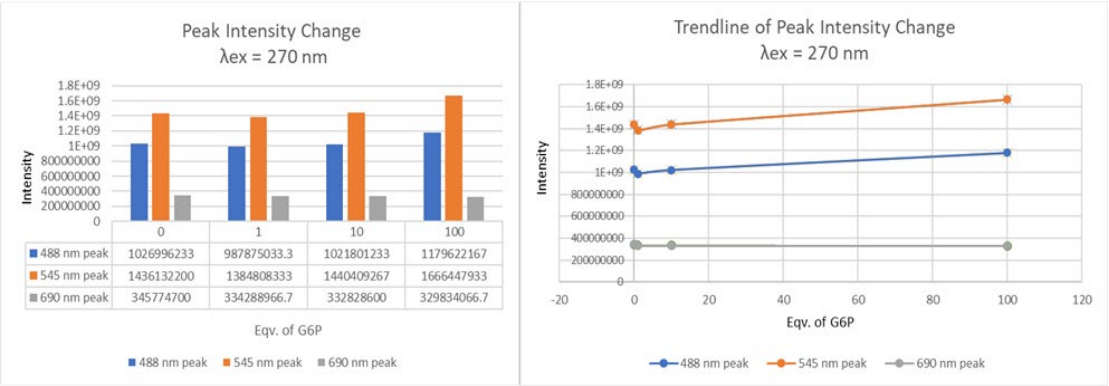


Figure 4.26 The trend of the three main peaks of the TbEu complex emission spectra after 100 eqv. G6P addition. (λex = 270 nm).

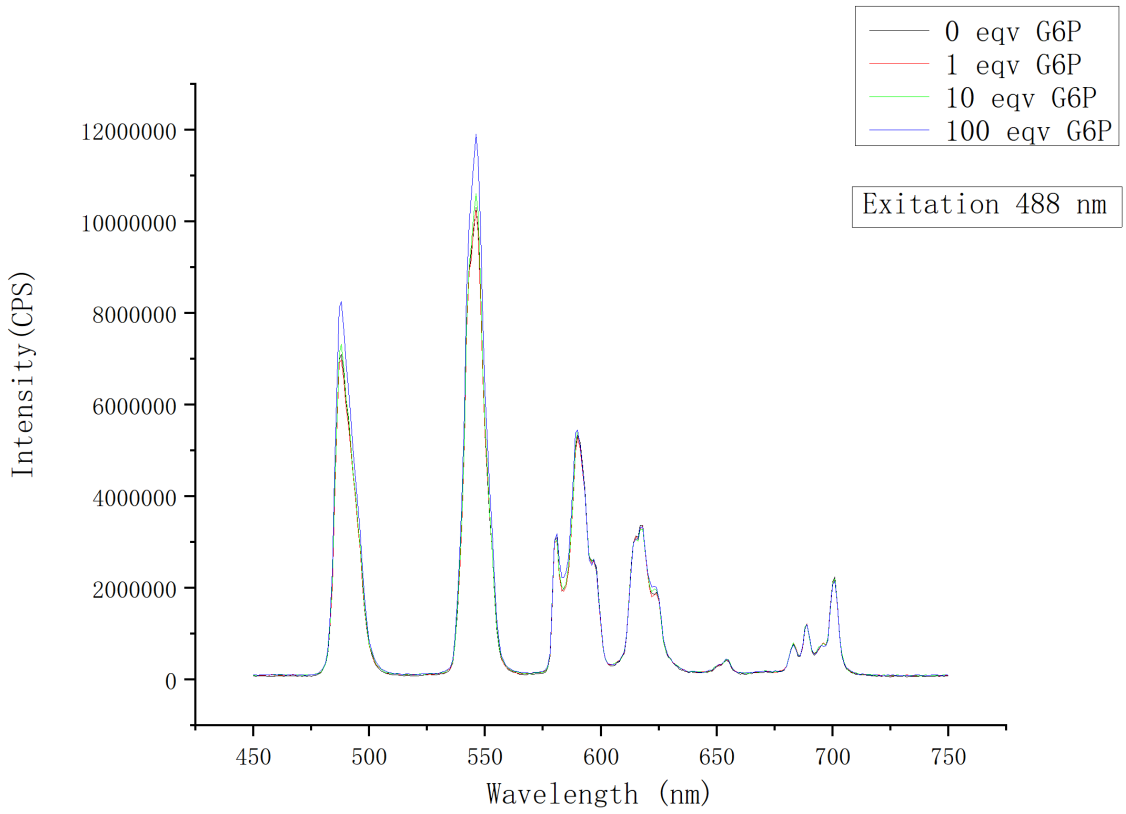


Figure 4.27 Overlay TbEu complex emission spectra before and after G6P addition. Emission spectra showing ratiometric response of Tb/Eu luminescence upon addition of G6P. (λex = 488 nm). HEPES buffer (20 mM, pH 7.4); TbEu heterometallic complex (2.5 × 10^{-4} mol/L); 25 ℃.

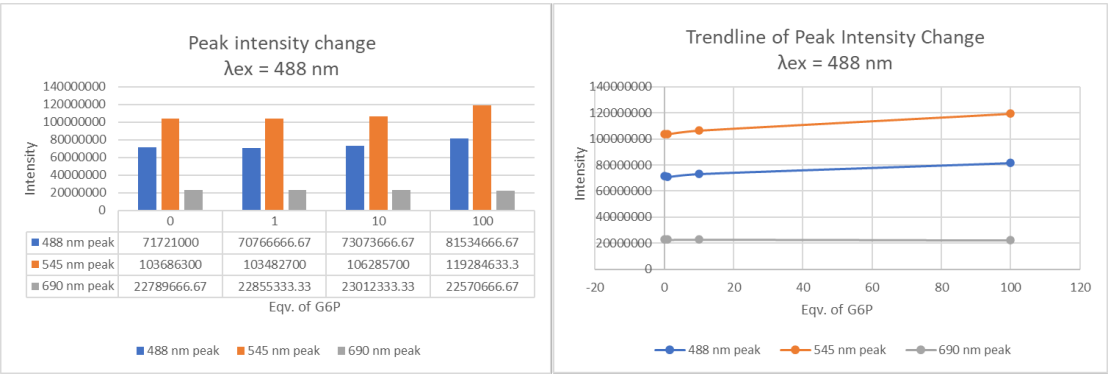


Figure 4.28 The trend of the three main peaks of the TbEu complex emission spectra after 100 eqv. G6P addition. (λex = 488 nm).

Excitation at 270 nm (through the chromophore), shown in Figure 4.25, or 488nm Tb^{3+} ($^7F_6$-$^5D_4$), shown in Figure 4.27, increases the intensity of the terbium-centred emission. At the same

time, there is essentially no change to the europium-centred emission, shown in Figure 4.26 & 4.28. This is a consequence of relatively small changes in the separation of the aryl chromophore and the lanthanide, and implies a reduction in the number of quenching pathways at the metal centre.

When considering the spectra obtained following excitation at 398 nm, shown in Figure 4.22, it is clear that the europium emission is relatively more intense than in the case of excitation at 488nm, shown in Figure 4.27. This is to be expected, since 398 nm excites the europium centre directly, while excitation at 488 can only give rise to europium emission following energy transfer from terbium. Indirect excitation via the chromophore at 270 nm (Figure 4.25) results in population of both centres, though it is notable that the spectrum is still dominated by terbium-centred emission lines.

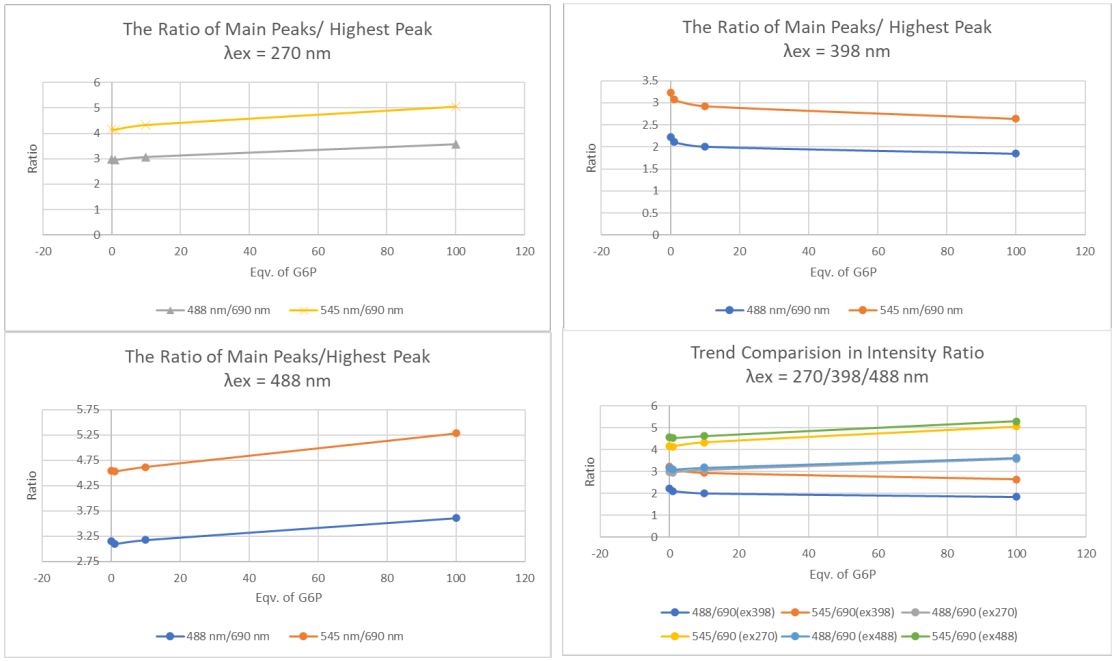


Figure 4.29. The ratio of the two main Tb emission peaks, 488 nm, 545 nm, vs the Eu emission peak, 690 nm, of the TbEu complex emission after 100 eqv. G6P addition. (λex = 270/398/488 nm).

Figure 4.29 shows the trend of Tb emission vs Eu emission after adding 0 to 100 eqv. of G6P. The trend of both λex = 270/488 nm grow up, but for the λex = 398 nm drops down. Excitation at 398 nm is in an anomalous relation to the others. This may be a consequence of the similarity in Energy between the Europium $^5L_6$ state and the Terbium $^5D_3$ state, shown in Figure 4.30. In such a system, these states can equilibrate as a consequence of resonant Energy Transfer between them. This Energy Transfer is likely perturbed binding to G6P, possibly as a consequence of structural change. By contrast, excitation at 488 nm (Tb $^7F_6$ - $^5D_4$) can populate the $^5D_0$ and $^5D_7$ States of Eu^{3+}, but such energy transfer is irreversible owing to the large energy gap between donor and acceptor.

At 488 nm of excitation, it seems reasonable to assume that resonant energy transfer from terbium to europium is effectively instantaneous when compared to the Lifetimes of the terbium and europium emissive states. As such, the enhancement of the terbium Luminescence relative to that of europium can also be assigned to Changes in the Coordination Sphere of the Terbium Centre, and the Removal of proximate quenching oscillation at the terbium which will reduce non-radiative quenching, and enhance the terbium-centred Emission.

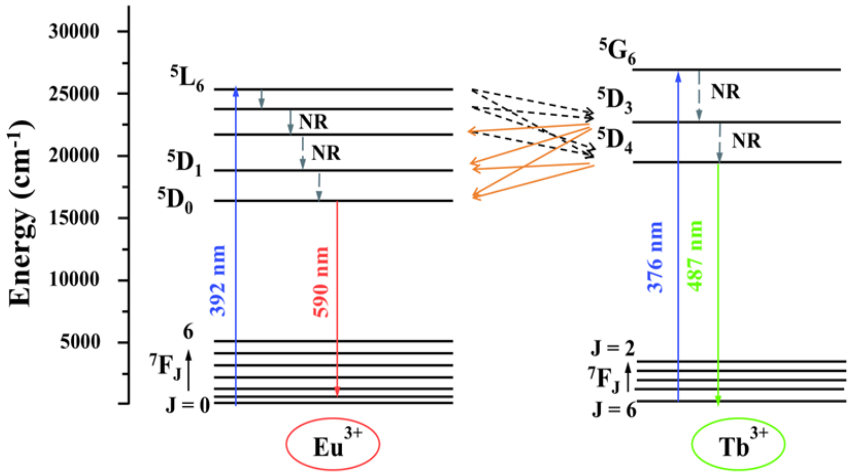


Figure 4.30. Proposed energy transfer pathway within the complex.

At 270 nm of excitation, the same logic can be applied to excitation through the chromophore. This will populate the excited state manifolds of both ions, meaning that the changes to the coordination sphere will dominate the observed changes in intensity in the same way that they do for 488 nm.

4.5 Coordination and Structural Characterisation

The luminescence measurements show similar results compared with the luminescence binding study. The photophysical data of q are summarised in Table 4.1. The number of water molecules that bind directly to Eu^{3+} or Tb^{3+} ions (q) can be calculated through luminescence lifetime measurements in H_2O and D_2O. The TbEu complex shows an average of 1.1 Eu and 0.8 Tb inner sphere water molecules. The EuTb complex shows 1.1 Eu and 0.8 Tb inner sphere water molecules on average.

Table 4.1 Photophysical properties of TbEu and EuTb complex recorded in H_2O and D_2O (l_{ex} as specified, 295 K). q = derived hydration numbers.

Compound	L_{ex} (nm)	L_{em} (nm)	t_{H_2O} (ms)	t_{D_2O} (ms)	q
Tb.Eu	270	700	0.63	2.35	1.1
	270	545	2.01	3.62	0.8
Eu.Tb	270	700	0.64	2.42	1.1
	270	545	2.10	3.70	0.8

On the basis of these data, it appears that both environments have similar degrees of inner sphere solvation.(However, it should be borne in mind that the accessibility of the metal may still differ; the relatively low solvation of the lanthanide in the heptadentate site is likely to be the consequence of the lipophilicity and bulk of the fourth pendent arm on the cyclen ring, while that of the octandentate site is the direct consequence of coordination to all but one of the available positions for water to bind to the lanthanide. In the case of the heptadentate site, low solvation does not preclude binding of a guest, indeed it could encourage binding of guests which can bind to the lanthanide while also having hydrophobic interactions with the fourth arm. By contrast, binding of a guest to the octadentate site would require a simple guest to displace water, or a chelating guest to displace water and one of the pendent donor groups; both these options are thermodynamically less favourable,making binding unlikely.

Addition of glucose-6-phosphate results in a negligible change in the luminescence lifetime at both metal centres, regardless of the location of europium and terbium. This suggests that there is no change in the overall solvation at the metal centres, with both still having essentially one bound water. This apparent contradiction with the steady-state luminescence spectra can be rationalised in terms of carboxylate being a monodentate ligand to the lanthanide. In such circumstances, a monodentate ligand will not need to displace water from the lanthanide bound in the heptadentate binding site, meaning that the overall observed q value is not influenced. This observation lends further weight to the suggestion that q values alone are not always an infallible method for establishing guest binding.

4.6 Conclusion

In conclusion, the use of bimetallic complexes presents a more complex picture than might originally have been imagined, though they still have potential as quantitative agents to probe anion binding. It is clear from the results described in this Chapter that many factors need to be taken into account beyond simplistic ideas about solvent displacement by anions. Excitation at 398 nm, the direct excitation of Eu^{3+}, which also indirectly excites terbium, likely through energy transfer from the higher excited state. The addition of G6P disrupts this delicate balance, thereby suppressing Tb^{3+} emission while leaving Eu^{3+} emission relatively stable. By contrast, under 270 nm excitation through the aryl chromophore or 488 nm excitation through Tb^{3+} direct excitation, the G6P binding increases the terbium emission while europium emission stays stable. It is notable that energy transfer between lanthanide ions cannot be neglected: Furthermore, it presents a complicated picture far beyond a simple one in which the emissive state of the donor lanthanide transfers energy to the acceptor state of the emissive lanthanide; this can lead to apparently unusual phenomena where a red emssive system can sensitise green light emission as a consequence of energy transfer in the upper manifold of excited states. As such, it is clear that all processes need to be considered in future studies of multimetallic systems. Overall, this work highlights the promise of heterometallic lanthanide complexes as responsive probes, but also emphasises the need for a deeper understanding of energy transfer and structural dynamics in order to design future multimetallic sensing platforms rationally.

4.7 References

(1) Tropiano, M.; Kenwright, A. M.; Faulkner, S. Lanthanide Complexes of Azidophenacyl-DO3A as New Synthons for Click Chemistry and the Synthesis of Heterometallic Lanthanide Arrays. *Chemistry–A European Journal* **2015**, *21* (15), 5697-5699.

(2) Routledge, J. D.; Zhang, X.; Connolly, M.; Tropiano, M.; Blackburn, O. A.; Kenwright, A. M.; Beer, P. D.; Aldridge, S.; Faulkner, S. Lanthanide complexes that respond to changes in cyanide concentration in water. *Angewandte Chemie* **2017**, *129* (27), 7891-7894.

(3) Jauregui, M.; Perry, W. S.; Allain, C.; Vidler, L. R.; Willis, M. C.; Kenwright, A. M.; Snaith, J. S.; Stasiuk, G. J.; Lowe, M. P.; Faulkner, S. Changing the Local Coordination Environment in Mono- and Binuclear Lanthanide Complexes through “Click” Chemistry. *Dalton Trans.* **2009**, *32*, 6283–6285.

(4) Hong, L.; Lin, W.; Zhang, F.; Liu, R.; Zhou, X. Ln [N $(SiMe_3)_2]_3$-catalyzed cycloaddition of terminal alkynes to azides leading to 1, 5-disubstituted 1, 2, 3-triazoles: new mechanistic features. *Chemical Communications* **2013**, *49* (49), 5589-5591.

(5) Rostovtsev, V. V.; Green, L. G.; Fokin, V. V.; Sharpless, K. B. A stepwise huisgen cycloaddition process: copper (I)-catalyzed regioselective" ligation" of azides and terminal alkynes. *Angewandte Chemie International Edition* **2002**, *41* (14), 2596-2599.

Chapter 5 Summary

This thesis investigated a series of responsive multinuclear lanthanide complexes for their interactions with glycolytic metabolites. The work focused on europium(III) and terbium(III) systems and on how their luminescence changes upon the addition of guest molecules such as glucose-6-phosphate (G6P) and fructose-1,6-bisphosphate (FBP). The change in coordination environment, self-assembly, and energy transfer are also studied in this work.

Chapter 2 showed that binuclear nitro-m-xylyl lanthanide complexes (Ln.NMM) can bind phosphate-containing glycolytic metabolites. This binding caused changes in luminescence, paramagnetic NMR spectra, and CEST proton exchange study. The results showed that glucose phosphate binding changes the coordination environment around the lanthanide and reduces non-radiative quenching, which changes europium emission. Preliminary CEST studies also suggested that these systems may be useful for imaging applications.

Chapter 3 investigated competitive binding and energy transfer in heterometallic supramolecular assemblies formed between Eu.NMM and Tb.iphth complexes. The formation of the assembly enabled energy transfer from terbium to europium. The addition of G6P or FBP disrupted the assembly and changed the energy-transfer process. As a result, terbium emission increased while europium emission decreased. These studies showed that G6P or FBP can be used for displacement sensing for such a system.

Chapter 4 introduced a new class of heterometallic europium–terbium complexes containing both seven- and eight-coordinate lanthanide centres. These complexes were designed to create different coordination environments for phosphate guest binding. The complexes were successfully synthesised using CuAAC click chemistry. Photophysical and binding studies were then carried out. The results showed that G6P binding caused changes in luminescence intensity.

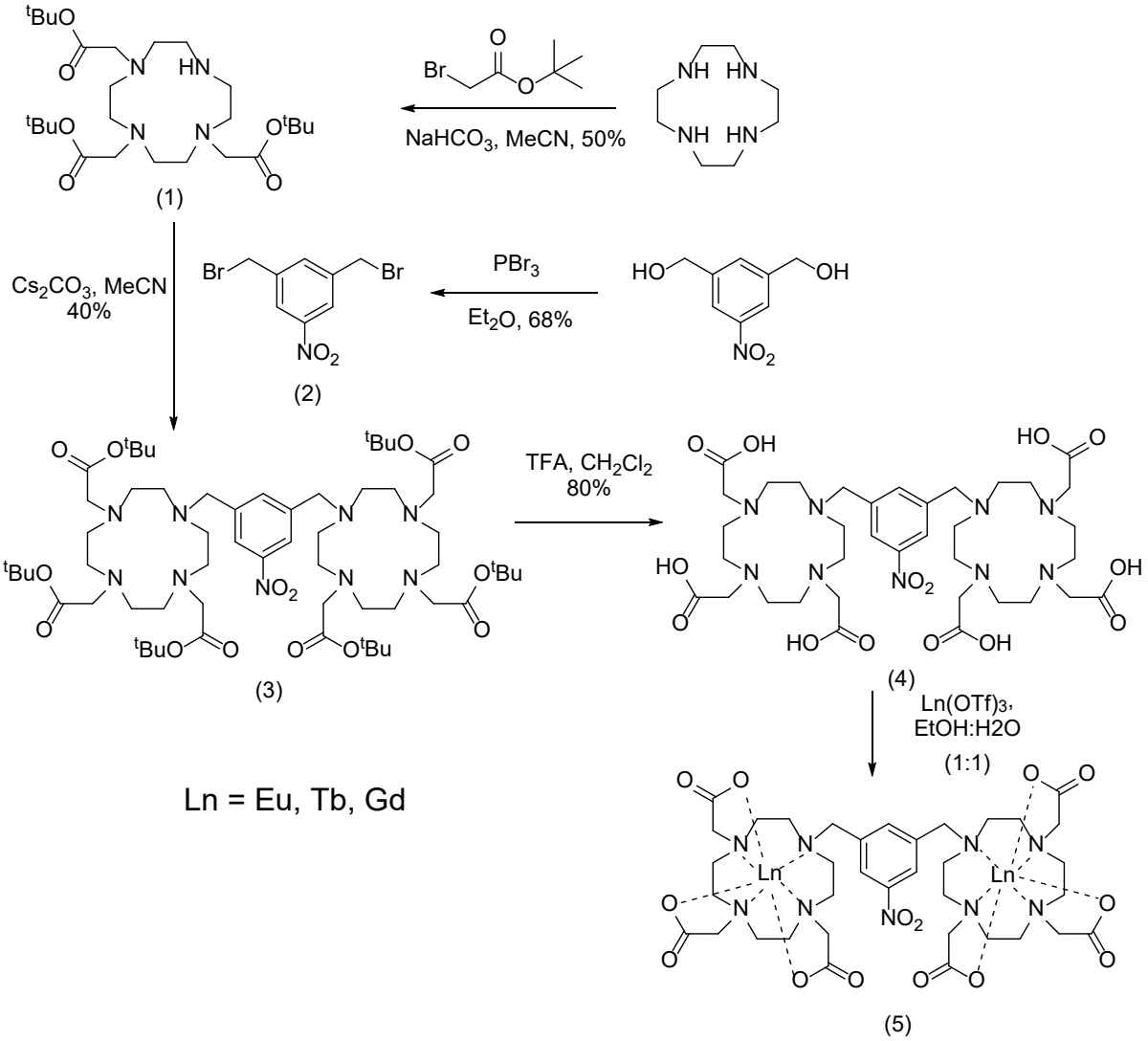
Overall, this thesis demonstrated that coordination environment, ligand design, self-assembly, and intermetallic energy transfer can be used to create lanthanide systems with tunable luminescence behaviour. The work improved the understanding of heterometallic europium–terbium complexes and their photophysical behaviour. It also provided useful design strategies for the future development of luminescent probes for metabolic sensing and bioimaging applications.

Chapter 6 Experimental

6.1 Synthesis and chemical characterisation

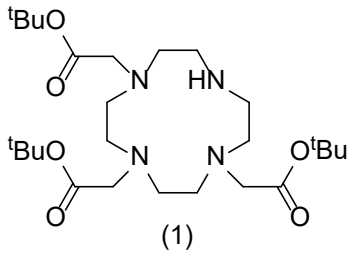
General Considerations

DO3A-tert-butyl ester was synthesised according to a previously reported procedure.[1] All reagents were of laboratory grade and obtained from established commercial suppliers. Deionised water was purified using a Milli-Q Millipore system prior to use. NMR spectra were acquired on either a Bruker Avance III HD nanobay spectrometer (9.4 T; ^{1}H 400.2 MHz, ^{13}C 100.6 MHz) or a Bruker NEO 600 instrument equipped with a broadband helium cryoprobe (^{1}H 600.4 MHz, ^{13}C 151.0 MHz), and the resulting data were processed using MestreNova software. Mass spectrometric analyses were performed using a Waters LCT Premier or an Agilent 6120 mass spectrometer. Infrared spectra were recorded for solid samples on a PerkinElmer FT-IR spectrometer fitted with an attenuated total reflectance (ATR) accessory. UV–visible absorption measurements were obtained using a PG Instruments T-60 UV–visible spectrophotometer.



Scheme 5.1 Reaction scheme of synthetic route to Ln.NMM.

1,4,7,10-Tetraazacyclododecane-1,4,7-triacetate tert-butyl triester (1)



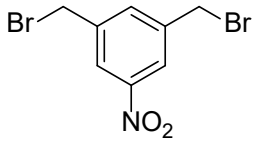
(1)

(1) is prepared in accordance with a modified procedure.[1]

A cooled (0 °C) suspension of 1,4,7,10-tetraazacyclododecane (4.00 g, 22.50 mmol) and sodium bicarbonate (6.26 g, 74.25 mmol) in freshly distilled acetonitrile (135 mL) was stirred for 30 min prior to the slow addition of tert-butyl bromoacetate (11 mL, 74.25 mmol) over 30 min. The reaction mixture was then allowed to reach room temperature and maintained under stirring for 48 h. Insoluble material was removed by filtration, and the filtrate was concentrated under reduced pressure to afford a crude solid. This residue was suspended in toluene (200 mL) and stirred for 72 h to extract soluble impurities, which were removed by filtration. The remaining solid was collected and dried under vacuum to give the purified product.

Yield: 7.01 g, 50%. ^{1}H NMR ($CDCl_3$, 600.4 MHz) δ (ppm) 10.03 (1H, br. s), 3.37 (4H, s), 3.29 (2H, s), 3.09 (4H, br. m), 2.90 (12H, br. m), 1.45 (27H, d). ^{13}C NMR ($CDCl_3$, 151.0 MHz) δ (ppm) 170.79, 169.90, 82.12, 81.97, 58.51, 51.65, 49.50, 47.80, 28.51, 28.47. ES^+ MS (*m/z*) 515.4 ($[M + H]^+$).

3,5-Bis(bromomethyl)nitrobenzene (2)



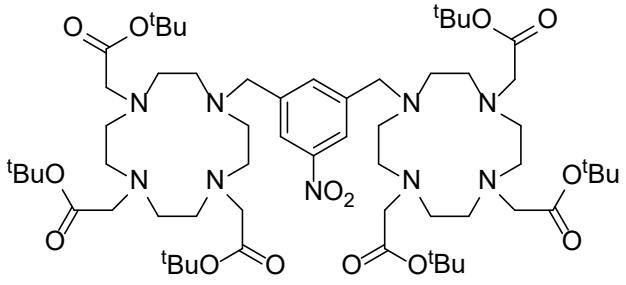
(2)

(2) is prepared in accordance with a reported procedure.[2]

5-Nitro-m-xylene-α,α′-diol (2.00 g, 10.92 mmol) was dissolved in diethyl ether (50 mL) with stirring and cooled to 0 °C. A solution of phosphorus tribromide (2 mL) in ether (30 mL) was then added slowly, and the reaction mixture was maintained at 0 °C for 6 h before being allowed to warm to room temperature and stirred for a further 12 h. The reaction was quenched by careful addition to crushed ice, followed by extraction with ether (5 × 40 mL). The combined organic extracts were washed sequentially with aqueous sodium carbonate solution and water, then dried over anhydrous sodium sulfate. Removal of the solvent under reduced pressure afforded the product as a white solid.

Yield: 2.29 g, 68%. ^{1}H NMR ($CDCl_3$, 400.2 MHz) δ (ppm) 8.19 (2H, d, *J*=1.7 Hz), 7.75 (1H, t, *J*=1.7 Hz,), 4.52 (4H, s). ^{13}C NMR ($CDCl_3$, 100.6 MHz) δ (ppm) 148.68, 140.52, 135.40, 123.82, 30.77. ES^+ MS (*m/z*) 325.2 ($[M+NH_4]^+$).

α,α'-Bis(DO3A tert-butyl triester)-3,5-dimethylnitrobenzene (3)



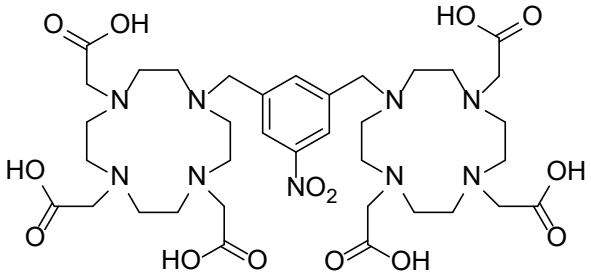
(3)

(3) is prepared in accordance with a modified procedure.[3]

Under a nitrogen atmosphere, 1,4,7,10-tetraazacyclododecane-1,4,7-triacetate tert-butyl triester (3.82 g, 6.42 mmol) was dissolved in anhydrous acetonitrile (125 mL), and caesium carbonate (5.96 g, 18.34 mmol) was added in one portion. A solution of 3,5-bis(bromomethyl)nitrobenzene (1.13 g, 3.67 mmol) in dry acetonitrile (10 mL) was then introduced, and the reaction mixture was heated at reflux for 72 h. Upon cooling to room temperature, the mixture was clarified by filtration to remove inorganic solids and concentrated under reduced pressure. The residue was dissolved in dichloromethane (125 mL) and washed with saturated brine (5 × 125 mL). The organic layer was dried over magnesium sulfate and concentrated to afford a dark yellow oil. The crude product was purified by silica gel column chromatography using a dichloromethane/acetone/methanol eluent with a gradual increase in methanol content; the target hexaester was isolated at a solvent composition of 80:10:10 (v/v/v).

Yield: 1.23 g, 40%. ^{1}H NMR ($CDCl_3$, 600.4 MHz) δ (ppm) 8.54 (2H, s), 8.04 (1H, s), 3.75 (4H, br.), 3.51 – 2.05 (44H, br. m), 1.44 (54H, s). ^{13}C NMR ($CDCl_3$, 151.0 MHz) δ (ppm) 173.72, 172.63, 148.88, 139.48, 123.80, 83.18, 83.00, 82.69, 58.30, 56.20, 55.70, 49.71, 28.26, 28.24, 27.90. ES$^+$ MS (*m*/*z*) 1176.7 ([M + H]$^+$), 1198.7 ([M + Na]$^+$), 589.8 ([M + 2Na]$^{2+}$).

α,α'-Bis(H_3.DO3A)-3,5-dimethylnitrobenzene (4)



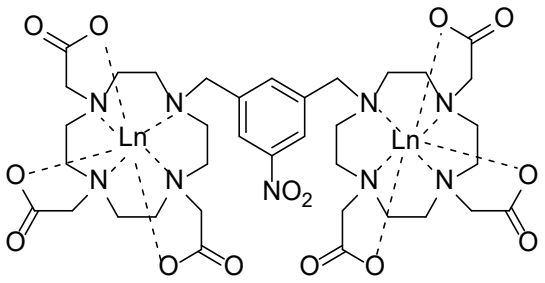
(4)

(4) is prepared in accordance with a modified procedure.[3]

The protected ligand α,α′-bis(DO3A tert-butyl triester)-3,5-dimethylnitrobenzene (3) (0.70 g, 0.55 mmol) was dissolved in dichloromethane (9.1 mL), and a solution of trifluoroacetic acid in dichloromethane (6.4 mL TFA in 5.3 mL DCM) was added slowly. The reaction mixture was stirred at ambient temperature for 48 h, after which all volatile components were removed under reduced pressure to give an orange oil. Residual trifluoroacetic acid was eliminated by repeated co-evaporation with methanol and ethanol. The residue was subsequently dissolved in a minimal volume of methanol, and diethyl ether was added to induce precipitation of the product. The resulting white solid was collected by filtration and dried under reduced pressure.

Yield: 0.37 g, 80%. ^{1}H NMR (D_2O, 600.4 MHz) δ (ppm) 8.35 (2H, s), 8.23 (1H, s), 4.58-2.55 (48H, br. m). ^{13}C NMR (D_2O, 151.0 MHz) δ (ppm) 169.24, 163.31, 163.07, 162.84, 162.60, 148.17, 125.51, 119.25, 117.32, 115.39, 113.45, 55.88, 54.90, 53.83, 50.25, 47.81. ES^+ MS (*m*/*z*) 840.3 ($[M + H]^+$), 862.3 ($[M+ Na]^+$).

α,α'-Bis(Ln.DO3A)-3,5-dimethylnitrobenzene (5)



(5)

Method 1:

The ligand α,α′-bis(H_3·DO3A)-3,5-dimethylnitrobenzene (4) (27.5 mg, 0.033 mmol) and europium(III) triflate (47.3 mg, 0.079 mmol) were dissolved in a 1:1 mixture of ethanol and water (660 µL, c_{ligand} = 0.05 M) in a sealed mass-spectrometry vial. The solution was heated at 50 °C with stirring for 24 h using a metal heating block. The pH was subsequently adjusted to neutral or slightly basic by incremental addition of 1 M NaOH (6–7 equiv., 126 µL total), introduced portionwise (3 + 2 + 1–2 equiv.) with 1 h stirring intervals between additions to promote complete metalation; after each addition, the vial was resealed and returned to the heating block. Following a total reaction time of 48 h, the resulting insoluble material was removed by centrifugation, and the supernatant was clarified by filtration through a 0.2 µm

syringe filter. Excess europium salts were removed by dialysis against water, and solvent removal by lyophilisation afforded the product as a pale yellow solid.

Eu: Yield: 30 mg, 8 %. ^{1}H NMR (D_2O, 400 MHz) δ (ppm) 34.55, 34.27, 28.70, 24.66, 24.61, 19.97, 15.11, 11.21, −1.04, −2.90, −4.10, −5.22, −6.85, −7.50, −8.16, −9.02, −10.87, −11.64, −14.61, −17.18,−18.18. MALDI-TOF HRMS (m/z) 1139 (M^+), 1162 ($[M + Na]^+$). UV-vis (H_2O) λ (I/Imax) 211 (1.00), 266 (0.43) nm.

Tb: Yield: 32 mg, 10 %. ^{1}H NMR peaks are too broad to assign. MALDI-TOF HRMS (m/z) 1153 ($[M + H]^+$).

Gd: Yield: 24 mg, 12 %. MALDI-TOF HRMS (*m*/*z*) 1149, 1150 ($[M + H]^+$).

Method 2:

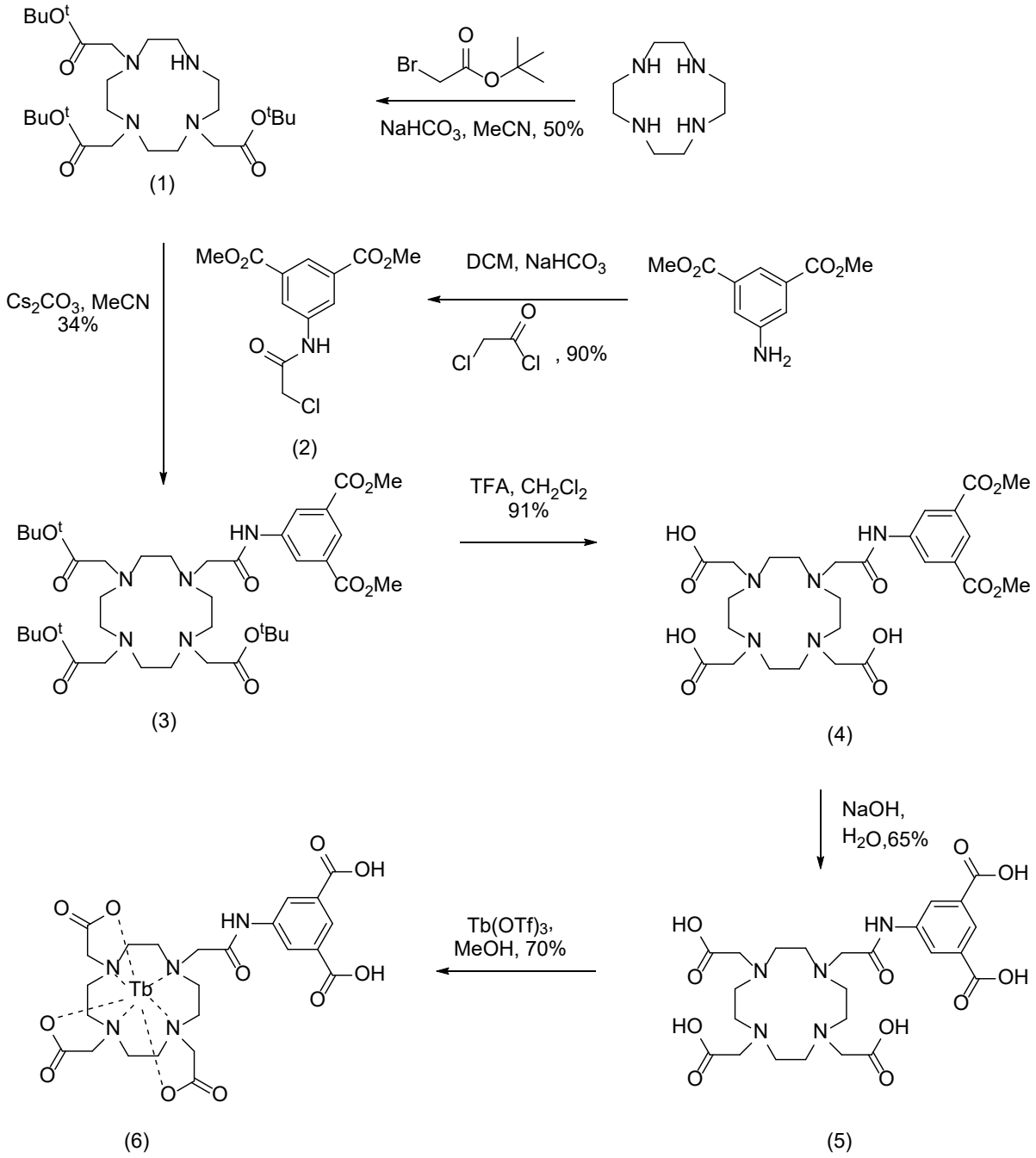
Ln = Eu, Tb

The ligand α,α′-bis(H_3·DO3A)-3,5-dimethylnitrobenzene (4) (50–100 mg, 1.0 equiv.) and europium(III) triflate (3.0 equiv.) were combined in acetonitrile (2.5–5 mL) in a sealed microwave vial. The resulting solution was heated at 90 °C with stirring for 144 h using a metal heating block. After cooling, the reaction mixture was adjusted to neutral or slightly basic pH by addition of 1 M NaOH, inducing formation of an insoluble solid, which was removed by

centrifugation. The supernatant was further clarified by passage through a 0.2 μm syringe filter. Excess europium salts were removed by dialysis against water, and the solvent was subsequently removed by lyophilisation to afford the product as a pale yellow solid.

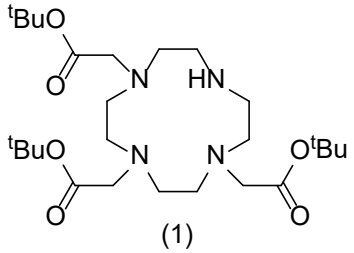
Eu: Yield: 60 mg, 32 %. ^{1}H NMR (D_2O, 400 MHz) δ (ppm) 34.66, 34.37, 28.75, 24.63, 24.51, 19.92, 15.09, 11.11, −1.14, −2.80, −4.20, −5.29, −6.89, −7.54, −8.18, −9.08, −10.82, −11.44, −14.51, −17.28,−18.38. MALDI-TOF HRMS (m/z) 1139 (M^+), 1140 ($[M+H]^+$). UV-vis (H_2O) λ (I/Imax) 210 (1.00), 265 (0.41) nm.

Tb: Yield: 39 mg, 30 %. ^{1}H NMR peaks are too broad to assign. MALDI-TOF HRMS (m/z) 1174 ($[M + Na]^+$). UV-vis (H_2O) λ (I/Imax) 209 (1.00), 266 (0.35) nm.



Scheme 2. Full synthesis route of Terbium-isophthalate complex.[4]

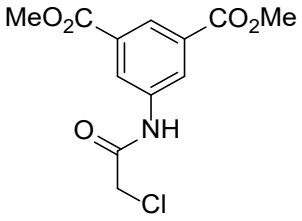
1,4,7,10-Tetraazacyclododecane-1,4,7-triacetate tert-butyl triester (1)



(1)

(1) is prepared in accordance with a modified procedure and reported above.[1]

l,3-Dimethyl-5-(amino carbonyl methylene chloride isophthalate) (2)

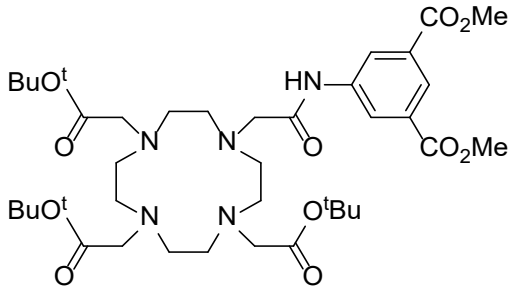


(2)

(2) is prepared in accordance with a reported procedure.[4]

Yield: 1.95 g, 90%. ^{1}H NMR ($CDCl_3$, 600.4 MHz) δ (ppm) 8.60 (1H, s, NH), 8.45 (3H, s, Ar-H), 4.22 (2H, s, CH2-Cl), 3.85 (6H, s, $2CH_3$). ^{13}C NMR (MeOD, 151.0 MHz) δ (ppm) 165.24, 164.31, 138.17, 133.52, 125.39, 53.88, 43.81. ES^+ MS (*m*/*z*) 308.3 ($[M + Na]^+$). IR-ATR *v* (cm^{-1}) 1715 (C=O), 1680 (C=O), 1544 (N-H).

l,4,7,10-Tetraazacyclododecane-l,4,7-tri(*tert*-butoxycarbonylmethyl)-10-(dimethyl-5-isophthalato acetamide) (3)

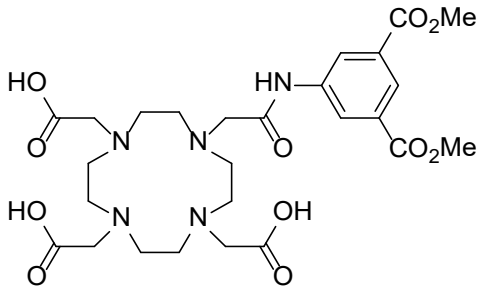


(3)

(3) is prepared in accordance with a reported procedure.[4]

Yield: 0.89 g, 34 %. ^{1}H NMR ($CDCl_3$, 600.4 MHz) δ (ppm) 8.52 (2H, s, Ar-H), 8.35 (1H, s, Ar-H), 3.92 (6H, s, $2CH_3$), 3.15 – 3.40 (24H, m, N-CH_2 and NCH_2CO), 1.30 – 1.55 (81H, m, CCH_3). ^{13}C NMR ($CDCl_3$, 151.0 MHz) δ (ppm) 170.8, 165.28, 139.15, 124.39, 82.30, 59.88, 55.24, 51.66, 50.81. ES$^+$ MS (*m*/*z*) 764.3 ($[M + H]^+$), 785.8 ($[M + Na]^+$). IR-ATR *v* (cm^{-1}) 1718 (C=O), 1682 (C=O).

l,4,7,10-Tetraazacyclododecane-l,4,7-triacetate-10-(dimethyl-5-isophthalato acetamide) (4)

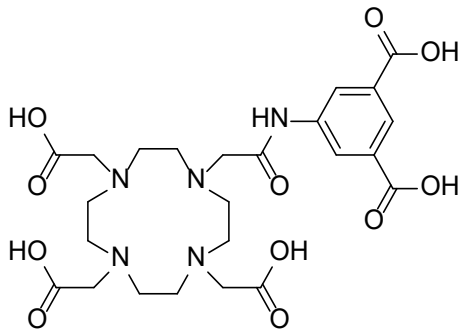


(4)

(4) is prepared in accordance with a reported procedure.[4]

Yield: 0.54 g, 91 %. ^{1}H NMR (D_2O, 600.4 MHz) δ (ppm) 8.26 (1H, s, Ar-H), 8.15 (2H, s, Ar-H), 3.88 (6H, s, $2CH_3$), 3.10 – 3.60 (24H, m, N-CH_2 and NCH_2CO). ^{13}C NMR (D_2O, 151.0 MHz) δ (ppm) 168.4, 163.70, 131.15, 126.40, 115.64, 59.88, 55.94, 50.40. ES^+ MS (*m*/*z*) 596.3 ($[M + H]^+$). IR-ATR *v* (cm^{-1}) 1720 (C=O), 1664 (C=O), 1576 (N-H).

l,4,7,10-Tetraazacyclododecane-l,4,7-triacetate-10-(dicarboxylic acid-5-isophthalato acetamide) (5)

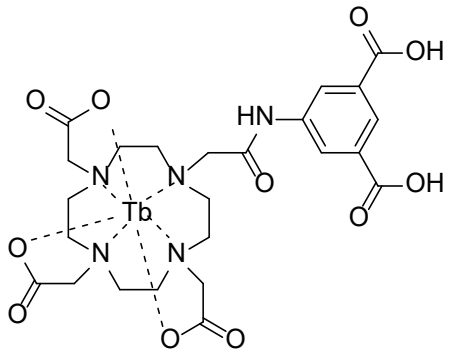


(5)

(5) is prepared in accordance with a reported procedure.[4]

Yield: 140 mg, 65 %. ^{1}H NMR (D_2O, 600.4 MHz) δ (ppm) 7.94 (1H, s, Ar-H), 7.80 (2H, s, Ar-H), 2.20 – 3.30 (24H, m, N-CH_2 and NCH_2CO). ^{13}C NMR (D_2O, 151.0 MHz) δ (ppm) 180.3, 173.8, 137.70, 125.50, 120.64, 58.30, 56.80. ES^+ MS (*m*/*z*) 568.4 ($[M + H]^+$), 590.3 ($[M + Na]^+$). IR-ATR *v* (cm^{-1}) 3320 (O-H), 1694 (C=O), 1589 (N-H).

l,4,7,10-Tetraazacyclododecane-l,4,7-tris(acetate)-l0-(dicarboxylicacid-5-isophthalato acetamide) terbium complex (6)



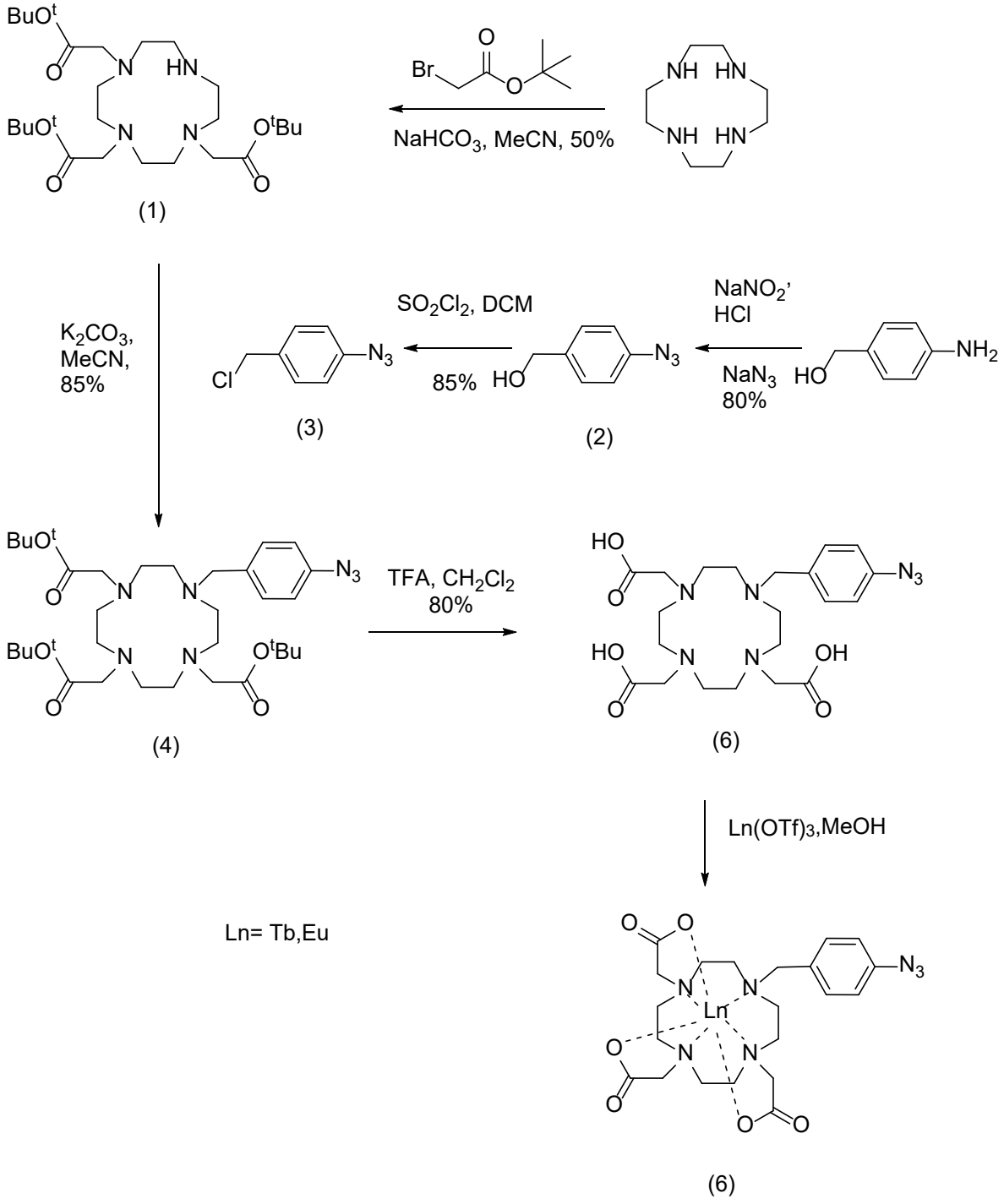
(6)

(6) is prepared in accordance with a reported procedure.[4]

Yield: 30 mg, 70 %. ^{1}H NMR (D_2O, 400 MHz) δ (ppm) 260.50, 245.90, 234.52, 169.54, 137.87, 124.20, 119.23, 85.11, −52.20, −64.10, −75.70, −77.85, −97.50, −100.16, −129.02, −144.80, −352.60, −364.61, −407.40. MALDI MS (m/z) 746 ($[M + Na]^+$). IR-ATR *v* (cm^{-1}) 3422 (O-H), 1690 (C=O), 1616 (N-H).

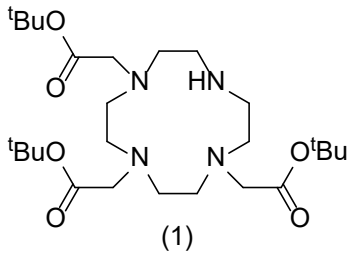
Chapter 4 Synthesis and chemical characterisation

Part 1: Azidobenzyl-DO3A complex



Scheme 5.3 Full synthesis route of Azidobenzyl-DO3A complex.

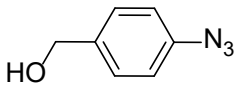
1,4,7,10-Tetraazacyclododecane-1,4,7-triacetate tert-butyl triester (1)



(1)

(1) is prepared in accordance with a modified procedure and reported above.[1]

(4-Azidophenyl)methanol (2)

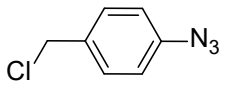


(2)

(2) is prepared in accordance with a reported procedure.[5]

Yield: 1.25, 90 %. ^{1}H NMR ($CDCl_3$, 400 MHz) δ (ppm) 7.35 (2H, d, *J*= 8.4 Hz), 7.02 (2H, d, *J*= 8.4 Hz), 4.65 (2H, s), 1.76 (1H, br). ^{13}C NMR ($CDCl_3$, 151.0 MHz) δ (ppm) 139.3, 137.5, 128.6, 120.2, 62.5.

1-Azido-4-(chloromethyl)benzene (3)

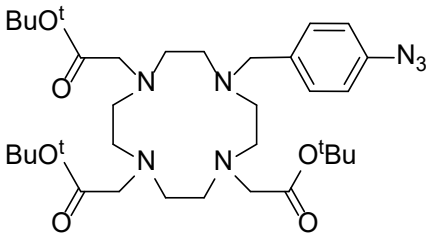


(3)

(3) is prepared in accordance with a reported procedure.[5]

Yield: 1.12, 85 %. ^{1}H NMR ($CDCl_3$, 400 MHz) δ (ppm) 7.37 (2H, d, *J*= 8.5 Hz), 7.02 (2H, d, *J*= 8.5 Hz), 3.48 (2H, s).^{13}C NMR ($CDCl_3$, 151.0 MHz) δ (ppm) 140.3, 134.5, 129.6, 32.5.

Tri-tert-butyl-2,2',2''-(10-(4-azidobenzyl)-1,4,7,10-tetraazacyclododecane- 1,4,7-triyl)triacetate (4)

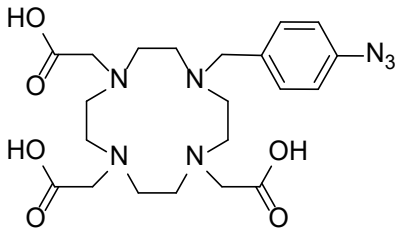


(4)

The triester (2.15 g, 3.55 mmol) was dissolved in anhydrous acetonitrile (120 mL), followed by the addition of potassium carbonate (0.82 g, 6.0 mmol) and 1-azido-4-(chloromethyl) benzene (3) (0.48 g, 3.6 mmol). The suspension was stirred at ambient temperature overnight, then filtered to remove inorganic salts and concentrated under reduced pressure. The resulting residue was purified by silica gel column chromatography using a gradient of methanol in chloroform (0–10%) to afford the product as a yellow solid.

Yield: 1.92 g, 85 %. ^{1}H NMR (DMSO, 400 MHz) δ (ppm) 7.43 (2H, d, *J* = 8.2 Hz), 7.07 (2H, d, *J* = 8.3 Hz), 3.63 (2H, s), 3.09 – 2.20 (22 H, m), 1.46 (27H, s). ES^{+} MS (m/z) 646.4 ([M + H]$^{+}$). ^{13}C NMR (DMSO, 151.0 MHz) δ (ppm) 173.44, 138.84, 132.39, 119.30, 82.31, 81.99, 57.23, 56.19, 55.96. IR-ATR *v* (cm^{-1}) 1690 (C=O).

2,2',2''-(10-(4-Azidobenzyl)-1,4,7,10-tetraazacyclododecane-1,4,7- triyl)triacetic acid (5)

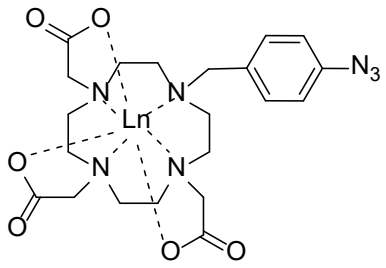


(5)

Compound (4) (1.8 g, 4.68 mmol) was dissolved in dry acetonitrile (100 mL), after which a premixed solution of trifluoroacetic acid and dichloromethane (1:1, 8 mL each) was introduced slowly. The reaction was maintained at room temperature with stirring for 24 h, then concentrated in vacuo to remove all solvents. The crude material was taken up in a small quantity of methanol, and diethyl ether was added to effect precipitation of the product as a white solid. The mother liquor was decanted, and the isolated solid was dried under vacuum to afford the target compound (5).

Yield: 1.06 g, 80 %. ^{1}H NMR (D_2O, 400 MHz) δ (ppm) 7.54 (2H, d, J = 8.2 Hz), 7.13 (2H, d, J = 8.3 Hz), 3.23 – 4.17 (26 H, m). ^{13}C NMR (D_2O, 151.0 MHz) δ (ppm) 167.50, 135.37, 131.21, 119.89, 94.91, 74.15, 48.46. ES^{+} MS (m/z) 478.5 ([M + H]$^{+}$). IR-ATR ν (cm^{-1}) 3312 (O-H), 1680 (C=O).

Lanthanide azidobenzylDO3A complexes (6)



(6)

General Synthetic Methods for Lanthanide AzidobenzylDO3A Complexes (6):

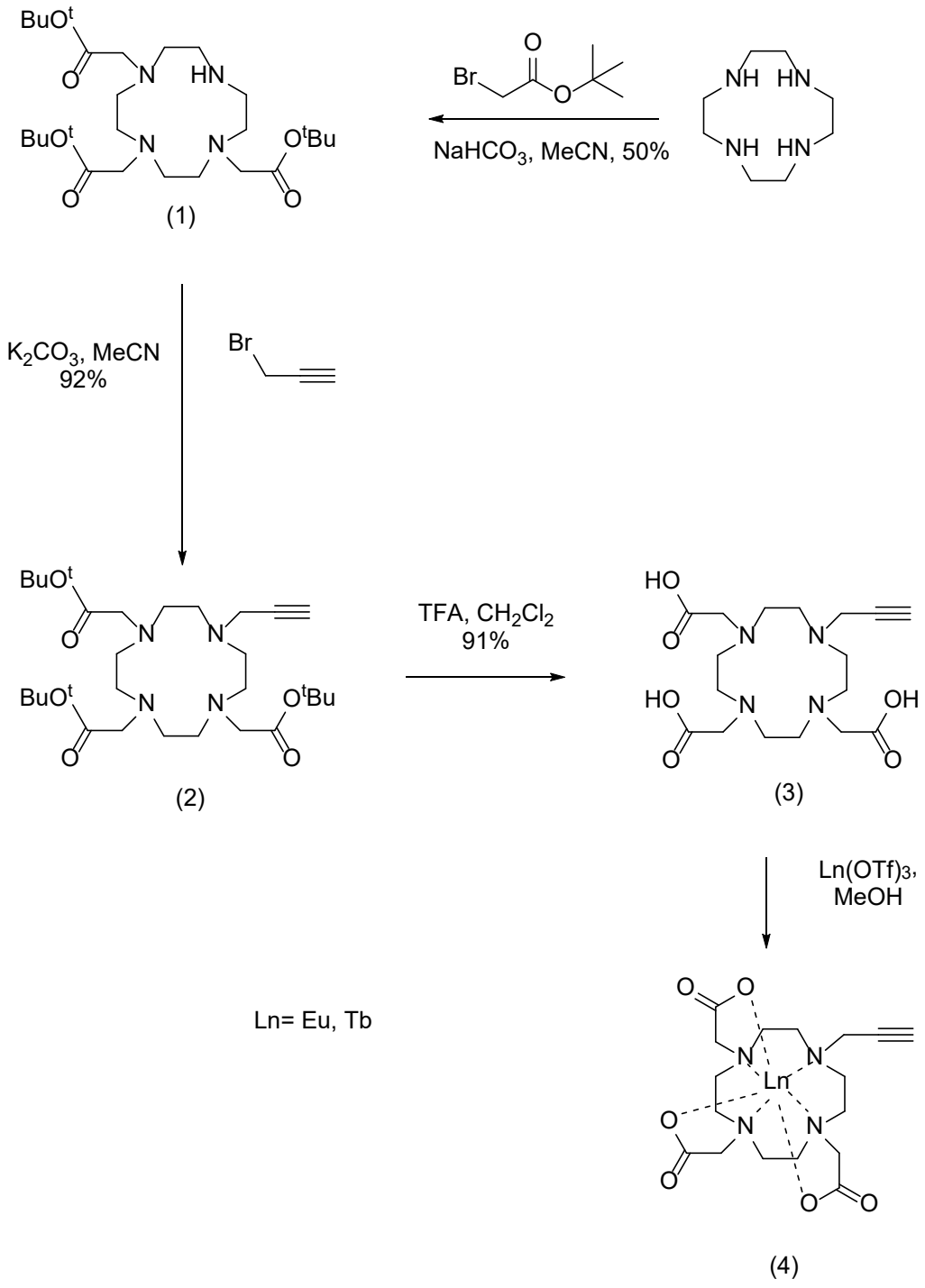
Ligand (5) was dissolved in methanol, followed by the addition of the corresponding lanthanide chloride hexahydrate. The resulting suspension was heated at 60 °C with stirring for 1 h, after which the pH was adjusted to approximately 4 by careful dropwise addition of aqueous sodium hydroxide (1 M). The mixture was then maintained at 60 °C under stirring for a further 48 h. After removal of the solvent, the residue was redissolved in methanol and the pH was raised to approximately 10 by gradual addition of 1 M sodium hydroxide solution. The resulting insoluble inorganic material was removed by centrifugation, and the

supernatant was clarified by passage through a syringe filter. Final removal of solvent by lyophilisation afforded the desired product.

Eu: Yield: 89 mg, 65 %. ^{1}H NMR (D_2O, 400 MHz) δ (ppm) 24.60, 7.28, -5.84, -7.76, -9.66, -15.60, -16.73, -18.83. Only resolved peaks observed outside the 0-5 ppm chemical shift range are included. ES^+ MS (*m*/*z*) 628.14 ($[M + H]^+$).

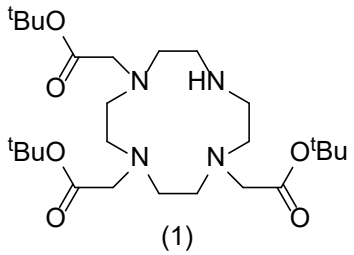
Tb: Yield: 72 mg, 51 %. ^{1}H NMR (D_2O, 400 MHz) δ (ppm) 308.0, 176.5, -52.42, -142.30, -188.25, -234.24, -264.10, -329.72. Only resolved peaks observed outside the -20–20 ppm chemical shift range are included. ES^+ MS (*m*/*z*) 634.15 ($[M + H]^+$).

Part two:



Scheme 5.4 Full synthesis route of the propargyl lanthanide complex.[6]

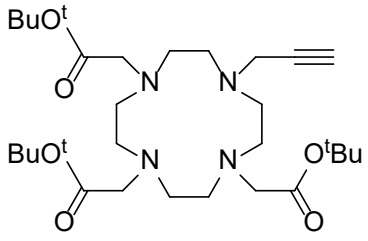
1,4,7,10-Tetraazacyclododecane-1,4,7-triacetate tert-butyl triester (1)



(1)

(1) is prepared in accordance with a modified procedure and reported above.[1]

Propargyl (DO3A *tert*-butyl triester) (2)

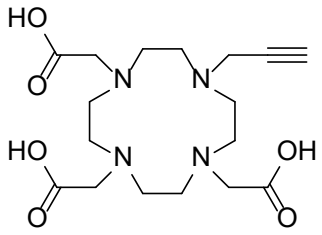


(2)

(2) is prepared in accordance with a reported procedure.[6]

Yield: 340 mg, 92%. ^{1}H NMR ($CDCl_3$, 400 MHz) δ (ppm) 3.40 – 2.80 (8H, br, NCH_2), 2.80 – 2.30 (12H, m, NCH_2), 2.16 (1H, br, C≡CH), 1.95 (4H, br. NCH_2R), 1.60 – 1.15 (27H, br. m, 3 ×^{t}Bu). ES$^+$ MS (*m*/*z*) 553 ([M + H]$^+$), 575 ([M +Na]$^+$).

Propargyl (H_3.DO3A) (3)

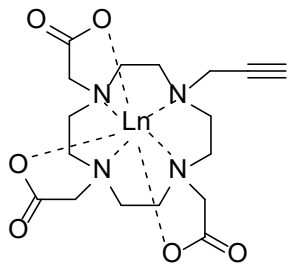


(3)

(3) is prepared in accordance with a reported procedure.[6]

Yield: 340 mg, 91 %. ^{1}H NMR (MeOD, 400 MHz) δ (ppm) 3.82 (8H, br. s, NCH2), 3.42 (8H, br. m, NCH2), 3.08 (8H, br. s, NCH2), 2.85 (1H, s, C≡CH). ES^+ MS (*m*/*z*) 385 ([M + H]$^+$).

Propargyl (Ln.DO3A) complex (4)



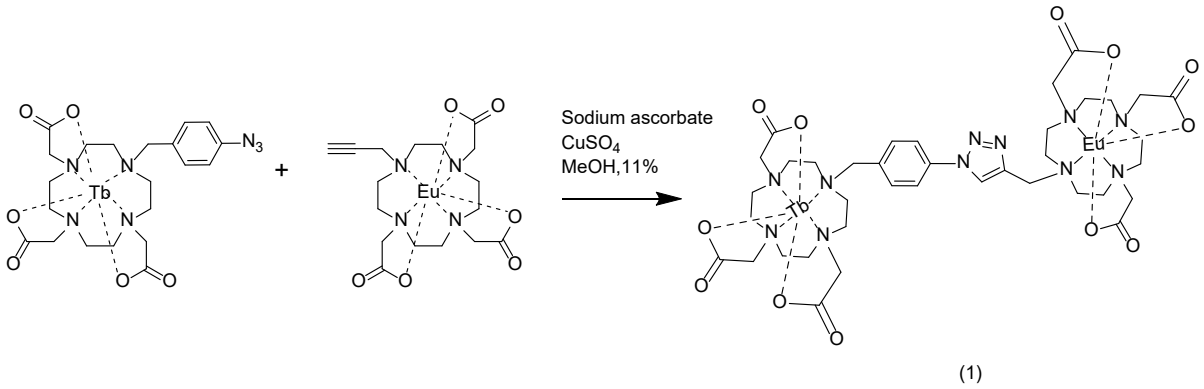
(4)

(4) is prepared in accordance with a reported procedure.[6]

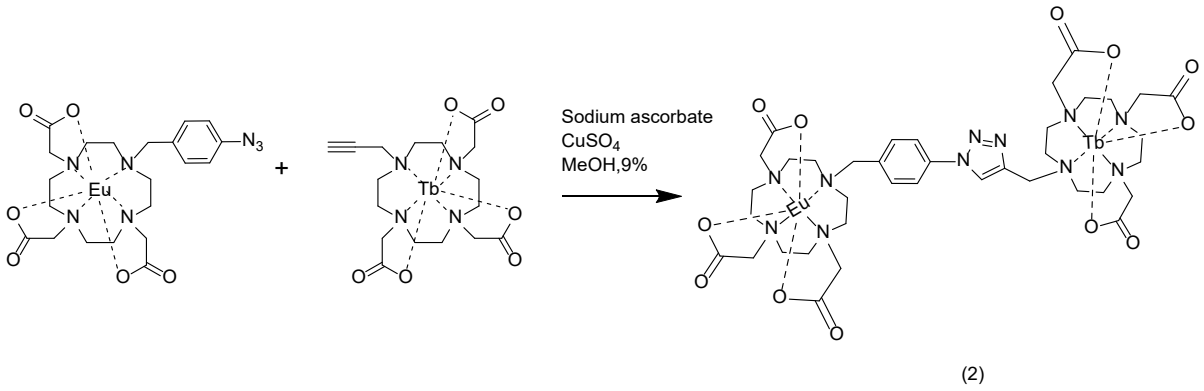
Eu: Yield: 93 mg, 60 %. ^{1}H NMR (D_2O, 400 MHz) δ (ppm) 25.92, 18.75, 18.52, 14.45, 10.24, −1.28, −5.96, −8.05, −10.18, −17.08, −18.16, −19.37. Only major resolved peaks outside the +10 to 0 ppm range are reported. MALDI-TOF HRMS (*m*/*z*) 535 ([M + H]$^+$).

Tb: Yield: 54 mg, 73 %. ^{1}H NMR (D_2O, 400 MHz) δ (ppm) 420.12, 408.33, 247.25, 198.50, 77.63, -75.78, -189.23, -320.35, -371.12, -389.60, -412.33. Only major resolved peaks outside the +50 to -50 ppm range are reported. MALDI-TOF HRMS (*m*/*z*) 541 ([M + H]$^{+}$).

Part three:



Scheme 5.5 Reaction scheme of synthetic route to TbEu complex.

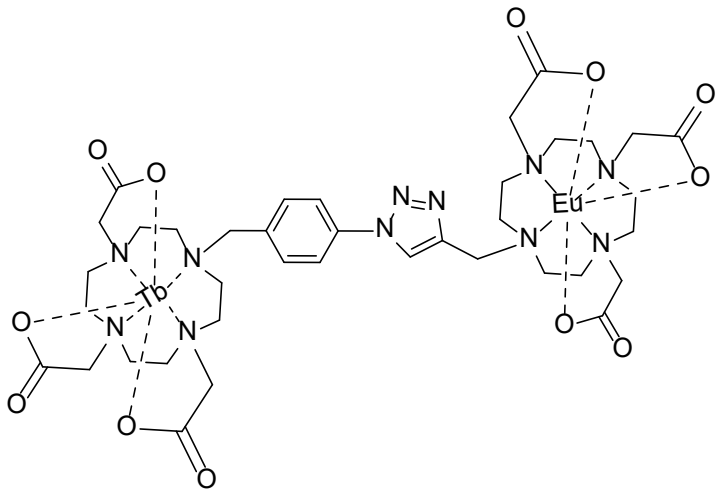


Scheme 5.6 Reaction scheme of synthetic route to EuTb complex.

General Synthetic Methods for Heterobimetallic Lanthanide Complexes (1) & (2):

Aqueous solutions of the propargyl-DO3A complexes (2 equiv.) and the azidobenzyl-DO3A complex (1 equiv.) were combined, followed by the addition of sodium ascorbate (10 mol %) and copper(II) sulfate (2 mol %) to generate the Cu(I) catalyst in situ. The reaction mixture was maintained at 40 °C with stirring for 3 days. The resulting solution was clarified by syringe filtration and purified by dialysis against water for 72 h using a 1000 MWCO membrane. Subsequent removal of water by lyophilisation produced a glassy residue, which was triturated with methanol and diethyl ether. The solid product was isolated and dried under high vacuum to afford a green solid. Isolated yields were determined relative to the azide starting material.

Heterobimetallic TbEu complex (1)

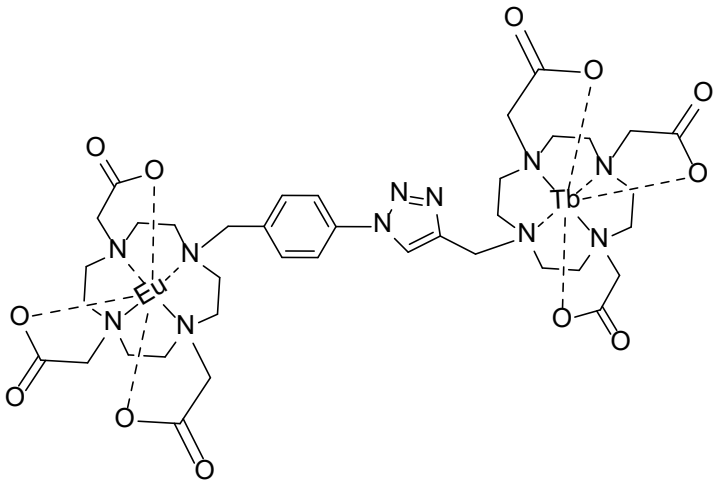


(1)

TbEu complex (1): Yield: 93 mg, 68%. ^{1}H NMR (D_2O, 400 MHz) δ (ppm) 236.00, 214.45, 128.11, 99.49, 90.49, 51.63, 22.27, 17.90, 15.88, 14.22, 12.40, -13.63, -15.39, -19.38, -20.94,

-58.18, -70.46, -81.80, -103.63, -115.57, -130.84, -157.31, -201.41, -356.02, -367.34, -406.77, -423.98.

Heterobimetallic EuTb complex (2)



(2)

EuTb complex (2): Yield: 93 mg, 68%. ^{1}H NMR (D_2O, 400 MHz) δ (ppm) 275.59, 225.28, 158.69, 124.56, 80.22, 54.57, 38.43, 23.32, 21.28, 19.38, 11.50, -10.37, -11.92, -15.39, -16.97, -18.52, -18.89, -36.09, -66.72, -83.58, -91.57, -115.01, -135.20, -163.74, -109.27, -207.68, -223.49, -275.79, -310.54, -370.43.

6.2 Photophysics Experimental

General Considerations

Luminescence measurements for the europium and terbium complexes were performed using a HORIBA FluoroLog-3 spectrofluorometer. Data analysis was carried out using OriginLab and Microsoft Excel. The excitation and emission monochromator slit widths were set to 10 and 2 nm, respectively, and an integration time of 0.1 s per point was employed to provide an optimal balance between spectral resolution and signal-to-noise across all experiments. Emission spectra were recorded between 450 and 750 nm in order to encompass both terbium- and europium-centred emission features.

A range of photophysical experiments was conducted; the study described in Section 3.6 is presented as a representative example.

3.6 Part 1: Experiment for Investigating the Energy Transfer between Eu.NMM and Tb.iphth.

Materials and Reagents

- Eu.NMM
- Tb.iphth
- HEPES buffer (20 mM, pH 7.4)
- Deionized water

Sample Preparation

All samples were prepared in 20 mM HEPES buffer. Stock solutions of Eu.NMM, Tb.iphth, and G6P were prepared at concentrations of 10^{-2} mol/L and diluted accordingly.

Sample	Composition
EuNMM only	2.5×10^{-4} mol/L EuNMM
Tb.iphth only	2.5×10^{-4} mol/L Tb.iphth
1:1 Eu + Tb	2.5×10^{-4} mol/L EuNMM + 2.5×10^{-4} mol/L Tb.iphth

Excitation-Emission Measurements

Step	Objective	Details
a.	Direct excitation of Tb^{3+}	λ<excitation> = 488 nm
b.	Antenna excitation	λ<excitation> = 270 nm
c.	Emission scan	λ<emission> = 450–750 nm

Part 2: Experiment for Competitive Binding Assay of EuNMM and Tb.iphth with G6P

Materials and Reagents

- Eu.NMM
- Tb.iphth
- Glucose-6-phosphate (G6P)
- HEPES buffer (20 mM, pH 7.4)
- Deionized water

Sample Preparation

All samples were prepared in 20 mM HEPES buffer. Stock solutions of Eu.NMM, Tb.iphth, and G6P were prepared at concentrations of 10^{-2} mol/L and diluted accordingly.

Sample	Composition
EuNMM only	2.5×10^{-4} mol/L EuNMM
Tb.iphth only	2.5×10^{-4} mol/L Tb.iphth
1:1 Eu + Tb	2.5×10^{-4} mol/L EuNMM + 2.5×10^{-4} mol/L Tb.iphth
1 eqv. G6P in 1:1 Eu + Tb	2.5×10^{-4} mol/L EuNMM + 2.5×10^{-4} mol/L Tb.iphth + 2.5×10^{-4} mol/L G6P
10 eqv. G6P in 1:1 Eu + Tb	2.5×10^{-4} mol/L EuNMM + 2.5×10^{-4} mol/L Tb.iphth + 25×10^{-4} mol/L G6P

Excitation-Emission Measurements

Step	Objective	Details
a.	Direct excitation of Tb^{3+}	λ<excitation> = 488 nm
b.	Antenna excitation	λ<excitation> = 270 nm
c.	Emission scan	λ<emission> = 450–750 nm

6.3 References

(1) Dadabhoy, A.; Faulkner, S.; Sammes, P. G. Long wavelength sensitizers for europium (III) luminescence based on acridone derivatives. *J. Chem. Soc., Perkin Trans. 2* **2002**, (2), 348-357.

(2) Chhikara, B. S.; Kumar, N.; Tandon, V.; Mishra, A. K. Synthesis and evaluation of bifunctional chelating agents derived from bis (2-aminophenylthio) alkane for radioimaging with 99mTc. *Bioorg. Med. Chem.* **2005**, *13* (15), 4713-4720.

(3) Placidi, M. P.; Natrajan, L. S.; Sykes, D.; Kenwright, A. M.; Faulkner, S. Bimetallic lanthanide complexes derived from macrocycle-appended *m*-xylyl derivatives: Synthesis and spectroscopic properties. *Helv. Chim. Acta.* **2009**, *92* (11), 2427–2438.

(4) Faulkner, S.; Matthews, J. Fluorescent complexes for biomedical applications. *Comprehensive Coordination Chemistry II* **2004**, *9*, 913-944.

(5) Hong, L.; Lin, W.; Zhang, F.; Liu, R.; Zhou, X. Ln [N $(SiMe_3)_2]_3$-catalyzed cycloaddition of terminal alkynes to azides leading to 1, 5-disubstituted 1, 2, 3-triazoles: new mechanistic features. *Chemical Communications* **2013**, *49* (49), 5589-5591.

(6) Jauregui, M.; Perry, W. S.; Allain, C.; Vidler, L. R.; Willis, M. C.; Kenwright, A. M.; Snaith, J. S.; Stasiuk, G. J.; Lowe, M. P.; Faulkner, S. Changing the Local Coordination Environment in Mono- and Binuclear Lanthanide Complexes through “Click” Chemistry. *Dalton Trans.* **2009**, *32*, 6283–6285.